ASSESSMENT OF FLOW CONDITIONS IN A NEW VORTEX-TYPE STORMWATER RETENTION POND USING A PHYSICAL MODEL

A Thesis

Submitted to the College of Graduate Studies and Research

in Partial Fulfillment of the Requirements

for the

Degree of Master of Science

in the

Department of Civil and Geological Engineering

University of Saskatchewan

Saskatoon

By

ROCKY CHOWDHURY

PERMISSION TO USE

In presenting this thesis in partial fulfilment of the requirements for a Postgraduate degree from the University of Saskatchewan, I agree that the Libraries of this University may make it freely available for inspection. I further agree that permission for copying of this thesis in any manner, in whole or in part, for scholarly purposes may be granted by the professor or professors who supervised my thesis work or, in their absence, by the Head of the Department or the Dean of the College in which my thesis work was done. It is understood that any copying or publication or use of this thesis or parts thereof for financial gain shall not be allowed without my written permission. It is also understood that due recognition shall be given to me and to the University of Saskatchewan in any scholarly use which may be made of any material in my thesis.

Requests for permission to copy or to make other use of material in this thesis in whole or part should be addressed to:

Head of the Department of Civil and Geological Engineering

University of Saskatchewan

57 Campus Drive

Saskatoon, Saskatchewan

Canada, S7N 5A9

ABSTRACT

The stormwater retention pond is a best management practice used for the improvement of runoff water quality before it discharges into larger surface waterbodies. A vortex-type retention pond, called the Nautilus Pond^{TM}, is a new design approach for stormwater retention ponds that is expected to produce an internal flow pattern in the pond that is more conducive to removal of sediments from runoff. Since many existing stormwater retention ponds were originally designed only for flood control, most of the ponds are subject to large dead zones, severe short-circuiting and short retention times, which can limit sediment retention in the ponds. In this study, the robustness of the design of the Nautilus Pond^{TM} was evaluated by assessing its residence time distribution (RTD) characteristics, flow pattern and sediment deposition patterns under various conditions of flow in the pond.

The study was carried out in two physical scale models of a simplified Nautilus Pond^{TM}: one with a scale ratio of 1:30.775 for an aspect ratio of 100:2, and the other with a scale ratio of 1:13.289 for a pond of 50:2 aspect ratio. The aspect ratio is the ratio of the pond diameter at its water surface (top width) to the depth of flow, 2 m at corresponding design flow rates, in the pond. First, the RTD characteristics and flow patterns in the ponds were investigated using tracer mass recovery and flow visualization tests allowing different times for steady flow development (flow development time) for the design flows corresponding to 4 m^3/s in the 100:2 prototype pond and 1 m^3/s in the 50:2 pond. Then, tracer tests were carried out at different flow rates to investigate its effects on the RTD characteristics in both model ponds. The deposition patterns of approximately 50 micron sediment particles (prototype size) were also observed. The best position of a berm around the pond outlet was determined for the 100:2 pond by comparing the RTD characteristics and the sediment deposition patterns in the pond for three different positions of the berm. The residence time distribution characteristics and the sediment deposition pattern were also assessed for the 50:2 pond with a berm placed in a position equivalent to the best position identified in the 100:2 pond tests.

It was found that the RTD curves at design flow rates of 4 m^3/s and 1 m^3/s for different flow development times were very similar to each other for both pond aspect ratios; the flow development time was found to have little effect on the flow characteristics of the ponds. The

average baffle factors, short-circuiting indices and Morril dispersion indices were 0.41, 0.20 and 4.1, respectively, for the 100:2 pond aspect ratio, whereas these were 0.23, 0.05 and 8.6 for the 50:2 pond.

The flow rate was found to have a significant effect on the RTD characteristics of both ponds. There were multiple peaks in the RTD curves for the lower flow rates tested for the 100:2 pond. This was thought to be a result of the low inflow momentum and high aspect ratio of the pond. As the flow rate was increased, the residence time distribution curve had a single, lower peak. In both ponds, an increase of flow rate caused the baffle factor and short-circuiting index to decrease and the Morril dispersion index to increase indicating that the inflow spent a shorter time in the pond.

The sediment deposition pattern tests in both ponds without the berm around the outlet showed that a higher quantity of sediments deposited in the outer peripheral region of 100:2 pond. The 50:2 pond deposited a small amount of sediment along the periphery due to the high velocity inflow jet and lower aspect ratio of the pond.

The best position of the berm among those tested was found to be at the 60% of pond bed radius from the center. Though the RTD characteristics for the 100:2 pond with different berm positions were very similar to each other, the 100:2 pond with the berm position at 60% of pond bed radius deposited most of the sediments outside the berm. The RTD characteristics in both ponds showed significant improvement with a berm at the 60% of radius position compared to the ponds without a berm. This improvement was more significant for the 50:2 pond than for the 100:2 pond. Further, the sediment deposition pattern in 100:2 pond with berm at 60% of bed radius showed that the larger sized sediment particles mainly deposited outside the berm and the finer particles deposited inside the berm. The 50:2 pond did not show any significant difference in particle size distribution of the sediments deposited inside and outside of the berm.

ACKNOWLEDGMENTS

I would like to acknowledge the guidance and support I received from my supervisors, Dr. Kerry Mazurek and Dr. Gordon Putz, throughout the M.Sc. program. I also thank my advisory committee members, Dr. Jim Kells, Dr. David Sumner and Dr. Moh Boulfiza, for their comments and suggestions about my research.

I thank technicians Mr. Dale Pavier, Mr. Brennan Pokoyoway, Mr. Adam Hammerlindl and Ms. Helen Yin for their support with the experimental setup in the laboratory.

I acknowledge the support of Mr. Cory Albers and Mr. Bernie Amell, Co-Owners of Source2Source Inc., about the design and operation of Nautilus Pond™.

I thank my fellow colleagues in the Hydrotechnical Lab for providing support in various ways throughout my research work.

I also acknowledge the financial support provided by Natural Science and Engineering Research Council of Canada (NSERC) to my supervisors in the form of Strategic Project Grants.

Last, but certainly not least, I thank my wife, Joyasree Dev, for her patience and encouragement in achieving this milestone.

DEDICATION

This thesis is dedicated to my mother, Chobi Chowdhury, and my sister, Bubli Chowdhury.

TABLE OF CONTENTS

LIST OF TABLES

LIST OF FIGURES

LIST OF SYMBOLS

A_R	pond aspect ratio;
$C(t)$	tracer concentration at the model outlet;
C_H	concentration of the highly concentrated tracer solution;
C_k	tracer concentration at the end of a time step;
C_{k+1}	tracer concentration measured at the beginning of a time step;
C_L	volume of the diluted solution;
D	diameter of the inflow jet;
d	fraction of dead spaces;
d_s	size of the settling particle;
d_*	dimensionless grain size diameter;
$E(t)$	residence time distribution function;
E_θ	dimensionless residence time distribution function;
$F(t)$	cumulative residence time distribution function;
F_r	Froude number;
G	specific gravity;
g	gravitational acceleration;
h	flow depth in the model;
h_w	head above weir crest upstream of the weir;
L_M	length in model;
L_P	length in prototype;
L_r	model to prototype length ratio;

M	total mass of recovered tracer;
ΔM_k	tracer mass exited at a time step;
m	fraction of perfectly mixed flow;
N_0	total mass of injected tracer;
n	number of measurements;
P	fraction of plug flow;
Q	flow rate;
R	tracer mass recovery rate;
R_e	inflow jet Reynolds number;
R_0	Rossby number;
t	time;
Δt	length of a time step;
t_d	theoretical retention time;
t_f	flow development time;
t_g	experimental retention time;
t_i	time required for the first tracer particle to reach outlet;
t_k	time at the beginning of a time step;
t_{k+1}	time at the end of a time step;
t_p	time to reach peak tracer concentration at the outlet;
t_{10}	time required for the 10% of tracer mass to leave the pond;
t_{50}	time required for the 50% of tracer mass to leave the pond;
t_{90}	time required for the 90% of tracer mass to leave the pond;
U	velocity;

U_i average velocity of flow in inlet pipe;

V_f flow volume in the model;

V_H volume of the highly concentrated tracer solution;

V_L volume of the diluted solution;

v_r radial velocity component;

v_s settling velocity;

v_ϑ circumferential velocity component;

y flow depth;

ν kinematic viscosity;

φ latitude.

Ω angular frequency of the planetary motion; and

ω Coriolis frequency.

CHAPTER 1: INTRODUCTION

1.1 Background

Several best management practices have been developed over time in order to improve surface water runoff quality by removing sediments and pollutants and control flooding. These management practices include dry detention basins, wet retention ponds, and infiltration basins. Dry detention basins hold stormwater runoff for a particular period of time and then completely discharge into larger water bodies at a slower rate than would occur if not captured in the pond (Erickson et al. 2013). Wet retention ponds maintain a permanent pool of water, which keeps the runoff in the pond for a longer period of time than dry detention basins. The long retention time allows sediments to be removed through gravitational settling and nutrients as well as other pollutants to be removed through complex chemical and biological processes. As a result, wet retention ponds can remove more sediments and pollutants than dry ponds. Infiltration basins have been reported to have the highest removal efficiency of sediments and pollutants from stormwater runoff (Clar et al. 2004). However, the infiltration basin is rarely used due to possible groundwater contamination. Therefore, the wet retention pond is considered the most efficient best management practice available for removing sediments and pollutants from stormwater runoff (United States Environmental Protection Agency (USEPA) 1983; Clar et al. 2004).

Most wet retention ponds, however, were initially designed as flow attenuation structures to control flooding, as surface water quality was not a major concern for planners before the 1980's (USEPA 1983; Wu et al. 1996; Clar et al. 2004). The Clean Water Act legislated in 1972 in the United States was amended in 1987 to include the management of urban stormwater pollution and stormwater permit programs for urban areas or industry (National Research Council (NRC) 2008). In 1997 – 2001, regulations for Total Maximum Daily Loads of various pollutants were introduced in the U.S. and assigned as effluent limitations in stormwater permits. Recently the Province of Alberta has introduced Maximum Allowable Loads for suspended sediments and pollutants to achieve surface water quality objectives (McDonald 2013).

Since surface water quality was now of concern, the quality of stormwater runoff was studied by various researchers to investigate its contribution to the sediments and pollutants of

surface water bodies. USEPA (2002) reports that storm water runoff is one of the four major human induced sources of water pollution in surface water bodies. It contains high percentages of suspended solids, organic substances, metal, nitrogen, phosphorus, and salt (USEPA 1983; Wang et al. 2004; Hunt et al. 2008). Existing retention ponds were tested to check their ability to improve water quality by removing suspended solids and other pollutants. It was found that the stormwater retention ponds do improve water quality somewhat. For example, USEPA (1983) monitored nine retention ponds and the removal efficiency for total suspended solids varied between 5%-91%. Total suspended solids are the suspended particles in the water that are larger than 2 micron in size. Though the variability in removal efficiencies was attributed to the different physical setup of each pond, low removal efficiencies of the ponds were caused by the presence of large dead zones, short circuiting and short retention times. Dead zones are the areas of stagnant water in the pond and short circuiting is the movement of flow directly from the pond inlet to outlet. These characteristics are the direct result of flow behaviors that in turn depend on pond geometries.

Attempts to modify the design of stormwater retention ponds for better removal of sediments and pollutants have been focused on the length to width ratio of the pond to increase flow path, adding a sub-surface berm or island near the inlet to minimize short-circuiting, and more effectively positioning the inlets and outlets (Persson 2001). However, these ponds are still subject to significant short-circuiting and dead spaces (Persson 2001). The internal flow pattern of the pond was never considered in design as a means of improving water quality.

Albers and Amell (2010) presented a new vortex-type retention pond design called the Nautilus Pond^{TM} to improve the flow pattern through ponds in hopes of providing greater improvements in water quality in their pond. The new pond receives inflow through a peripheral inlet and flow exits through an elevated outlet at the pond center. Thus a vortex is created with its center at the outlet so that the entire pond recirculates. A sketch of the Nautilus Pond^{TM} in plan and in a cross-sectional view is shown in Figure 1.1. Sediments are intended to deposit along the long flow path created by the vortex near the outer edges of the pond. A circular berm is often placed around the outlet to help stabilize and improve the flow conditions. The best position for the berm is one of the issues studied herein. The spiral flow pattern in the vortex is expected to provide a longer residence time in the pond allowing more time for the physical, chemical and

biological processes to remove pollutants and sediments. Short circuiting from inlet to outlet and dead space in the pond is reduced in the Nautilus Pond™ (Albers and Amell 2010).

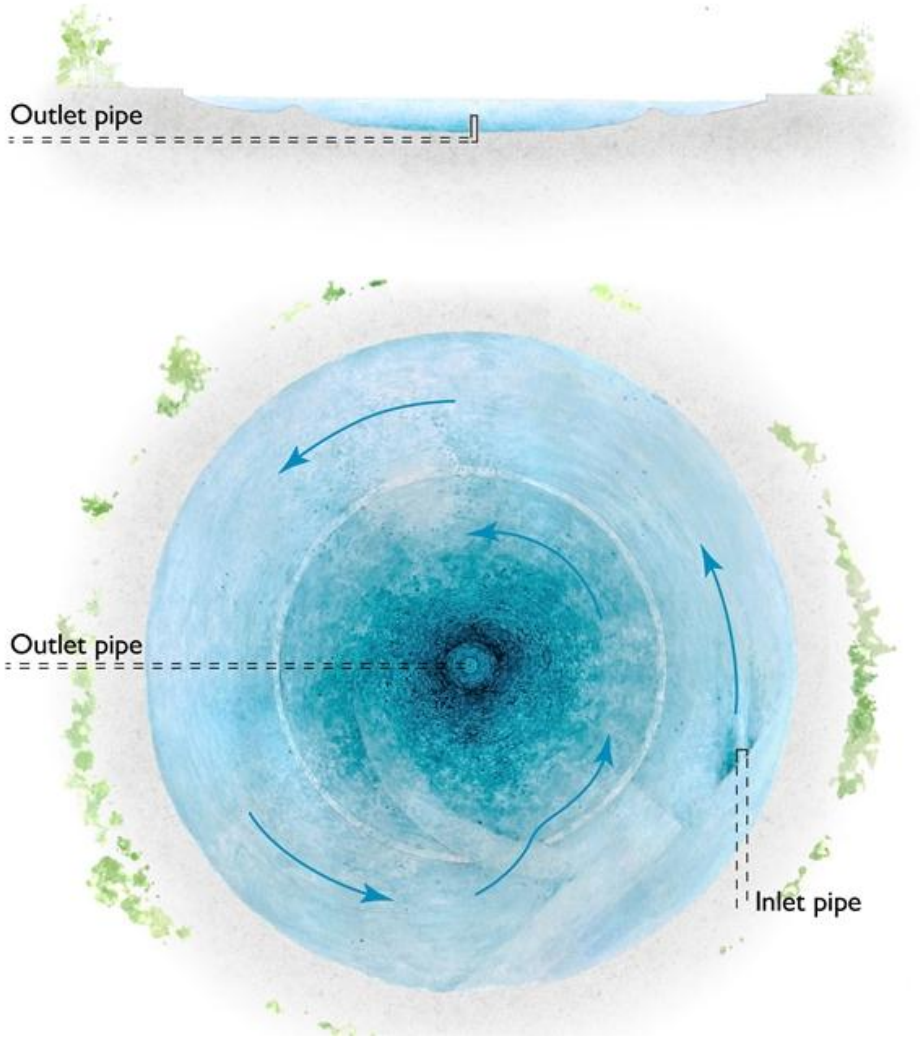

Figure 1.1: Cross-sectional profile and plan of a Nautilus Pond™
(permission for use was obtained from Source2Source Inc. on April 27, 2015)

Vortex technology in the form of vortex type settling basins has been used in the past to remove sediments from irrigation and power canals (Mashauri 1986; Paul et al. 1991; Athar et al. 2002; Keshavarzi and Gheisi 2006; Chapokpour 2011; Ansari and Athar 2013). Sullivan et al. (1974), Heinking and Wilcoxon (1985), and Luyckx and Berlamont (2004) similarly studied the Swirl concentrator. Unlike the Nautilus Pond™, both of these devices use secondary flow created by the circulating peripheral inflow to remove sediment through a central outlet (Athar et al. 2002). Secondary flow is created due to the deceleration of flow near the bed. The low velocity in the

bottom layers of a circulating flow is unable to create a strong centrifugal force to counteract the radially inward pressure gradient of the flow. Therefore flow near the bed tends to move radially inward whereas the top flow layers of high velocity follow a circulating path. A high kinetic energy in inflow is required in order to create a strong secondary flow to remove sediments through a central outlet and achieve high removal efficiency (Sullivan et al. 1974; Mashauri 2011). The volume and kinetic energy of stormwater runoff inflows are often highly variable and therefore the existing conventional vortex-based devices are not effective in treating stormwater runoff.

1.2 Objectives

The objective of this research is to investigate the performance of the Nautilus Pond™ design over a range in operating conditions by conducting testing in a physical scale model of the pond. The specific objectives are the following:

1. To investigate the flow development time[1], residence time distribution (RTD - the distribution of flow times particles spend inside a pond), and flow pattern under a steady state inflow in hydraulic models equivalent to common Nautilus Ponds™ designs of 100 m and 50 m diameter each of 2 m depth;

2. To investigate the effects of flow rate on RTD characteristics of the pond;

3. To investigate the sediment deposition pattern in the Nautilus Ponds™ for sediment added to the flow as continuous feed for particles equivalent to 50 μm diameter in the prototype pond;

4. To determine the best of the three positions of a berm used to improve flow and residence time characteristics for the pond; and

5. To investigate the effect of a berm at its best position on the sediment deposition pattern in the pond.

[1] In this thesis, the flow development time is the time from initiation of flow in the model before a test is started.

1.3 Scope of the Research

This research on a vortex-type stormwater retention pond was carried out using a physical scale model. The model was used to test two prototype pond designs of 100 m and 50 m diameters and 2 m flow depths. The steady flow rates used in the model to test the 100:2[2] and 50:2 ponds were equivalent to 4 m^3/s and 1 m^3/s for the prototype flow, respectively. The berm around the outlet for the 100:2 pond model was tested at three different positons. The 50:2 pond model was tested with the same relative berm position at which the 100:2 pond model achieved the longest retention time. Sediment deposition pattern tests were carried out to identify the location of deposited sediments. Computational fluid dynamics modelling was not used in this research to analyze pond hydraulics.

1.4 Organization of the Thesis Document

The thesis document consists of five chapters. For the following chapters, Chapter 2 provides a literature review of typical existing pond conditions and considerations for the physical modelling of the pond. Chapter 2 also involves discussion of how to evaluate flow patterns and the residence time in ponds. Chapter 3 discusses the design procedure and construction of the hydraulic model, experimental setup and details of the testing program. Chapter 4 presents the test results, analysis and discussion of the results. Chapter 5 highlights the conclusions derived from this study and the recommendations for further research.

[2] 100 m and 50 m diameter Nautilus Ponds™ of 2 m depths are referred as the 100:2 and 50:2 ponds, respectively.

CHAPTER 2: LITERATURE REVIEW

2.1 Introduction

The literature review presented in this chapter consists of a discussion of the conditions at typical stormwater retention ponds, as well as the criteria for the development of a hydraulic model of a pond. Flow visualization and tracer studies to investigate flow characteristics are also discussed. The conditions of existing stormwater retention ponds have been studied in terms of sediment removal efficiency of existing ponds and the operation and maintenance costs of ponds. An understanding of the deposition of sediment in existing retention ponds is of strong interest for the design of the Nautilus Pond^{TM}.

2.2 Existing Stormwater Retention Ponds

The sediment removal efficiencies of wet retention ponds have been found to be highly variable. Sediment removal efficiency can be defined as the mass of sediments retained in the pond as percentage to the total sediment load into the pond. The sediment mass retained is calculated from the difference of total sediment load in the inflow and outflow over a specified time. Sometimes the removal efficiency is calculated based on the difference in event mean concentration of sediment in the inflow and outflow instead of the total load in the inflow and outflow (Gain 1996). The sediment removal efficiency usually depends on the pond geometry, rainfall intensity and duration, land use characteristics of the watershed, area of the pond as percentage of the watershed area and vegetation in the pond (Ferrara and Witkowski 1983; Kantrowitz and Woodham 1995; Wu et al. 1996; Mallin et al. 2002).

Ferrara and Witkowski (1983) measured the removal efficiency of total suspended solids for three typical wet retention ponds for three storms. The sediment removal efficiencies for the three ponds were found vary from 32% – 80%, 20.3% – 77.6% and 13.6% – 24% for the three storms; the removal efficiencies were found to increase with rainfall intensity. This was because the more intense storms produced more runoff and carried greater percentages of coarse sediments that settle more quickly in the pond. Though the inflow sediment concentration was found to vary throughout the storm duration, the outflow sediment concentration was found to be relatively constant during the same period (Ferrara and Witkowski 1983). Comings et al. (2000) and

Takaijudin et al. (2011) also reported an increased removal of sediments in conventional stormwater ponds with a high inflow rate of runoff. Conversely, Wu et al. (1996) reported 100% sediment removal in a pond during some storm events. However, the storm duration was so small in those cases that the pond was able to retain all runoff in its permanent volume.

Wu et al. (1996) studied sediment removal efficiencies of three wet retention ponds and the long term removal efficiencies were found to be 41%, 62% and 93%. They reported that the sediment removal efficiency is proportional to the surface to area ratio of the pond. The surface to area ratio is the ratio of the pond surface to the corresponding watershed area. However, the increasing rate of removal efficiency decreased significantly for surface to area ratios greater than 2% (Wu et al. 1996). Therefore, a robust cost-benefit analysis was recommended for designing ponds large in size as a means of increasing the sediment removal efficiency of the pond.

Pond geometry was also shown to be an influential factor in determining sediment removal efficiency of wet retention ponds. Persson (2001) reported that ponds having higher length to width ratios experience less short circuiting effects and can have better sediment removal efficiencies. Comings et al. (2000) studied two ponds: the first was U-shaped pond having a large permanent pool volume; the second was a three-cell pond with rectangular-shaped cells with a much smaller permanent pool volume as compared to the U-shaped pond. The U-shaped pond was found to remove 81% of total suspended solids, whereas only 61% was removed by the pond having three cells. The first two cells of the three-cell pond were reported to have severe short-circuiting, which was considered responsible for the lower removal efficiency of the pond. The third cell had a diagonal flow path that contributed most in removing the sediments from the pond. The longer flow path of the U-shaped pond and the significantly larger permanent pool volume were thought to be the causes for the increased sediment removal efficiency in the pond (Comings et al. 2000).

As suggested above, the sediment removal efficiency of a wet retention pond also depends on the particle size of sediments in the inflow. The sediment sizes in the inflow in turn depend on the land use characteristics and rainfall intensity in the watershed (Liebens 2001). Liebens (2001) reported that inflow sediments may contain 26% – 85% of sand, 6% – 51% of silt and 5% – 35% of clay depending on the residential or commercial use of the areas. The runoff from commercial

areas has been reported to contain larger quantities of fine sediments as compared to residential areas (Liebens 2001).

Greb and Bannerman (1997) studied removal efficiencies of different sized particles in a wet retention pond for 16 storm events. The pond was located in a watershed consisting of 97% residential area and 3% commercial area. The pond was an irregular leaf-shaped structure with an island in the middle of the pond. The pond inflow was reported to carry 9% sand, 40% silt and 51% clay. The average removal efficiencies of the pond for different storm events were found to be 99%, 93% and 74% for the particles greater than 0.062 mm, between 0.062 – 0.004 mm and less than 0.004 mm, respectively. The efficiencies were calculated using the event mean concentrations of different samples instead of total loads in each size of sediments. However, it shows that the inflow runoff containing a higher fraction of fine sediments will usually have lower removal efficiency and vice versa.

The Ontario Ministry of Environment and Energy, (OMEE) (1994) and Yousef et al. (1994) studied sediment accumulation rates in stormwater retention ponds. Yousef et al. (1994) derived a relationship between the sediment accumulation rate and the ratio of the pond surface area to the contributing drainage area for nine retention ponds. The sediment accumulation rate in a pond was found to increase very sharply for pond surface to drainage area ratios less than 2% and became nearly constant at 10 mm per year for the pond surface to drainage area ratios greater than 4% (Yousef et al. 1994). OMEE (1994) found an asymptotically proportional relationship between the storage capacity, which is an indicator of sediment accumulation rate, and sediment removal efficiencies of the pond. The derivation of this relationship, however, did not consider the effect of upstream development, poor sediment controls and other site specific factors that may have simultaneous effects on the sediment accumulation data of different ponds.

The location of sediment deposition in the pond is equally important and can be an indicator of the sediment removal efficiencies of retention ponds. Usually the coarse particles tend to settle near the inlet and the finer particles travel a longer distance toward the outlet before settling or exiting the pond (Verstraeten and Poesen 2001). Yousef et al. (1994) and Verstraeten and Poesen (2001) studied the pattern of deposited sediments in conventional stormwater retention ponds. Yousef et al. (1994) found that the width-averaged depth of deposited sediment was about 180 mm

throughout the pond. However the average sediment depth along the outlet side of the rectangular pond was 245 mm, which shows that a lot of the sediments traveled the entire flow path of the pond and may exit through the outlet. The study of Verstraeten and Poesen (2001), using the dry density of sediment throughout the pond, showed that the deposited sediment density was the highest near the inlet and slowly became less dense along the length toward outlet. However, the sediments deposited near the outlet did not follow this particular pattern and was reported to have a higher density of sediments. Often a small area forebay is installed near a pond's inlet to deposit most of the coarse sediments in the inflow (Gharabaghi et al. 2006). This forebay may need more frequent maintenance than the main pond due to its ability to deposit a high percentage of sediments.

2.3 Operation and Maintenance Costs of Stormwater Retention Ponds

The design of a stormwater retention pond should take into account the annual operation and maintenance costs in addition to the construction costs during design. Since both construction costs and operation and maintenance costs are highly site specific, the operation and maintenance costs are often compared to the capital cost as an indicator of cost for each site (Livingston et al. 1997). The operation and maintenance tasks usually include regular inspection, removal of debris, maintenance of inlets and outlets, vegetation control, vector control and administrative work. Strassler et al. (1999) and the California Department of Transportation (CALTRANS) (2004) found that the annual operation and maintenance cost of a conventional stormwater retention pond is initially about 3% – 6% of its capital cost. However, the total operation and maintenance cost of a conventional stormwater retention pond over a 20-year life cycle was estimated to be about 26% of the capital cost when all of the costs were adjusted (considering a 4% inflation rate in each year) (CALTRANS 2004).

Sediment removal is one of the major maintenance works required for a stormwater retention pond. Strassler et al. (1999) reported that the sediment removal is required every 5 years from forebays and every 20 years from the main retention pond. OMEE (1994) recommended a sediment removal frequency of 10 years as a design target for stormwater retention ponds though the actual removal frequency is site specific and depends on land use characteristics, permanent and active pool volumes, development activities near the corresponding site and the sediment accumulation rate in the pond. Sediment cleanups may also need to be performed if the sediment

removal efficiency of a pond is reduced by 5% due to the accumulation of sediments on the pond bed (OMEE 1994).

Drake and Guo (2008) obtained sediment removal cost data of stormwater retention ponds through interviews with the City of Mississauga, City of Waterloo, Town of Markham and the City of Ottawa. The sediment removal cost was found to be in the range of $200,000 – $500,000. This large cost for sediment removal and its frequency warrants that these costs should be incorporated during design. A well-designed pond should retain most of the sediments in the pond as well as not require frequent cleanup of the entire pond to maintain its high removal efficiency. Drake and Guo (2008) recommended that municipalities must set high standards for pond design if the costs of regular monitoring and frequent sediment removal are to be avoided later.

2.4 Physical Hydraulic Modelling

A hydraulic model is an important tool to study the robustness of the design of stormwater retention ponds through investigation of the flow characteristics in the model. Flow characteristics can be investigated to assess whether the flow pattern is favorable to produce high sediment removal efficiencies in the pond.

There are two conventional practices to study the flow characteristics in hydraulic systems: the physical model; and the numerical model. A physical model is a laboratory scale representation of a real world prototype and a numerical model is a mathematical representation of flow processes. The main advantage of physical modelling is that it can replicate complex flow characteristics and transport processes for which a reliable solution through computer simulation cannot be developed (ASCE 2000). Studies with physical models may incorporate important nonlinear variables in the flow that might be unknown prior to the study (Peakall et al. 1996). Physical modelling can be employed without any measured field data and can be used to study the design and operation of unbuilt hydraulic structures. The disadvantages of the physical models are the potential requirements for a large space in the laboratory, high cost, pumping capacity, requirements for a data collection system and so on. Scale ratios in a physical model can be limited due to the effects of surface tension, viscosity and roughness whereas scale ratios can be neglected in a numerical model (Kobus 1980).

The comparisons between physical and numerical models are important to understand the benefits, limitations and applications of both types of models. Most of the limitations of a physical model do not exist in a numerical model. However the major limitation of a numerical model is the approximation of equations through various assumptions and the unavailability of empirical coefficients (Grayman et al. 1996). Most of the flow processes in hydraulic engineering cannot be defined by a closed set of equations, causing limitations on the general prediction capabilities of numerical models (Kobus 1980). The numerical model can also be limited due to the resolution of the model. Therefore the physical model is limited toward the upper end of scale due to limitations in laboratory space whereas numerical models are limited toward the lower end of scale due to the limitations in small grid size or high resolutions (Kobus 1980). Kobus (1980) recommended using physical models for the study of local flow processes and numerical models for the large scale flow processes (Kobus 1980). Considering the limitations in each case sometimes both physical and numerical modeling are carried out for a particular hydraulic study.

Similitude is the most important condition for physical modelling. It is required for accurate representation of hydraulic phenomena in a physical model. Three criteria need to be fulfilled in order to ensure model-prototype similitude (Kobus 1980; Sharp 1981; ASCE 2000). These are geometric similarity, kinematic similarity, and dynamic similarity. Geometric similarity is achieved by maintaining a constant ratio between all prototype and model dimensions. Model velocities, accelerations and time need to maintain a constant ratio with the prototype are required in order to ensure kinematic similarity. If kinematic similarity can be achieved accurately, the model flow will have the same shape of streamlines as the prototype. Geometric similarity must be achieved in order to ensure kinematic similarity and the kinematic similarity is automatically achieved if the dynamic similarity criteria are satisfied in the model (ASCE 2000). Dynamic similarity requires that the driving and resisting forces acting on the model flow need to have a constant ratio with the prototype at all points. Geometric, kinematic and dynamic similarities together ensure the exact similitude between model and prototype.

Dimensional analyses had been carried out in the past in order to determine similitude criteria with quantifiable mathematical parameters (ASCE 2000; Novak et al. 2010). Dimensional analyses with the variables acting on the free surface flows yielded several dimensionless parameters that must be evaluated in the model and prototype in order to maintain proper

similitude. These dimensionless parameters are the Reynolds number, Froude number, Weber number and Euler number that represent viscous forces, gravitational forces, surface tension forces and pressure forces respectively in a flow (ASCE 2000; Novak et al. 2010).

Scaling of all forces simultaneously acting in prototype flow is theoretically possible but would require the use of different fluids in the model and prototype (Kobus 1980; Quarini et al. 1996; ASCE 2000; Gill and Pugh 2009). However the use of a different fluid in a model is very expensive and impractical due to the fact that fluids with accurately scaled hydraulic properties almost never exist. One way to deal with this complexity is to ensure the exact similitude only for the most dominant force acting on the flow in the prototype while keeping other forces within certain limits so that the non-dominant forces do not create different flow regimes than in the prototype flow.

Since the gravitational force is dominant in most free surface flows, the Froude number is usually kept equal in the model and prototype (Kobus 1980; ASCE 2000; López et al. 2008; Waldron 2008). Considering an equal Froude number as the primary criterion, the scaling relationship for other parameters can be developed in the design of the hydraulic model. The scaling relationships based on Froude scaling laws are given in Table 2.1, where L_P and L_M are lengths in the prototype and model, respectively, and L_r is the length scale ratio for the model.

Table 2.1: Scaling relationships based on Froude scaling laws

Parameter	Scale ratio
Length	$L_r = \frac{L_M}{L_P}$
Area	L_r^2
Velocity	$L_r^{0.5}$
Flow Rate	$L_r^{2.5}$
Time	$L_r^{0.5}$

Khan et al. (2013) and Farjood et al. (2015) used a physical model for the study of conventional stormwater retention ponds. Khan et al. (2013) used a scale ratio of 1:10 to design the physical model for a rectangular-shaped prototype pond with sloping sides. Since gravity is the dominant force in the flow of stormwater retention ponds, Froude scaling laws were used as the primary design principle for the physical model. The scale ratios for the vertical and horizontal dimensions in the model were kept equal to avoid complexities in model similitudes. Farjood et al. (2015) also used this physical model to study the effect of baffles on the flow characteristics of a stormwater pond.

Although there have been few physical models built of stormwater retention ponds reported in the literature, there have been physical models built for other similar cases of flow. For example, Falconer and Tebbutt (1986), Bishop et al. (1993), Grayman et al. (1996), and Yu et al. (2008) used physical models in the study of clearwells. Clearwells are large shallow reservoirs for storage of treated water to provide retention time for reaction of chlorine and its retention times are often measured using tracer tests. Froude scaling laws were also used in the design of these clearwell physical models. Bishop et al. (1993) and Falconer and Tebbutt (1986) compared the hydraulic parameters obtained from the tests in the Froude scaled physical model with the corresponding prototype clearwell and they showed close similarity. Therefore, Froude scaling laws can be considered as the appropriate criteria for the scaling of clearwell models and by extension to stormwater retention ponds due to the similar flow situation.

Falconer and Tebbutt (1986) used both distorted and undistorted physical models of clearwells to measure longitudinal velocity fields and they found identical velocity fields in both models. However, dispersion due to vertical velocity gradients have been found to be exaggerated and dispersion due to transverse velocity gradients has been found to be underestimated using a distorted physical model (Fischer and Holley 1971). Ali et al. (1978) reported different mixing patterns for the distorted and undistorted physical model of the same prototype clearwell. Therefore, the use of different scale ratios in the horizontal and vertical direction may change the dispersion characteristics in the physical model and proper similitude may not be achieved. ASCE (2000) recommended not using a distorted model where the flow pattern similitude is important in the model. Flow pattern similitude is one of the major objectives in the modelling of stormwater

retention ponds. The results of the studies cited above indicate that a model of a stormwater retention pond should not be distorted.

Model distortion, however, is sometimes considered in order to avoid surface tension effects and increase turbulence in the flow. Any effects due to surface tension are usually negligible in the flow of real world water bodies. When the flow depth and velocity becomes small in a physical model due to the use of the same scale ratio in the horizontal and vertical directions, surface tension in the model may become significant. Novak and Čábelka (1981) discussed several criteria to keep the surface tension effects minimized in a physical model. These include the following: the minimum depth of flow should be greater than 15 mm; and the minimum wave celerity should be greater than 0.23 m/s. These conditions generate a minimum Weber number of 11-12, which may also be used as a limiting condition (Novak et al. 2010). The Weber number is the square root of the ratio of the inertial force to the surface tension force acting in the flow. Kobus (1980) and ASCE (2000) suggested keeping a minimum 25 mm and 30 mm flow depth, respectively, to have negligible surface tension effects in a physical model. However the use of surface-active agents can lower the surface tension effects and the thresholds of the Weber number may be increased (Kobus 1980).

In another flow situations with similar features to a vortex-type retention pond, Sullivan et al. (1974), Mashauri (1986), and Paul et al. (1991) investigated the sediment removal efficiency of a vortex settling basin and swirl concentrator with a physical model. The vortex settling basin and swirl concentrator are 1.0-2.5 m diameter circular basins with a very low diameter to depth ratio. The basin uses secondary flow characteristics of a high velocity vortex to move sediments towards the central outlet and remove sediments with a small amount of flow (Mashauri 1986). The secondary flow is created due to the radial variation of tangential velocity components in the vortex flow (Yang 2009). Quarini et al. (1996) found an outward radial velocity component near the bed of a circular physical model when the inlet was at the center of the model and the outlet weir was at the model periphery. Since centrifugal acceleration resulting from the circulating flow in the model was much less than gravitational acceleration, gravity was considered the dominant force and Froude scaling laws were used in the design of the physical model (Mashauri 1986; Paul et al. 1991). The centrifugal acceleration can be calculated considering the inflow velocity as the tangential velocity since the radial and vertical components of inflow velocity are negligible as

compared to the tangential velocity. The ratio of the square of the tangential velocity to the basin radius gives the centrifugal acceleration. Therefore, Froude scaling laws can be used for the design of the vortex-type retention pond physical model if the centrifugal acceleration is much smaller than the gravitational acceleration.

Odgaard (1986), Knauss (1987), Kiviniemi and Makusa (2009), and Kleynhans (2012) investigated the critical submergences in the formation of air entraining vortices over hydraulic structure intakes using scale models. The critical submergence is the smallest depth of water above the intake for which air stops entraining into the intake through vortices. Gravity was considered as the dominant force and scaling was done accordingly for the physical model. However, it was stated that the physical models designed based on Froude scaling laws may underestimate the possibility of vortex formation in the model due to the scale errors in viscosity (Sharp 1981). Therefore, higher velocities than that given by Froude scaling laws are sometimes used to more accurately simulate the air entraining vortices over hydraulic intakes (Sharp 1981; Knauss 1987). Novak et al. (2010) stated that the viscous forces in the swirling flow can be neglected if the ratio of the Reynolds number to Froude number is greater than 50,000. The surface tension effects can also be neglected in swirling flow when the Weber number is greater than 11 (Novak et al. 2010).

Hai-feng et al. (2009) and Kiviniemi and Makusa (2009) considered the Coriolis force as one of the contributors in vortex formation. The Coriolis force is created due to the rotation of the earth and its relative importance is determined measured by the Rossby number. The Rossby number is defined by the ratio of the inertial force to the Coriolis force. It is a dimensionless parameter given by Equation [2.1] (Hai-feng et al. 2009).

$$R_0 = \frac{U}{L\omega} \qquad [2.1]$$

where U is the characteristic velocity, L is the characteristic length and ω is the Coriolis frequency with $\omega = 2\Omega \sin\varphi$, where Ω is the angular frequency of planetary rotation and φ is the latitude. If the Rossby number is less than 1, this indicates a strong Coriolis effect in vortex formation whereas a higher Rossby number indicates a negligible contribution of Coriolis force in vortex formation. Therefore, the Rossby number should be calculated for the modelling of vortex-type

retention ponds to see if the Coriolis force has significant effect on the formation of the central vortex.

2.5 Flow Visualization Studies

To monitor the flow pattern and estimate the mean velocities in physical models, flow visualization studies have been commonly used. Flow visualization studies are usually carried out using surface floats, submerged drogues, or potassium permanganate solution or food coloring dye (Falconer and Tebbutt 1986; Quarini et al. 1996). However, the most appropriate technique would be the one that accurately defines the flow characteristics. The floats or drogues used in flow visualization studies should be very small and have low inertia in order to have the same movement pattern as the actual flow (ASCE 2000). If drogues are used they must be submerged up to near the bed so that they represent depth average velocity (Falconer and Liu 1987). If dye is used in the study, it must produce high contrast images with still photography or video recordings.

The understanding of the mixing processes of dye in the flow is important in order to understand the appropriateness of using dye in the flow visualization studies. Though any micro scale observation of the shape of eddies is unimportant in flow visualization studies of stormwater retention ponds, it is important to understand the risk of flow visualization images possibly being different than the real flow due to the diffusion of vorticities in visualized flow. The diffusion of vorticities cause a reduction in amplitudes of fluctuating vorticities (Gursul et al. 1990). Gursul et al. (1990) reported that the diffusion of vorticities depends on the Reynolds number of the flow and the distance between the dye injection point and flow pattern visualization point.

When dye is injected into the flow, the small scale eddies distort the shape of the injected dye and create a concentration gradient at a small scale. The local concentration gradients at a small scale become uniform with the spreading of dye through the molecular diffusion process (Fischer et al. 1979). However, turbulent diffusion is dominant in turbulent flow. Turbulent diffusion occurs due to the fluctuation of large scale eddies. Though this process simultaneously occurs in all directions, turbulent diffusion is mainly responsible for dispersing of dye in the lateral and vertical directions. The longitudinal dispersion process due to velocity gradient plays the major role in spreading dye in the longitudinal direction. The dimensionless forms of the longitudinal

dispersion coefficients for laboratory channels were reported to be 150 – 392 whereas the same dimensionless coefficients for transverse and vertical mixing were 0.09 – 0.26 and 0.05 – 0.067 respectively (Fischer et al. 1979). The several orders of magnitude higher coefficients for longitudinal dispersion show that the most of the dye travels with the flow in the longitudinal direction and accurately define the flow characteristics.

2.6 Tracer Studies

The flow characteristics in a physical model can be determined in a quantitative manner using tracer studies whereas the flow visualization studies often give only a qualitative assessment of flow characteristics. Tracer study results can be used to determine how long the flow particles spend inside a waterbody. This is termed the residence time distribution (RTD). The shape of the RTD curves obtained from tracer studies can be interpreted using mathematical parameters to quantify the flow characteristics in waterbodies.

2.6.1 Conducting Tracer Studies

Tracer studies usually involve injection of a tracer at the inflow of the system and the tracer concentration at the outlet is measured at regular time intervals (Wolf and Resnick 1963). However a successful tracer study requires selection of the appropriate tracer material, tracer injection method, appropriate tracer mass, frequency of outflow sample collection at the outlet and accurate measurement of flow and tracer concentration at the outlet. Detailed procedures for conducting tracer studies for varied conditions can be found in Wilson et al. (1986) and Teefy (1996).

The flow characteristics in a physical model of a stormwater retention pond can be defined by the retention time, baffle factor, dead space fraction, mixing characteristics and short-circuiting. Mixing characteristics are determined using the plug flow and complete mixed flow fractions and the dispersion index of flow. Dead space represents the area of the waterbody where flow is stagnant and short circuiting is the movement of inflow directly to the outlet using the shortest flow path. A complete list of parameters used to interpret RTD curves and define flow characteristics is given in Table 2.2 (Hart 1979; Bishop et al. 1993).

As shown in Table 2.2, one of the ways to define flow characteristics is to calculate the fractions of plug flow and complete mixed flow in the system. Plug flow and complete mixed flow

are two ideal flow characteristics often present together in waterbodies (Danckwerts 1953). All fluid particles move with equal velocity in a plug flow system and there is no longitudinal dispersion. As a result, all particles in a plug flow system experience an equal retention time that is equal to the theoretical retention time of the flow (Levenspiel 2012). The theoretical retention time is the ratio of the flow volume to the flow rate in the model. In contrast to plug flow in a complete mixed flow system, the inflow is instantaneously and uniformly mixed with the existing fluid (Levenspiel 2012).

Table 2.2: Mathematical parameters to interpret residence time distribution curve

Parameter	**Definition**
t_i	Time required for the first tracer particle to reach outlet.
t_{10}, t_{50} and t_{90}	Time required for the 10%, 50% and 90%, respectively, of total tracer mass to pass through the outlet.
t_d	Theoretical retention time determined from the ratio of system volume to the flow rate.
t_p	Time to reach peak concentration.
t_g	Mean retention time or time to reach the centroid of the time series concentration curve.
$\frac{t_g}{t_d}$	Index of average retention time.
$\frac{t_{50}}{t_d}$	Index of mean retention time.
$\frac{t_{90}}{t_{10}}$	Morril dispersion index.
$\frac{t_i}{t_d}$	Short-circuiting index.
$\frac{t_p}{t_d}$	Index of modal retention time.
P, m, d	Fraction of plug flow, complete mixed flow and dead space, respectively.

The fraction of plug flow and completely mixed flow can be determined using the time series concentration data obtained from tracer tests to fit a theoretical model of the flow system. The theoretical models of any continuous flow system, which may involve mixing, chemical reactions, heat transfer or mass transfer, have been developed considering either plug flow or complete mixed flow in the system. Wolf and Resnick (1963) presented a theoretical model considering plug flow, mixed flow, dead space and short-circuiting together. Rebhun and Argaman (1965) presented a simplified version of the model of Wolf and Resnick (1963) by neglecting short-circuiting as defined in the original model. Short-circuiting in the Wolf and Resnick (1963) model was defined as a fraction of inflow that reaches instantaneously to the outlet. The Rebhun and Argaman (1965) model is given by

$$\ln\left(1-F\left(\frac{t}{t_d}\right)\right)=-\frac{1}{(1-P)(1-d)}.\frac{t}{t_d}+\frac{P}{1-P} \qquad [2.2]$$

where F is a residence time distribution function representing fraction of tracer material that already left the system, and P, d, t and t_d represent the plug flow fraction, dead space fraction, time and theoretical retention time, respectively. If $\ln\left(1-F\left(t/t_d\right)\right)$ calculated from the experimental data is plotted against t/t_d, it should generate a straight line. The slope of the straight line would be $-1/((1-P)(1-d))$ and the intercept of vertical axis would be $P/(1-P)$. The plug flow and dead space fraction can be calculated by solving the equations for the slope and the intercept of the vertical axis. Since the fraction of plug flow was considered with respect to the active volume and short-circuiting was neglected, the mixed flow as a fraction of active volume can be calculated by subtracting the plug flow fraction from unity (Rebhun and Argaman 1965). Therefore, flow characteristics in a waterbody can be defined in quantitative manner using tracer studies. Liem et al. (1999), Roy et al. (2002), Hurtig (2003), and Yu (2009) used the Rebhun and Argaman (1965) model to fit time series concentration data obtained from tracer tests in clearwells and calculated fractions of plug flow, mixed flow and dead space.

2.6.2 Examples of Previous Research Studies using Tracer Tests

Examples where tracer studies have been used to assess flow behavior in cases similar to the Nautilus Pond™ include Falconer and Tebbutt (1986), Dunn et al. (1991), Bishop et al. (1993),

and Crozes et al. (1999) who conducted tracer studies in the physical models of large reservoirs used as clearwells. The disinfection abilities of clearwells were assessed by determining hydraulic parameters from RTD curves obtained using tracer studies. The RTD characteristics were also used to recommend required changes in the geometric designs of clearwells in order to improve their disinfection characteristics. Alkhaddar et al. (2001) and Phipps et al. (2008) used tracer studies for the physical model of the hydrodynamic vortex separator in order to determine the mean retention time and optimize geometric designs.

Holland et al. (2004) and Kjellin et al. (2006) used tracer studies in field scale studies of wetlands and retention ponds. Holland et al. (2004) assessed the effects of changing flow rates and flow depths on the normalized residence time distribution curve of a wetland using tracer tests. Kjellin et al. (2006) estimated short-circuiting and the mean retention time of a wetland using tracer studies. Holland et al. (2004) and Kjellin et al. (2006) used Rhodamine WT and radioactive water with hydrogen isotopes, respectively, as tracer materials. Both studies used the continuous feed method for injecting tracer into the wetland. Holland et al. (2004) did not find any significant effects of flow rates on RTD characteristics and the short-circuiting and mixing in the wetland were found to increase with flow depth (Holland et al. 2004).

Khan et al. (2013) conducted tracer tests in a physical model of a stormwater retention pond to optimize the size, orientation and position of a floating treatment wetland in order to have the best hydraulic performance in the pond. Rhodamine WT solution was used as the tracer material and a slug of 10 mL 1000 PPM Rhodamine WT solution was injected 720 mm upstream of the opening of model inlet. The outlet concentration was measured with a Seapoint Rhodamine Fluorometer at a frequency of 100 samples per second. The tests were carried out for a duration of more than twice the theoretical retention time and at least 90% of the dye was recovered. The RTD curve derived from the Fluorometer measurements showed two peaks. The early high peak indicated severe short-circuiting in the pond and a much smaller peak which was found later represented the mixing characteristics of the pond. The long tails of the RTD curve indicated the presence of dead space in the pond.

Farjood et al. (2015) also used RTD curves obtained from tracer studies to assess the hydraulic performance of a stormwater retention pond with solid and porous baffles. The tests

were carried out in a physical model using Rhodamine WT as tracer material. The tracer was injected uniformly across the width of the pond near the inlet. This was in sharp contrast to the conventional method of tracer injection as slug or continuous feed a point within the inlet. The hydraulic performances were assessed and compared using t_5, t_{10} and t_{90}, which represent the times required from 5%, 10% and 90% of tracer mass to leave the model. The studies of Khan et al. (2013) and Farjood et al. (2015) show that the tracer studies in physical models and resulting residence time distribution curves can be used to assess flow characteristics in stormwater retention ponds.

2.7 Scaling of Sediment Deposition

Scaling of sediment transport in physical modelling largely depends on the objectives of the study. A dimensional analysis with the parameters involved in sediment transport processes shows that the sediment transport depends on Froude number, model Reynolds number, Shields number, particle Reynolds number, particle sizes and settling velocity (Julien 2002). In a model scaled with Froude scaling laws, similitude in model Reynolds numbers may be neglected as long as the model flow is in a similar turbulent range to the prototype. The transport of bed materials in a physical model of hydraulic structures can be neglected if the Shields number of the bed material is less than 0.03; the model can be considered a rigid bed model in that case (Julien 2002).

Particle fall velocity is considered important for similitude when suspended load is considered (Abderrezzak et al. 2014). The unhindered settling velocity of discrete fine particles can be predicted using Stokes law, given by

$$v_s = \frac{g\left(G\text{-}1\right)d_s^{\,2}}{18\nu} \qquad [2.3]$$

where v_s, g, G, d_s and v are the particle settling velocity, gravitational acceleration, specific gravity of the particle, particle size and kinematic viscosity of the falling medium, respectively. Stokes law was derived based on the assumption that the fluid has uniform density and viscosity throughout the settling medium, the settling path is vertical and straight, the particle is not accelerating, the shape of the particle is spherical and the particle Reynolds number is less than 0.5 (Farrell and Sherman 2015). Peakall et al. (1996) considered a particle size of 0.1 mm as the

upper limit for Stokes law instead of the particle Reynolds number of 0.5 for particles falling in water. The particle Reynolds number can be defined by

$$R_p = \frac{v_s d_s}{\nu} \qquad [2.4]$$

When boundary layer separation becomes important in the case of larger particles, Stokes law cannot accurately predict the settling velocity of particle (Peakall et al. 1996). Stokes law considers only viscous forces affecting the settling process. In the case of larger particles, separation and turbulence affects the settling process and the settling velocity can be better predicted using Newton's law. Newton's law shows that the settling velocity is proportional to the square root of the particle size. Gill and Pugh (2009) reported the following empirical equation developed by U.S. Bureau of Reclamation and originally reported by Dodge (1983) for settling velocity of sand particles as

$$v_s = 0.8 d_s^{\,2} \qquad [2.5]$$

$$v_s = 0.11 d_s^{\,0.5} \qquad [2.6]$$

Equations [2.5] and [2.6] are applicable for particles less than 0.3 mm and greater than 0.3 mm, respectively, and they are the empirical forms of Stokes law and Newton's law respectively. Julien (2002) presented an alternate equation to define settling velocity,

$$v_s = 8\left[\left(1 + 0.0139 d_*^{\,3}\right)^{0.5} - 1\right]\left(\frac{\nu}{d_s}\right) \qquad [2.7]$$

where d_* is the dimensionless grain size diameter, which is given by

$$d_* = [g(G-1)/\nu^2]^{1/3} d_s \qquad [2.8]$$

If both the geometrically scaled model particle size and the prototype particle size are either greater than 0.3 mm or less than 0.3 mm and both settling velocities can be represented by the same settling velocity law, the geometric scaling of particle size is appropriate in those cases as it produces the equivalent settling velocity of particles in the model as suggested using Froude scaling laws (Peakall et al. 1996). However, if the geometric scaling gives model particle sizes smaller than 0.3 mm whereas the prototype particle sizes are larger than 0.3 mm, a size adjustment

of model particle is required to make the settling velocity equivalent to the prototype. The use of model sediments with different specific gravity than prototype would also require the adjustment of the geometrically scaled particle size in the model in order to make the settling velocity equivalent to the prototype.

If the Shields parameter of the bed material is greater than 0.06, the transport of bed material becomes important and the model needs to be considered as movable bed model (Julien 2002). Julien (2002) reported four similitude criteria required to be simultaneously satisfied for accurate scaling of movable bed rivers. They are similitudes with Froude scaling laws, resistances, dimensionless grain size diameters and Shields parameters. If these four criteria cannot be simultaneously satisfied, then similitudes for either Froude number or dimensionless grain size diameter may be kept out of consideration in the scaling process.

Gill and Pugh (2009), Ho et al. (2010) and Kleinhans et al. (2014) considered similitude in Shields number and dimensionless unit sediment transport for model and prototype along with the geometric scaling of particles. Geometric scaling ensures similitudes in Froude number and resistance in model and prototype which are required as reported in Julien (2002). If the dimensionless unit sediment transport criteria and Shields number criteria are satisfied and proper similitude is achieved, a Shields number vs grain Reynolds number plot for the prototype and scaled model would superimpose on each other. However, the Shields parameter vs grain Reynolds number plots with only geometrically scaled particles put model and prototype points far apart from each other. Gill and Pugh (2009) and Ho et al. (2010) used three different methods to bring Shields parameter vs grain Reynolds number plots for model and prototype close to each other. These are adjusting particle size to equate scaled fall velocity, use of lightweight sediment materials in model and adjusting the model slope. These scaling criteria have been illustrated with a flowchart in Figure 2.1, prepared based on the studies of Julien (2002), Gill and Pugh (2009) and Ho et al. (2010).

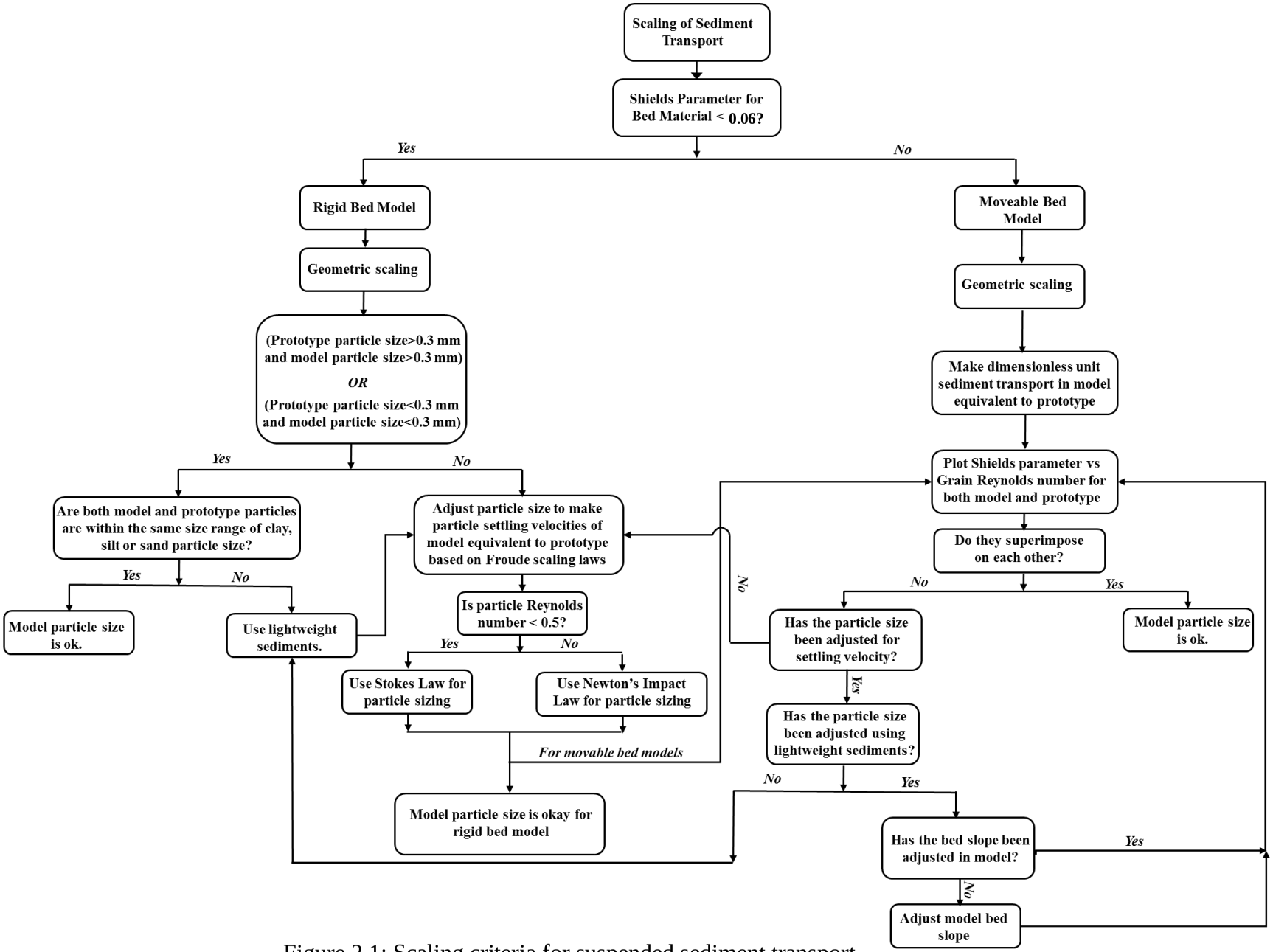

Figure 2.1: Scaling criteria for suspended sediment transport

Scaling of sediment transport, however, often cannot achieve proper similitude as the scaled particles sizes may not be readily available and production of those particular size particles can be very expensive. In addition to that geometrically scaled particles sometimes can be so small that the cohesion characteristics of particles may be altered. The motion of sand and silt particles is mainly dominated by gravity, whereas the motion of fine silts and clay particles is dominated by inter-particle electrostatic forces (ASCE 2000). Therefore the use of different materials in a model might be necessary in order to increase the size of the model sediments.

Some examples of sediment materials that had been used in modelling so far are ground walnut shells, Bakelite, crushed brown coal, polystyrene and so on (ASCE 2000). The specific gravities of these sediment materials are in the range of 1.04–1.50. When sediments are marginally denser than water, it must be checked whether surface tension interferes with the submergence ability of the sediments. The model sediments also should not be susceptible to abrasion or fracture during transport with flow in the model. Gorrick and Rodriguez (2014) recommended not using lightweight sediments when there is oscillatory movements of flow and sediments into the model. The oscillatory movement may increase the inertial forces acting on lightweight sediments and prevent natural settling of sediments as predicted in theory.

2.8 Summary

The review of previous studies on stormwater retention ponds shows that the sediment removal efficiencies of existing ponds are highly variable and often influenced by several local and environmental factors such as rainfall characteristics, land use, particle sizes and so on. The low removal efficiencies are attributed to the presence of short-circuiting and dead spaces in the pond. In addition to that, the existing ponds have significant maintenance costs due to the need for dredging every 5−20 years. It has been recommended to design ponds in such a way they have a high sediment removal efficiency but lessen operation and maintenance cost through the life cycle of the pond by limiting the areal extent of the deposition zone.

The study of the flow behavior in a stormwater retention pond can be carried out in a laboratory using a physical model. The physical model should be designed using Froude scaling laws. In order to achieve proper similitude with the prototype, an undistorted physical model is preferable to a distorted one. The Reynolds number characterizing the flow in the model should

be great enough to minimize the viscous effects and the depth should be greater than 30 mm in order to avoid any surface tension effect.

Flow visualization studies and tracer studies have been carried out in the past in order to study flow characteristics. Flow visualization studies provide qualitative assessments of the flow pattern whereas tracer tests help to assess flow characteristics in a quantitative manner. Retention time, short circuiting, the dispersion index and the fraction of plug flow, perfect mixed flow and dead space can be calculated from tracer studies.

Previous studies on scaling of sediment transport were reviewed. Scaling based on settling velocity, Shields parameter, dimensionless grain size diameter and sediment concentrations have been used so far in experimental studies. Settling velocity has been used as the primary scaling criteria where only suspended load is important and Shields parameter was considered the primary criteria where bedload is important. Lightweight materials may sometimes be used in the model if the scaled particle sizes are too small to maintain the same cohesion characteristics of prototype particles.

CHAPTER 3: METHODOLOGY

3.1 Background

The Nautilus Pond™ is circular in plan. It has side slopes of 3H:1V or 5H:1V depending on the site characteristics and local safety concerns. The pond can be built with an aspect ratio between 100:2 and 50:2 with 2 m depth. The aspect ratio is the ratio of the diameter at the water surface to the corresponding depth of the pond at the peak flow rate. The peak flow rates for these two ponds are considered to be 4 m^3/s and 1 m^3/s, respectively. The inlet or inflow enters the pond along its periphery and the longitudinal axis of the inlet pipe makes a 30° angle with a tangent line to the pond circumference at the point of entrance. The inlet is oriented to cause anticlockwise vortex flow in the pond. The invert of the circular inlet pipe of Nautilus Ponds™ is usually kept 300 mm above the pond bed and projects a small distance into the pond. The inlet pipe diameters reported by Source2Source Inc. are 1.60 m for the 100:2 pond and 0.80 m for the 50:2 pond. The pond outlet or outflow is located at the center of the pond. The outlet is an elevated structure that maintains a permanent pool in the pond. It is a circular pipe of 1.80 m diameter in the 100:2 pond and 1.20 m diameter in the 50:2 pond. The outlet pipe extends vertically into the pond up to near the water surface. The outlet is closed at its top and is perforated between 50% and 75% of its total height. Therefore the permanent pool depth in the Nautilus Pond™ is equivalent to the 50% of the height of the outlet. The detailed design of the outlet pipe follows the standard manhole design by Lafarge Canada Inc.

A berm is often placed inside the pond around the outlet. The berm is trapezoidal in cross section and has 3H:1V side slopes with the top of the berm at 2.50 m above bed. The berm extends along the entire circumference of the pond. Source2Source Inc. specifies the width of the berm across its top is 0.50 m. The best radial position of the berm is not known and is a variable in this study. There is a small opening in the berm to let the flow move toward the central outlet. The width of the berm opening is one-twelfth of the circumferential length of the berm and the base of the opening is at 300 mm above the bed in this section. The opening is positioned to allow the inflow to complete at least one full circle before it enters the central portion of the pond enclosed by the berm.

This chapter discusses the details of the experimental program used to evaluate the flow characteristics of the Nautilus Pond™. Tests were carried out using a laboratory physical model of the pond. First the development of the physical model is discussed. This is followed by a description of the experimental setup and details of the testing program. Finally, details of the procedures for the tracer tests, flow visualization tests and sediment deposition tests used in these experiments are discussed.

3.2 Hydraulic Model

3.2.1 Design Criteria

The design of the physical model was carried out using Froude scaling laws since the Nautilus Ponds™ have free surface flows and gravity is the dominant force. The model was designed so that ponds of 100:2 and 50:2 aspect ratios could be tested using the same model with different flow depths and flow rates for each aspect ratio. Scale ratios of the models were selected based on the considerations of available space in laboratory, cost, minimum flow depth, pump capacity and inlet and outlet diameters. The inlet and outlet diameters needed to be approximately equal to the standard internal diameters of Schedule 40 or Schedule 80 PVC pipe.

Considering these criteria, 1:30.775 and 1:13.289 scale ratios were selected for 100:2 and 50:2 prototype ponds respectively. Vertical and horizontal scale ratios were kept equal. The scaled flow depths were 65 mm for the 100:2 pond model and 150 mm for the 50:2 pond model at the peak flow rates. Kobus (1980) reported a 30 mm minimum flow depth is required to overcome any surface tension effects in the model.

The scaled peak flow rates for the models corresponding to the 100:2 and 50:2 prototype ponds were 0.76 L/s and 1.55 L/s, respectively, and the supply pump for the model had sufficient capacity to deliver these flows. The model overflowed to an underground reservoir from which a sump pump with a capacity of 1.26 L/s pumped it to the domestic sewer. Although the 1.55 L/s test flow rate was greater than the sump pump capacity, no additional temporary pumping was required because 60,000 L of storage was available in the reservoir which provided sufficient equalization capacity to handle the maximum flow duration required in the model tests.

The scaled sizes of the inlets and outlets were 52 mm and 59 mm, respectively, for the 100:2 pond model and 60 mm and 90 mm, respectively, for the 50:2 pond model. The invert of the inlet pipe was kept about 10 mm and 23 mm above the bed for models corresponding to the 100:2 and 50:2 prototype ponds, respectively.

The flow in the model was in the turbulent subcritical regime. The Froude number in the model was calculated based on the inflow jet velocity and the flow depth in the model. Since the velocity was different at different radial positions of flow and it was not measured quantitatively, instead the Froude number was calculated based on the inflow jet velocity which provides an estimate of the state of flow regime. Table 3.1 shows the Froude numbers at different flow rates. Since the flow was subcritical at the inflow jet for all flow rates and the flow velocities in the model are less than the inflow jet velocity, the flow in the model can be considered subcritical too. The Froude number is calculated by

$$F_r = \frac{U_i}{\sqrt{gh}} \qquad [3.1]$$

where U_i is the inflow jet velocity considering full flow at the inlet pipe, g is the gravitational acceleration and h is the flow depth in the model.

Table 3.1: Reynolds numbers and Froude numbers in the scale model

Model corresponding to prototype pond	Model flow rates, L/s	Depth, mm	Reynolds number	Froude number
100:2	1.00	84	18,900	0.53
	0.76	65	14,400	0.46
	0.60	62	11,400	0.37
	0.40	54	7,570	0.26
	0.10	34	1,890	0.08
50:2	1.55	148	24,600	0.43
	1.20	116	19,000	0.38
	0.80	94	12,700	0.28
	0.20	76	3,170	0.08

The turbulence characteristics in the model were ensured by observing the mixing of dye in the flow. Since there are no boundary walls on both sides of the flow cross-section in the circular flow and several components of velocities act together toward different directions, the flow cross-section at different radial positions could not be accurately identified. As a result, the Reynolds number for the flow inside the model could not be accurately calculated. However, the inflow jet was kept fully turbulent by ensuring its Reynolds number was greater than 3000 for most of the flow rates (Rajaratnam and Flint-Petersen 1989). In the case of the fully turbulent jet, the spreading of the jet becomes independent of the Reynolds number (Rajaratnam and Flint-Petersen 1989). Table 3.1 shows the inflow jet Reynolds number calculated for different flow rates in both models. The inflow jet Reynolds number is calculated by

$$R_e = \frac{UD}{\nu} \qquad [3.1]$$

where U is the average velocity of flow in the inlet pipe, D is the diameter of the inflow jet at the nozzle and ν is the kinematic viscosity of water at 10° C temperature. The calculated Reynolds number was less than 3000 for 0.10 L/s flow rate in the 100:2 pond model; but it is still far greater than the minimum threshold of turbulent inflow jet. Though the calculations of all Reynolds numbers were carried out considering full pipe flow at the inlet and the circular jet, the 0.10 L/s and 0.40 L/s flow rates in the 100:2 pond model and 0.20 L/s flow rate in the 50:2 pond model did not produce full pipe flow at the inlet and the circular jet. The inlet pipe was not fully submerged at these flow rates. Therefore the actual jet Reynolds numbers are higher than those given.

3.2.2 Model Construction

The hydraulic model was constructed using 5/8" marine grade plywood sheets and 2"x4" lumber. It was set above an elevated base of 915 mm height. The model base was also constructed with plywood sheets and kept open in the middle in order to install the central outlet pipe under the model bed. The construction drawing of the Nautilus Pond™ model is shown in Figure 3.1.

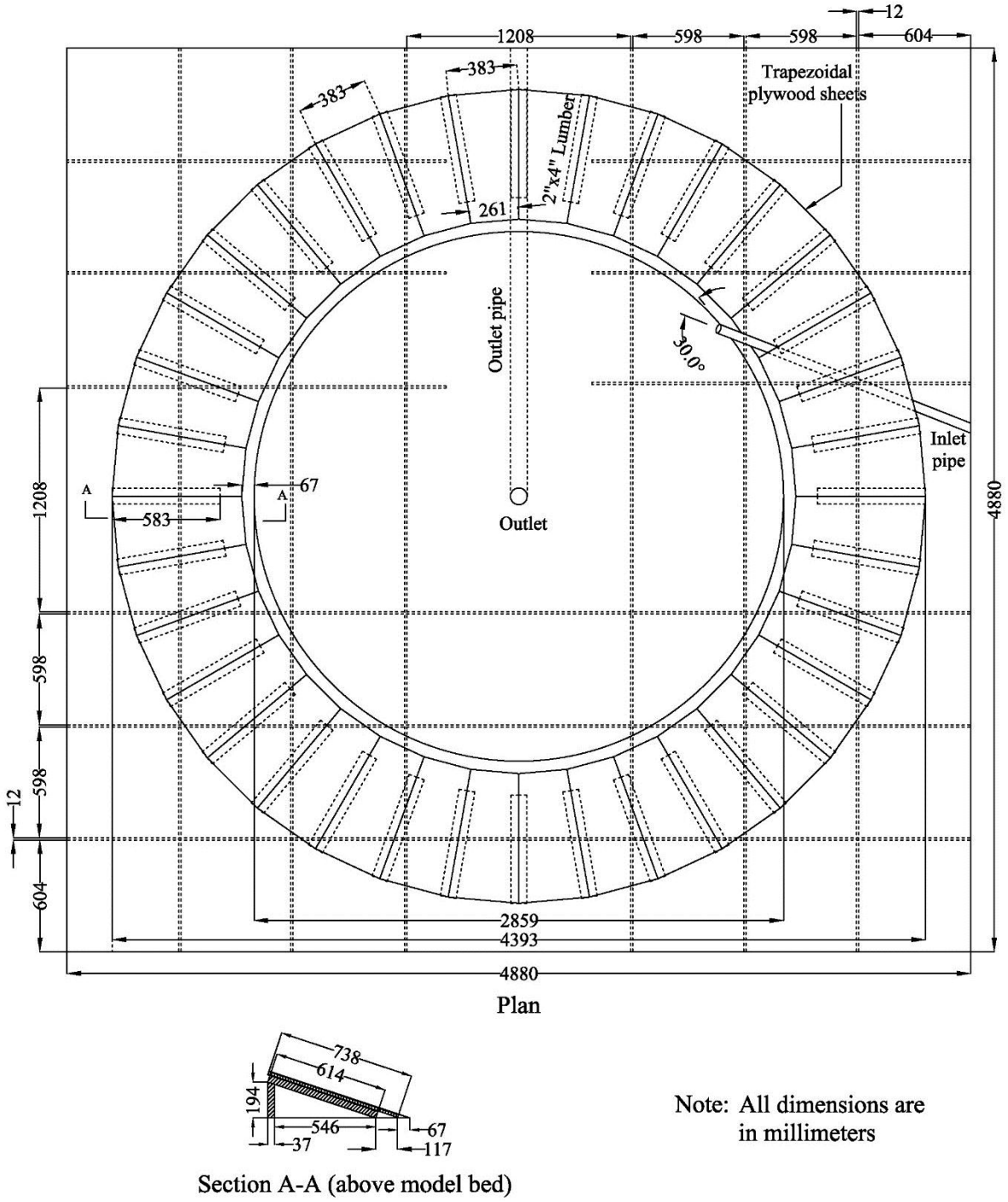

Figure 3.1: Construction drawing of the scale model of Nautilus Pond^{TM}

The model was circular in plan as in the prototype. The side slope was constructed with thirty six trapezoidal plywood sheets of 383 x 261 x 738 mm dimensions so that they fit the smaller bottom circle of 2859 mm diameter and the larger top circle of 4393 mm diameter. The 383 mm

and 261 mm dimensions are of the two parallel sides of the trapezoidal sheets and 738 mm is the vertical distance between them. The trapezoidal-shaped plywood sheets were symmetrical about their longitudinal axis. Each trapezoidal sheet was supported by two frames of 2”x 4” lumber along its long edges and each frame supported two long edges of two adjacent trapezoidal sheets. The 2” x 4” lumber frame consisted of one vertical member of 194 mm length and one 614 mm member inclined in 3H:1V slopes. The lumber frame and trapezoidal plywood sheets were placed along a circle of 2859 mm diameter drawn on the model bed. The model bed was constructed with 5/8” plywood sheets placed in double layers. All of the joints in the base and side slopes were sealed with silicone to make them waterproof. The model was painted with oil based primer and paint to make the plywood sheets waterproof and durable. The constructed model is shown in Figure 3.2.

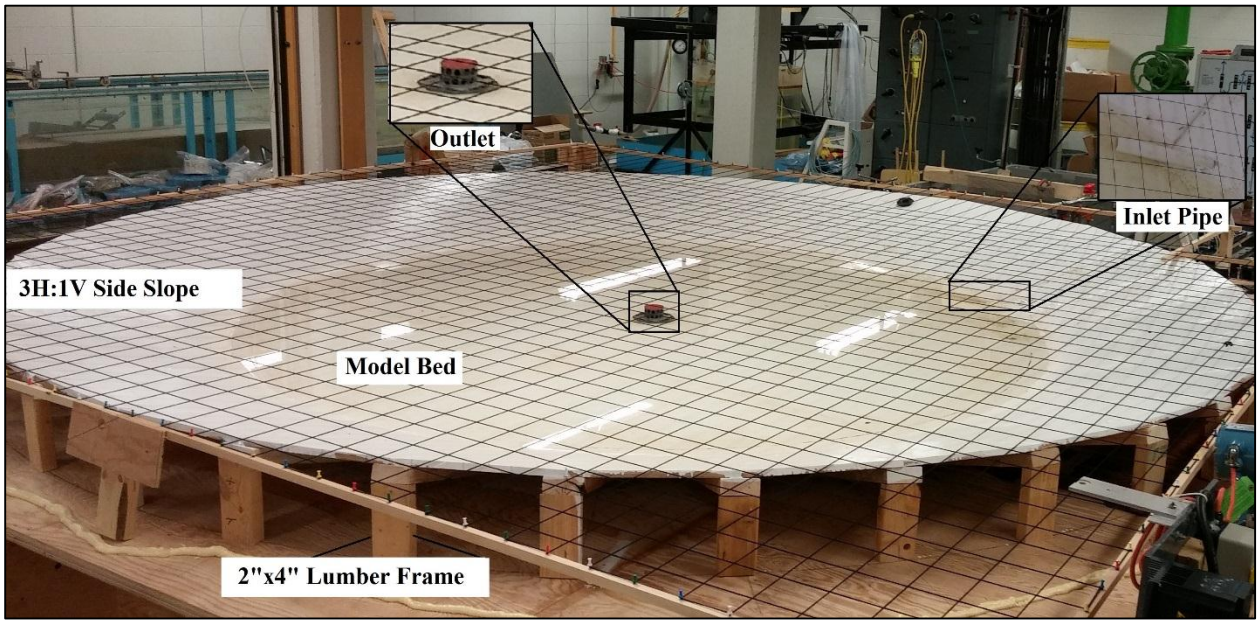

Figure 3.2: Constructed hydraulic model

PVC pipes were used as inlet and outlet pipes in the model. The internal diameter of the inlet pipes were 51.5 mm for the 100:2 pond model and 61.5 mm for the 50:2 pond model. These dimensions are slightly different than the scaled diameters of the inlet pipes that were 52 mm for the 100:2 pond model and 60 mm for the 50:2 pond model. However, the small differences did not have significant impacts on the flow conditions. For example, the velocity was found to be only 2.0% higher for the 100:2 pond model and 4.8% lower for the 50:2 pond model than the expected inflow velocities with perfectly scaled inlet sizes. The inlet pipe was projected about 300 mm into the 100:2 pond model and 200 mm into the 50:2 pond model. It was installed at a 30^{o} angle with

the tangent of the periphery at the point of entrance into the model. The inlet pipe was equipped with tracer injection and sediment injection ports, which were installed about 1.3 m upstream of the inlet to allow for complete mixing of tracer and sediments with the water before entering the model. The inlet was supplied with water by a 3 hp centrifugal pump, with a magnetic flow meter installed between the pump and inlet at the model to measure the flow rate.

The outlet of the Nautilus Pond™ is at the center of the pond bed. Detailed sketches of outlets used in the model are shown in Figure 3.3 and 3.4. The diameters of the outlet pipes were 58 mm and 89 mm for the 100:2 and 50:2 models respectively. The outlet heights were 60 mm for the 100:2 pond model and 145 mm for 50:2 pond model. The outlets in both prototype ponds were closed at the top and perforated between 50 and 75% of their height. This height range for perforating the outlet could not be maintained for the 100:2 pond model in order to maintain the required 65 mm water level at the desired design flow rate. Therefore, an initial design for the perforations to pass the required outflow at the design flow rate was constructed and tested. Some additional trials were conducted with rubber stoppers in some holes. This was done until the desired depth was steady at the design flow rates. There are 16 perforations of 16 mm diameter and 15 perforations of 9 mm diameter that were kept opened for the 50:2 pond model outlet to stabilize the flow depth at 148 mm. For the 100:2 pond model, 9 perforations of 14 mm diameter were kept open to stabilize the water level at 65 mm depth. Photographs of the outlets for the two models are shown in Figure 3.5(a and b).

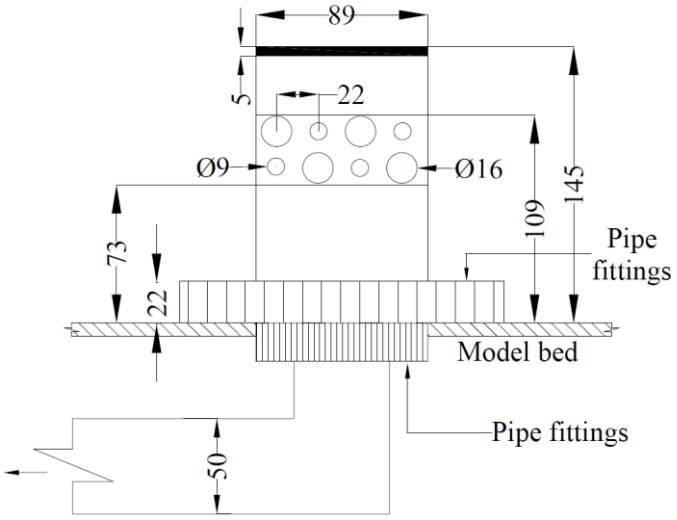

Note: All dimensions are in millimeters

Figure 3.3: Details of the outlet for the 50:2 pond model

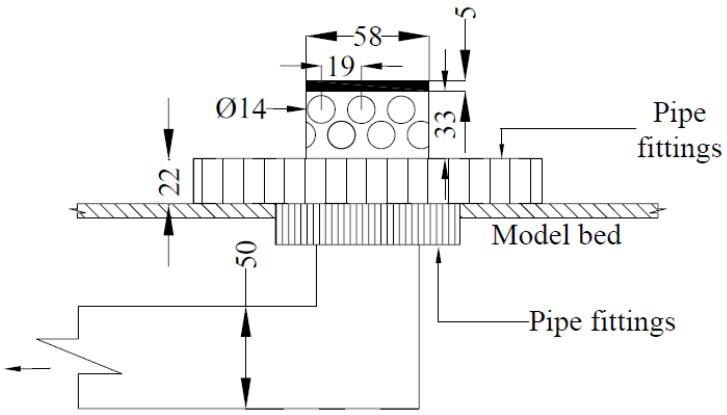

Note: All dimensions are in millimeters

Figure 3.4: Details of the outlet for the 100:2 pond model

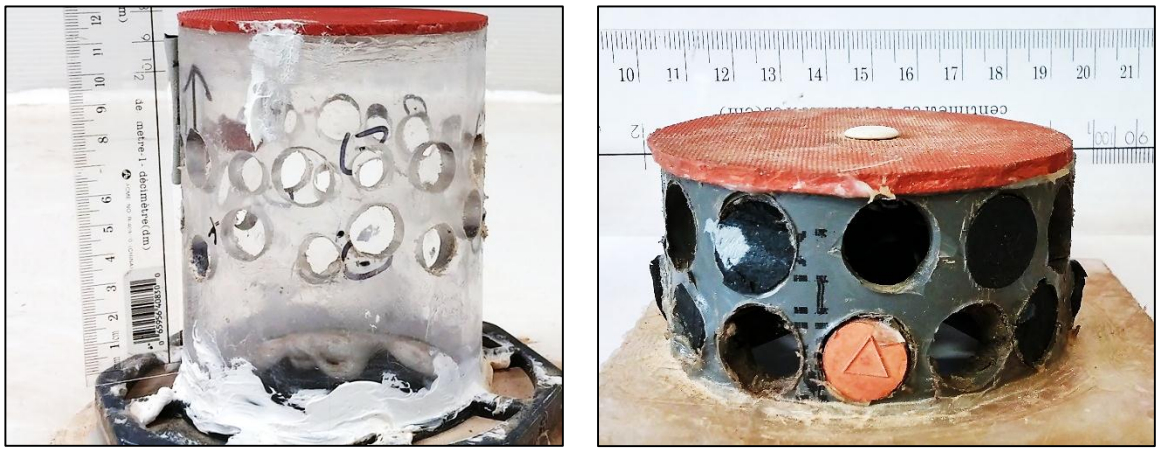

(a) (b)

Figure 3.5: Photograph of outlet for (a) 50:2 pond model and (b) 100:2 pond model

A valve was installed in the outlet pipe in order to control the flow if required and to let any entrapped air out of the pipe. The entrapped air may reduce the flow carrying capacity of outlet after the initiation of flow in the model and prevent the water level from becoming stable. The valve was installed about 3.40 m downstream of the outlet, near a joint between the outlet pipe and the weir tank. The valve was closed and opened a few times upon the initiation of flow to let out any entrapped air.

3.2.3 Model Operation and Experimental Setup

The constructed scale model was operated in conjunction with the water supply system to the model and measurement systems. Figure 3.6 shows a schematic of the full experimental setup. A 50 mm City of Saskatoon fresh water supply line with capacity of about 8.1 L/s fed a laboratory flume. The flume is 1.21 m wide, 0.75 m deep and 25.4 m long and capable of storing up to 23,050 L of water. It was used as a reservoir to maintain a constant head for a 3 hp 3500/2900 RPM 60/50 Hz centrifugal pump with 5-1⁄16 inch impeller diameter and manufactured by Goulds Pumps. A 50 mm plastic tubing connected the centrifugal pump with the flume and supply water to the pump. The centrifugal pump and flow rate is controlled with a Toshiba three-phase 240V class variable frequency drive with inverter type VFS15 2022PM-W. The pumped water goes through a magnetic flow meter before entering into the model. A Rosemount 8732 magnetic flow meter system capable of measuring up to 23.5 L/s flow rates was used for flow measurements. Figure 3.7(a-c) shows the centrifugal pump, variable frequency drive and magnetic flow meter, respectively. The centrifugal pump and the magnetic flow meters were connected to the inlet pipe using 35 mm plastic tubing.

The inlet pipes for both ponds were schedule 40 PVC pipes that were about 1.0 m long. The tracer injection and sediment injection ports were installed about 1.3 m upstream of the inlet. The diameter of the tracer injection port is 4.1 mm and the sediment injection port is 7.7 mm. A 60 mL luer lock tipped injection syringe was used to inject tracer through this tracer injection port and a Masterflex 6-600 ppm peristaltic pump (Catalog No. 7553-20 and Serial No. 395937), manufactured by Cole-Parmer Instrument Co. was used to inject sediment into the inlet. Figures 3.8 and 3.9 show the tracer injection syringe and the peristaltic pump used for sediment injection, respectively.

The water level in the pond was measured by a small diameter 200 mm long graduated tube that was installed vertically; the lower end of the tube was connected near the model bed with a small diameter pipe. As a result, the depth of water column in the tube indicates the flow depth in the model. This vertical standpipe shown in Figure 3.6 acts as a piezometer.

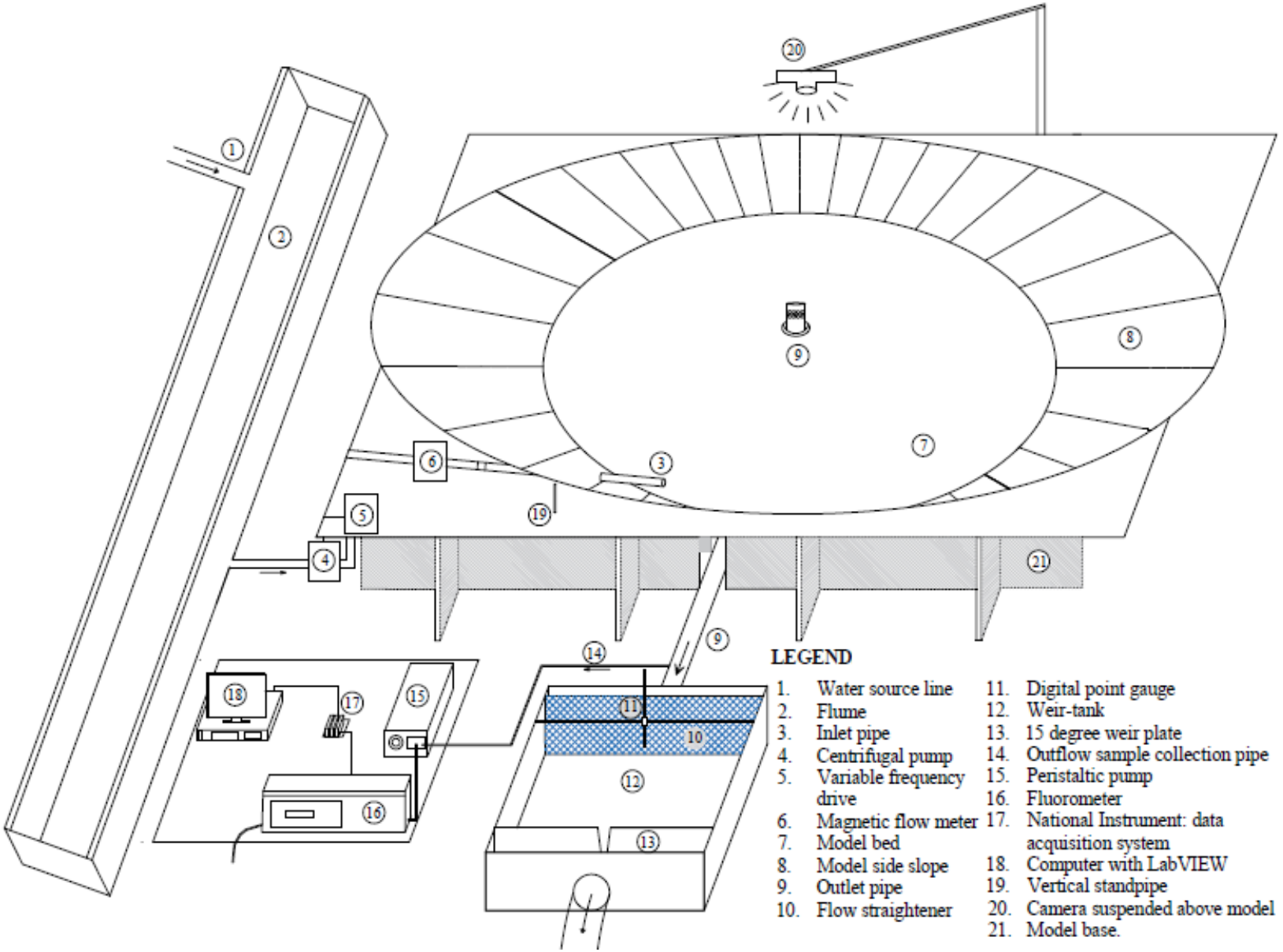

Figure 3.4: Schematic of experimental setup

(a)

(b)

(c)

Figure 3.5: (a) Centrifugal pump, (b) variable frequency drive and (c) magnetic flow meter

Figure 3.6: Tracer injection syringe

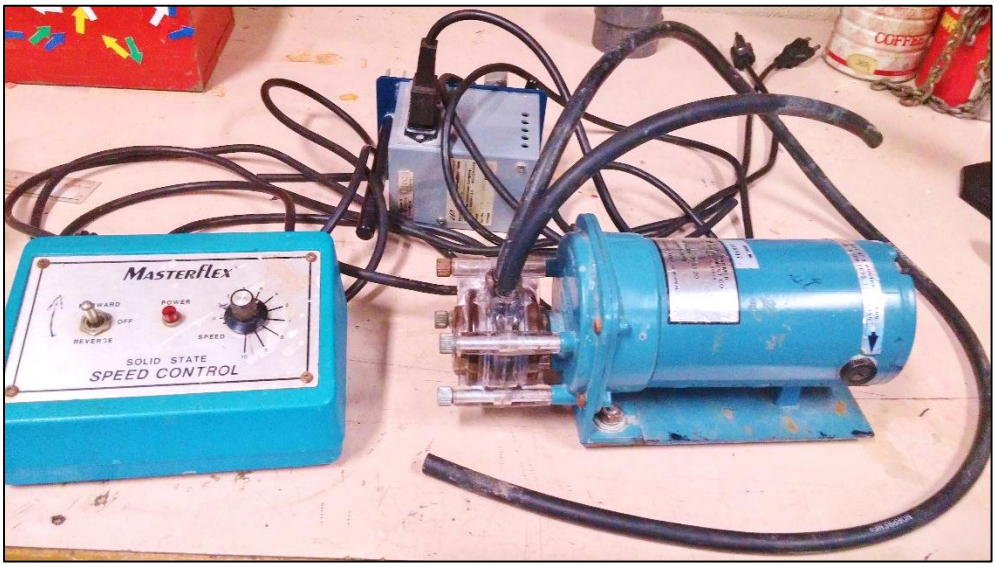

Figure 3.7: Peristaltic pump for sediment injection

The central outlet in the model is connected to a 3.57 m long and 50 mm diameter plastic tubing that is installed underneath the model bed and connects with a gate valve and a weir tank at the end of the outlet tubing.

A 4.8 mm diameter steel tube was installed for sampling at the intersection of the plastic outlet tubing and the weir tank to collect outflow samples for tracer concentration measurement. A sketch of the sampling tube details is shown in Figure 3.10. The sampling tube was vertically

attached at the inner face of the wall of the weir tank and extended up to the center of the opening where the outlet tubing connects to the weir tank. Then the sampling pipe was projected horizontally about 100 mm into the plastic outlet tubing. The steel sampling tube was 300 mm long in vertical direction and connected to a 2.25 m long plastic delivery pipe of 3.0 mm diameter. The other end of this plastic pipe was connected to a Masterflex peristaltic pump of model 7016 and manufactured by Cole-Parmer Instrument Co. The peristaltic pump collects outflow samples and injects into a Turner Design Fluorometer, model 10-AU-005-CE. The fluorometer is used to measure the concetration of fluorescent tracer in the outflow. A National Instruments data acquisition system, model NI cDAQ-9178, integrated with the LabVIEW software recorded the time series concentration data of the fluorometer as a text file on a computer. Figure 3.11(a-c) shows the fluorometer, peristaltic pump and data acquisition system, respectively.

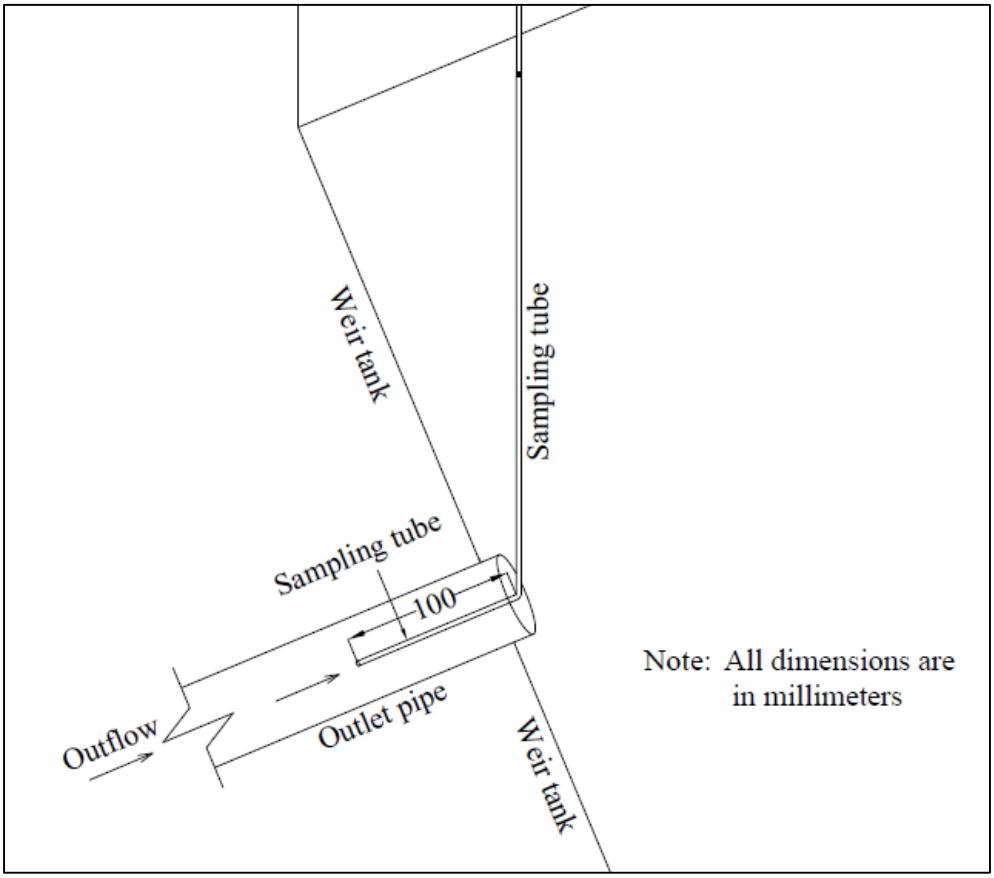

Figure 3.8: Sampling tube

(a)

(b)

(c)

Figure 3.9: (a) Fluorometer, (b) Peristaltic pump for outflow sample collection and (c) Data acquisition system

The weir tank was used to monitor the outflow rate using head-discharge relationship of a V-notch weir plate. A picture of the weir tank is shown in Figure 3.12. The weir tank, constructed in the Engineering Shops at the University of Saskatchewan, was initially designed with additional objectives of controlling the flow depth in the model in case of any test with unsteady state conditions at variable flow rates. Four trailer jacks with 907 kg lifting capacity each were attached at the four corners of the weir tank so that it could be moved up and down to control the flow depth in the model. It is a rectangular tank of 1.50 m length, 0.90 m width and 0.60 m depth. The weir tank is equipped with a 15° V-notch weir plate, a flow straigtener and a digital point-gauge. The weir plate is located 150 mm upstream from the outlet end of the weir tank. The crest of the V-notch weir plate is 170 mm above the bed. A digital point gauge was used to measure the head or flow depth in the weir tank. The digital point gauge was placed 1 m behind the weir plate

considering that the head measurement location for the weir needs to be at a distance of four times the head above the weir crest. Therefore, the weir tank could be used to measure a maximum flow rate corresponding to a 250 mm head above the weir crest. A flow straightner was placed just behind the digital point gauge. The flow straightener ensured that the momentum of flow from the model outlet is uniformly distributed throughout the tank cross section and there is uniform velocity profile throughout the cross section of the weir tank.

Figure 3.10: Photograph of the weir tank

The weir tank was calibrated to get a head-discharge relationship to monitor flow rates. The head in the tank was measured with a digital point gauge for 20 different flow rates. The calibrated head-discharge relationship obtained from these data is given in Figure 3.13. The flow rate was measured volumetrically by measuring the time to fill a bin of 61.5 L volume with the outflow of the weir tank. Measurements were not taken for very low flow rates for which the nappe was clinging to the wall of the weir plate. The best fit curve to the measurements is given by

$$Q = 3\times10^{-7} h_w^3 + 4\times10^{-5} h_w^2 + 0.0044 h_w - 0.1145 \qquad [3.2]$$

where Q and h_w are the flow rate and upstream head above the weir crest respectively.

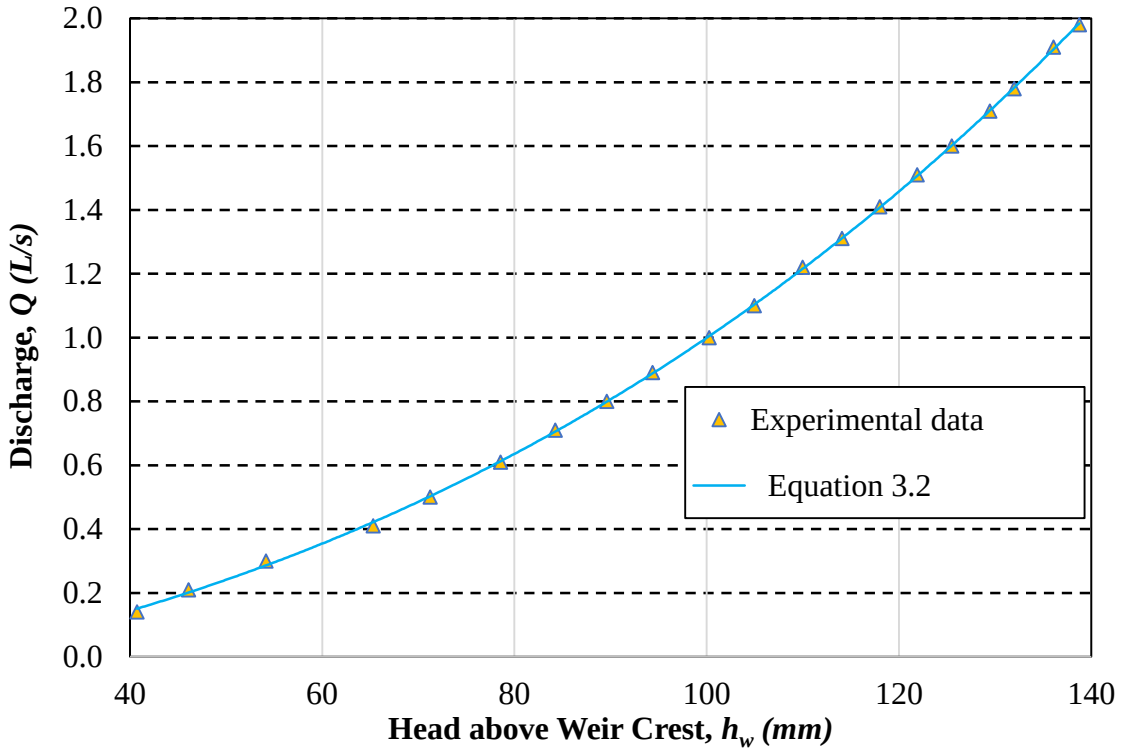

Figure 3.11: Head-discharge calibration curve of the weir tank

3.3 Details of Testing Program

The first objective of the research is to investigate the flow development time, residence time distribution characteristics and flow pattern in both the 100:2 and 50:2 pond at the design flow rates of 4 and 1 m^3/s, respectively. Therefore, tracer tests and flow visualization tests were carried out in the scale model at different flow development times to accomplish this objective. The flow rates in the model were 0.76 L/s and 1.56 L/s for the 100:2 and 50:2 pond model, respectively, and the flow depths were about 65 mm and 148 mm, respectively. The flow development times used in the model for the 100:2 pond were 10 min, 30 min, 2 hr, 3 hr, 4 hr, 5 hr, 6 hr and 12 hr and these are indicated by the Test # 1A-1H in Table 3.2. The dimensionless form of these flow development times are 1.0, 2.9, 11.5, 17.2, 23.0, 28.7, 34.4 and 68.8, respectively. The dimensionless flow development time was calculated by taking the ratio of the flow development time to the theoretical retention time of the model. The theoretical retention time is given by

$$t_d = \frac{V_f}{Q} \qquad [3.3]$$

where t_d, V_f and Q are theoretical retention time, flow volume and flow rate, respectively, in the model. Test # 2A-2G in Table 3.2 shows the flow visualization tests in the 100:2 pond model and the flow development times were 30 min, 2 hr, 3hr, 4 hr, 5 hr, 6 hr and 12 hr for these tests. Test # 8A-8F and 9A-9F indicates the tracer tests and the flow visualization tests, respectively, for the 50:2 pond model. The dimensionless flow development times used for these tests were 0.9, 2.9, 11.8, 17.8, 23.7 and 70.4. These are similar to the dimensionless flow development times used for the 100:2 pond model.

Table 3.2: Testing program

Test #	Scale model corresponding to prototype	Position of annular ring	Test Type	Flow rate (L/s)	Depth (mm)	Flow development time	Dimensionless flow development time
1A	100:2	NA	Tracer test	0.76	65	10 min	1.0
1B	100:2	NA	Tracer test	0.76	65	30 min	2.9
1C	100:2	NA	Tracer test	0.76	65	2 hr	11.5
1D	100:2	NA	Tracer test	0.76	65	3 hr	17.2
1E	100:2	NA	Tracer test	0.76	65	4 hr	23.0
1F	100:2	NA	Tracer test	0.76	65	5 hr	28.7
1G	100:2	NA	Tracer test	0.76	65	6 hr	34.4
1H	100:2	NA	Tracer test	0.76	65	12 hr	68.4
2A	100:2	NA	Flow visualization	0.76	65	30 min	2.9
2B	100:2	NA	Flow visualization	0.76	65	2 hr	11.5
2C	100:2	NA	Flow visualization	0.76	65	3 hr	17.2
2D	100:2	NA	Flow visualization	0.76	65	4 hr	23.0
2E	100:2	NA	Flow visualization	0.76	65	5 hr	28.7
2F	100:2	NA	Flow visualization	0.76	65	6 hr	34.4

Table 3.2 Cont'd

Test #	Scale model corresponding to prototype	Position of annular ring	Test Type	Flow rate (L/s)	Depth (mm)	Flow development time	Dimensionless flow development time
2G	100:2	NA	Flow visualization	0.76	65	12 hr	68.4
3	100:2	NA	Tracer test	0.1	34	47 hr	72.2
4	100:2	NA	Tracer test	0.4	54	18.5 hr	68.7
5	100:2	NA	Tracer test	0.6	62	14.4 hr	68.8
6	100:2	NA	Tracer test	1	84	12 hr	67.5
7	100:2	NA	Sediment deposition	0.76	65	3 hr	17.2
8A	50:2	NA	Tracer test	1.56	146	12 min	0.9
8B	50:2	NA	Tracer test	1.56	148	40 min	2.9
8C	50:2	NA	Tracer test	1.56	148	2.67 hr	11.8
8D	50:2	NA	Tracer test	1.56	147	4 hr	17.8
8E	50:2	NA	Tracer test	1.56	147	5.34 hr	23.7
8F	50:2	NA	Tracer test	1.56	148	16 hr	70.4
9A	50:2	NA	Flow visualization	1.56	146	12 min	0.9
9B	50:2	NA	Flow visualization	1.56	148	40 min	2.9
9C	50:2	NA	Flow visualization	1.56	148	2.67 hr	11.8
9D	50:2	NA	Flow visualization	1.56	147	4 hr	17.8
9E	50:2	NA	Flow visualization	1.56	147	5.34 hr	23.7
9F	50:2	NA	Flow visualization	1.56	148	16 hr	70.4
10	50:2	NA	Tracer test	0.2	76	53 hr	67.0
11	50:2	NA	Tracer test	0.8	94	17.8 hr	70.0
12	50:2	NA	Tracer test	1.2	116	15 hr	68.4
13	50:2	NA	Sediment deposition	1.56	147	4 hr	17.8
14	100:2	60%	Tracer test	0.76	68	3 hr	16.4

Table 3.2 Cont'd

Test #	Scale model corresponding to prototype	Position of annular ring	Test Type	Flow rate (L/s)	Depth (mm)	Flow development time	Dimensionless flow development time
15	100:2	60%	Sediment deposition	0.76	68	3 hr	16.4
16	50:2	60%	Tracer test	1.55	139	4 hr	18.9
17	50:2	60%	Sediment deposition	1.55	139	4 hr	18.9
18	100:2	70%	Tracer test	0.76	68	3 hr	16.4
19	100:2	80%	Tracer test	0.76	68	3 hr	16.4
20	100:2	80%	Sediment deposition	0.76	68	3 hr	16.4

The second objective is to study the effect of flow rates on the residence time distribution characteristics of the ponds. Therefore tracer tests were carried out in both models at different flow rates under steady state conditions. Tested flow rates in the 100:2 pond model were 0.1 L/s, 0.4 L/s, 0.6 L/s and 1.0 L/s and these are equivalent to 0.53 m^3/s, 2.10 m^3/s, 3.15 m^3/s and 5.25 m^3/s flow rates, respectively, in the 100:2 prototype pond. The dimensionless flow development times used for these tests were 72.2, 68.7, 68.8 and 67.5 for 0.1 L/s, 0.4 L/s, 0.6 L/s and 1.0 L/s, respectively. These tests are shown in Table 3.2 as Test # 3-6 for the 100:2 pond model. The flow rates tested in the 50:2 pond model were 0.2 L/s, 0.8 L/s and 1.2 L/s that are equivalent to 0.13, 0.52 and 0.77 m^3/s, respectively, in the corresponding prototype pond. The dimensionless flow development times were 67.0, 70.0 and 68.4 for 0.2, 0.8 and 1.2 L/s, respectively. These are shown in Table 3.2 as Test # 10-12 for the 50:2 pond model.

The third objective is to investigate the sediment deposition patterns in both models. Tests were carried out at 0.76 L/s and 1.55 L/s in the 100:2 and 50:2 pond models, respectively. The dimensionless flow development times were 17.2 and 17.8 for 100:2 pond and 50:2 pond, respectively. These are shown in Table 3.2 as Tests # 7 and 13 for the 100:2 and 50:2 pond models, respectively.

The fourth objective is to find the best position for a berm, constructed as annular ring in the model around the outlet, to improve the flow and residence time distribution characteristics in the pond. In order to accomplish this objective, tracer tests were carried out in the 100:2 pond

model with berm at a distance of 60%, 70% and 80% of the model bed radius from center. The dimensionless flow development time for all these tests was 16.4. The flow rates and flow depths were 0.76 L/s and 68 mm, respectively. These tests are shown in Table 3.2 as Test # 14, 18 and 19. A tracer test was also carried out in the 50:2 pond model with the berm at its best position indicated by tracer tesing in the 100:2 pond model. The dimensionless flow development time was 18.9 in this test. This is shown as Test # 16 in Table 3.2.

The fifth objective is to investigate the effect of the best position of the berm (constructed as an annular ring around the outlet in the model) on the sediment deposition pattern. The sediment deposition pattern tests were carried out in the both 100:2 and 50:2 pond model. The dimensionless flow development times were 16.4 and 18.9 for 100:2 and 50:2 pond models, respectively. These are shown as Test # 15 and 17 in Table 3.2. Test #20 was carried out to support the findings about the best position of the berm based on Test # 14, 18 and 19.

3.4 Details of Testing Procedures

3.4.1 Tracer Testing

The tracer testing involved preparation of tracer materials, calibration of the fluorometer, allowing a certain flow development time, injection of tracer material with appropriate concentration and volume, and measuring and recording the time series tracer concentration data in the model outflow.

3.4.1.1 Preparation of Tracer Materials

Rhodamine WT was used as tracer material in this study. It is one of the most commonly used tracers in field and laboratory studies of flow patterns and effluent mixing in water (Wilson et al. 1986). According to the material safety datasheet (Acros Organics 2011), the Rhodamine WT is not classified as a hazardous material and its toxicity level is unknown. However, it is recommended, when handling the 20% solution it is supplied in, to avoid inhalation and ingestion and use necessary personal protective equipment to avoid contact with eyes, skin and clothing (Acros Organics 2011).

Rhodamine WT, a fluorescent tracer, was used for calibrating the fluorometer used for concentration measurement of tracer in outflow. 1190 ppm and 2380 ppm Rhodamine WT

solutions were used as tracer in this research for the 100:2 and 50:2 pond model, respectively. These tracer concentrations were prepared from 20% Rhodamine WT solution with specific gravity of 1.19. 23.8 ppb, 59.5 ppb and 95.2 ppb Rhodamine WT were also prepared with serial dilution in order to calibrate and test the fluorometer. The dilution method of Rhodamine WT solution can be described by

$$C_H * V_H = C_L * V_L \quad [3.3]$$

where C_H and V_H are the concentration and volume, respectively, of the highly concentrated solution and C_L and V_L are the concentration and volume, respectively, of the diluted solution. Therefore the dilution of 5 mL 238 g/L (or 20%) Rhodamine WT tracer with deionized water into 1 L diluted solution produced 1190 ppm Rhodamine WT. Then the dilution of 1 mL 1190 ppm solution with deionized water into 100 mL diluted solution produced 11.9 ppm solution. Similarly the dilution of 2, 5 and 8 mL of 11.9 ppm solution into 1000 mL diluted solution produced 23.8, 59.5 and 95.2 ppb, respectively.

The dilution of 20% Rhodamine WT solution with deionized water should be started after washing all necessary equipment with tap water and then rinsing with deionized water. All equipment should be rinsed with a particular solution of Rhodamine WT for 2-3 times before using that equipment for that particular concentration. The equipment includes 3-4 small beakers for temporary storing of tracer, 1-5 mL pipettes to measure the volume of the highly concentrated tracer, 100 mL and 1000 mL volumetric flasks for dilution and a few brown jars to store Rhodamine WT solutions. All jars containing Rhodamine WT solution must be labeled with appropriate concentration and date of tracer preparation.

3.4.1.2 Calibration of the Fluorometer

The fluorometer was calibrated with 59.5 ppb or 71.4 ppb Rhodamine WT solution before beginning of tracer tests considering the standard concentration should be between 50-80% of the peak concentration in the linear range of the fluorometer readings. Then the calibration of the fluorometer was checked with 23.8 ppb and 95.2 ppb solution.

Calibration was carried out in three major steps. They are setting up the basic operating level, blanking the instrument and calibration with a standard Rhodamine WT solution. The basic

operating level of the fluorometer was set only once and in between 0-100 ppb. It involved loosening the sensitivity adjustment screw and setting the percentage of full scale reading to approximately 60% or 70% when using 59.5 ppb or 71.4 ppb standard, respectively, as the high concentration range. Once the basic operating level was set, blanking of the fluorometer was done using deionized water. The fluorometer was set to subtract the blank signal from the actual concentration reading. The last step was to calibrate the fluorometer with 59.5 ppb or 71.4 ppb standard solution. 59.5 ppb or 71.4 ppb was entered as input in the fluorometer before injecting tracer into the instrument. Then the standard was injected into the fluorometer 2-3 times and the calibration run. Once the calibration was finished, the fluorometer reading was checked with 23.8 ppb and 95.2 ppb standards of Rhodamine WT solution.

3.4.1.3 Tracer Test Procedures

The first step to run the tracer test was to fill up the model with water up to a level which would be the stable flow depth for the steady state condition for a particular flow rate in the model. This stable flow depth for a particular flow rate was determined beforehand by running that flow rate in the model for a few hours. After filling up the model to the stable depth, the inflow pump was shut off and outlet valve was closed. The valve at the centrifugal pump was also closed in order to stop any possible flow from the flume to the model through siphoning. Then the water in the model was kept at rest for about 15-20 minutes so that any motion of water in the model would be fully ceased. Next, the pump was turned on setting the variable frequency drive to obtain the desired flow rate and the valves at the inflow and outflow pipes were opened. Finally, the flow was kept running for certain flow development time (see Table 3.2) before injecting tracer into the model.

The slug input method was used to inject Rhodamine WT tracer in the inlet. A 60 mL injection syringe was used to measure tracer volume and inject it into the inlet pipe. The tracer injection process was done as fast as possible so that the time required to finish the injection process did not exceed $1/50^{th}$ of the theoretical retention time (Thirumurthi 1969). The time required for the tracer to travel from the injection point on the inlet pipe to the model inlet was recorded with a stopwatch.

The volume of the injected tracer material was dependent on the flow depth and the flow rate in the model. The injected tracer volume was selected so that the outlet tracer concentration did not exceed 100 ppb. The fluorometer that measures tracer concentration in the outflow provides the most accurate reading in the range of 0 - 100 ppb where the calibration curve is linear. The required volume of injected tracer was determined by several trial and error tracer tests with 1190 ppm and 2380 ppm concentration of tracer for the 100:2 and 50:2 pond models, respectively. Table 3.3 shows the volume and concentration of injected Rhodamine WT during different tests.

Table 3.3: Concentration and volume of the Rhodamine WT injected at inlet

Scale model corresponding to prototype	Flow rate (L/s)	Depth (mm)	Tracer Concentration (ppm)	Tracer Volume (mL)	Peak concentration readings in the fluorometer (ppb)	Dimensionless flow development time
100:2	1.00	84	1190	50	49	67.5
	0.76	65		30	58	68.4
	0.60	62		30	53	68.8
	0.40	54		30	76	68.7
	0.10	34		10	52	72.2
50:2	1.56	148	2380	50	68	70.4
	1.20	116		30	62	68.4
	0.80	94		20	59	70.0
	0.20	76		8	95	67.0

LabVIEW was used to record concentration readings from the fluorometer as soon as the tracer injection process was finished. The time lag between the injected tracer entering the model and the start of the LabVIEW recordings was measured with a stopwatch and added to the recorded times in LabVIEW. The concentration readings were taken at 1 s intervals. The peristaltic pump, which collected outflow sample from the center of the outlet pipe and injected through the fluorometer, was started beforehand.

The tracer tests were continued for four times the theoretical retention time or until the tracer concentration readings from the fluorometer became zero (Teefy 1996). During the tests the inflow and outflow rates, head in the flume and flow depths in the model were continuously monitored. The model outflow rates were monitored using the head of the weir tank measured with

a digital point gauge. When the tracer test was finished, the time lag between the tracer to reach the outlet and for LabVIEW to record the concentration reading was measured. This was done by pouring some highly concentrated Rhodamine WT tracer right at the outlet and recording the time to get a response in LabVIEW. This time lag was measured for each flow rate used in the tracer test and subtracted from the times recorded with the concentration readings in LabVIEW.

3.4.2 Flow Visualization Tests

Flow visualization tests were carried out to investigate the flow pattern in the model. First the entire model was covered with a 10 x 10 cm yarn grid to serve as a reference scale for any photographic images of the flow in the model. A GoPro camera was suspended above the model, which was capable of showing the entire model. This camera can be operated remotely through a wireless network. After running the flow for a certain flow development time, the flow visualization test was started.

Potassium permanganate and food coloring dyes were used for these tests. The dye was injected into the inlet through the dye injection port used for tracer studies. Squeeze bottles were used in this case to inject dye instead of a 60 mL syringe as a significantly larger volume of dye was needed than for tracer tests. Once the injection of dye was started, photographic images of the flow were taken at every 2-3 s. The dye injection at the inlet and the capturing of photographic images were continued until the full flow pattern was established in the model and the dye had mixed through the entire flow volume.

3.4.3 Sediment Deposition Pattern Tests

3.4.3.1 Sediment Scaling Criteria

In order to decide what particle size to use for the sediment deposition testing, the model was assumed to be a rigid bed model and sediment size was scaled according to the Froude scaling laws and considering the settling velocity of particles as the primary scaling criteria. Concern is for the settling velocity of suspended solids in the pond. According to the guidelines received from Source2Source Inc., the Nautilus Pond^{TM} is expected to remove particles greater than or equal to 50 micron therefore scaling was done for 50 micron particles. Linear scaling of 50 micron particles using scale ratios 1:30.775 and 1:13.289 give particle sizes in the range of clay and fine silt

respectively and this would alter the cohesion characteristics of the model sediments. Therefore, a lightweight sediment was used to increase the size of the scaled sediments.

At first the settling velocity of a 50 micron particle with specific gravity 2.65 was determined. Then, the calculated settling velocity was scaled using Froude scaling law for velocity and scale ratio of the corresponding model. The scaled settling velocity and the specific gravity of the lightweight sediment was used in Stokes law to calculate the required sizes of the lightweight sediments in the model.

3.4.3.2 Choice of Sediment Material

Ground walnut shells of specific gravity 1.2-1.4 were used as sediment material for testing in the model. When the prototype sediment particle size of 50 micron was scaled according to the settling velocity criteria, the scaled sizes of walnut shells were 50 micron and 61 micron for the 100:2 and 50:2 pond models, respectively. Since a single sized walnut shell sediment was not readily available, a flour grade of walnut shells having the size distribution given in Figure 3.14 was used for both pond models.

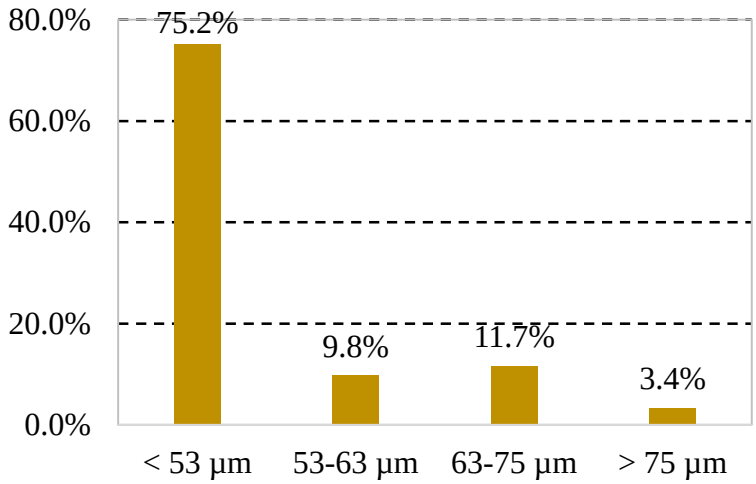

Figure 3.12: Particle size distribution of the ground walnut shells used for tests

The walnut shells used as sediments were also tested to determine their settling velocity. The measured settling velocities of 28 random particles were found to be in the range of 0.25 - 1.20 mm/s as compared to the theoretical settling velocities (calculated based upon Stokes' Law) of 0.27 mm/s and 0.41 mm/s for 50 micron and 61 micron particles, respectively. The settling velocity measurement was carried out in a graduated cylinder of 47 mm diameter and 356 mm

height set in vertical position and filled with water. Water in the cylinder was allowed to rest for 1.5 - 2 hr before beginning a test. Then some walnut shell powders were put at the top of the cylinder and allowed to free fall through the water in the cylinder. The motion of sediments through a 3 mm marked interval near the bottom of the cylinder was zoomed in and recorded in a high resolution video camera. The 3 mm test length was selected so that every single particle would be visible in the magnified version of that small length in the camera. The times required for 28 particles to travel through that 3 mm interval were measured with a stopwatch and the settling velocities were calculated. The individual particle was seen to be angular in shape in the settling velocity test.

3.4.3.3 Procedures for Sediment Deposition Pattern Tests

At first, flow in the model was kept running for a certain flow development time. Then sediment slurries were prepared with 2.3 and 5.9 kg of walnut shells for the 100:2 and 50:2 pond models. The sediment slurries were stored in a bucket and air bubbles coming out from the bottom were used to keep the sediments in suspension in a slurry. The sediment slurries were injected into the inlet through a peristaltic pump. Though the injection of the sediment slurry was finished after a short time, the flow was kept running until the flow in the model was cleared of turbidity. Then the deposited sediment in the model was captured in a photographic image with a GoPro camera suspended above the model.

In order to evaluate the sediment deposition patterns, samples of deposited sediments were collected from different areas of the model for sieve analysis. The sampling locations for models with and without berm are shown in Figure 3.15(a) and 3.15(b), respectively. Four samples were collected from outside of the 60% of base radius and two samples were collected from inside of the 60% of model bed radius from center. In the case of tests with berm in the model, four samples were taken outside the berm and two were taken inside the berm.

A wet sieving method was used for sieve analysis with the collected sample of the deposited sediments. The sediment samples were dried in an oven and stored in plastic bottles until the sieve analysis was carried out. The No. 270, 230 and 200 sieves of 53, 63 and 75 micron mesh openings were used for sieve analysis. Figure 3.16 shows the wet sieving setup used for sieve analysis. The sieve shaker (Gilson Company Inc., Model # SS-23) was set on a bucket making

grooves at the top edge of the bucket. Only two sieves can be put at a time between the base of the sieve shaker and its electronic control box. The setup was put on a sink so that the tap water could be used for washing during wet sieving. Finally, the sieve analysis was carried out following the standard procedures for wet sieve analysis outlined in ASTM C325 - 07 (2014).

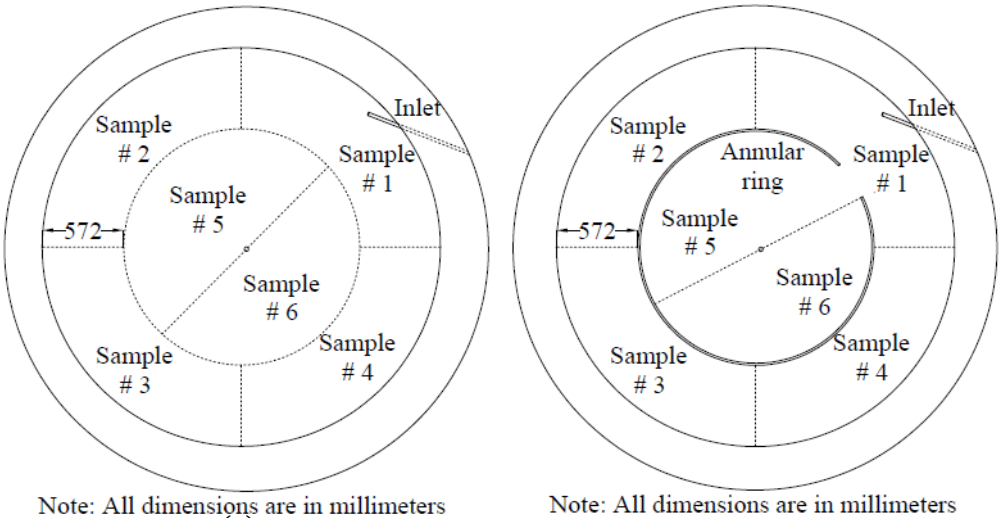

Figure 3.13: Sampling location of sediments in pond (a) without berm and (b) with berm

Figure 3.14: Sieve analysis setup

CHAPTER 4: ANALYSIS, RESULTS AND DISCUSSION

4.1 Introduction

The results obtained from the tracer, flow visualization and sediment deposition pattern tests are presented in this chapter. First, the method of analyses of the data are discussed. Then, the residence time distribution characteristics obtained from the tracer tests in the 100:2 and 50:2 pond models at different flow development times and at the peak flow rates are given. Next, tracer tests results for different flow rates and the sediment deposition patterns at the peak flow rates are presented. The best among the three different position of the berm was determined for the 100:2 pond model and the residence time distribution characteristics for both ponds with berm at this position are given. Finally the sediment deposition patterns in both models with berm placed at this position are presented and discussed.

4.2 Analysis of Tracer Test Data

The analysis of tracer tests data was carried out using the method described in Fogler and Brown (1992), Teefy (1996) and Levenspiel (2012). The measurements were the concentration of tracer, *C(t)*, at the model outlet at time, *t*. The tracer mass, ΔM_k, that exited from the outlet during the time interval $\Delta t = t_{k+1} - t_k$ is

$$\Delta M_k = (\frac{C_{k+1} + C_k}{2}) Q \Delta t \qquad [4.1]$$

where *Q* is the flow rate through the system. The total mass of recovered tracer is $M = \sum_{k=1}^{n-1} \Delta M_k$, where *n* is the number of measurements and the tracer recovery rate, *R*, is

$$R = \frac{M}{N_o} x100\%$$

where N_o is the mass of the injected tracer, which is calculated by multiplying the concentration and volume of the injected tracer.

There are two functions that represent the residence time distribution characteristics of flow. The function, *E(t)*, the residence time distribution (RTD) function, represents the fraction of tracer materials leaving the pond with time, and *F(t)*, the cumulative residence time distribution (CRTD) function, represents the fraction of tracer materials that have already left the pond before a particular time. *E(t)* and *F(t)* can be mathematically defined by

$$E(t) = \frac{C(t)}{\int_0^\infty C(t)dt} = \frac{QC(t)}{M} \qquad [4.2]$$

$$F(t) = \int_0^t E(t)dt \qquad [4.3]$$

Since *E(t)* is not dimensionless, a normalized residence time distribution function is required in order to compare the residence time distribution curves obtained under different test conditions. The normalized *E* function is

$$E_\theta = E(t)t_d \qquad [4.6]$$

where t_d is the theoretical retention time. The normalized *E* function is plotted against the dimensionless time, t/t_d to give the dimensionless residence time distribution curve.

The shapes of the residence time distribution curves are used to define the flow characteristics in the model. For example, the baffle factor refers to the dimensionless time for which *F(t)* = 0.1 and the short-circuiting index refers to the lowest dimensionless time for which *E(t)* or *F(t)* has a non-zero value. The fractions of plug flow, mixed flow and dead space can also be calculated by fitting the cumulative residence time distribution function to the Rebhun and Argaman (1965) model, as discussed in Chapter 2.

4.3 Results and Discussion

4.3.1 Tracer Tests at Different Flow Development Times

Figures 4.1 and 4.2 show the dimensionless residence time and the cumulative residence time distribution curves for the 100:2 pond model obtained from the tests where the flow was kept constant at 0.76 L/s (equivalent to the 4 m^3/s flow rate in the prototype). The flow development

times, t_f, were varied in these tests. The flow depth, h, was 65 mm in the model and eight tracer tests were carried out with the dimensionless flow development times, t_f/t_d, ranging from 1.0 –68.4.

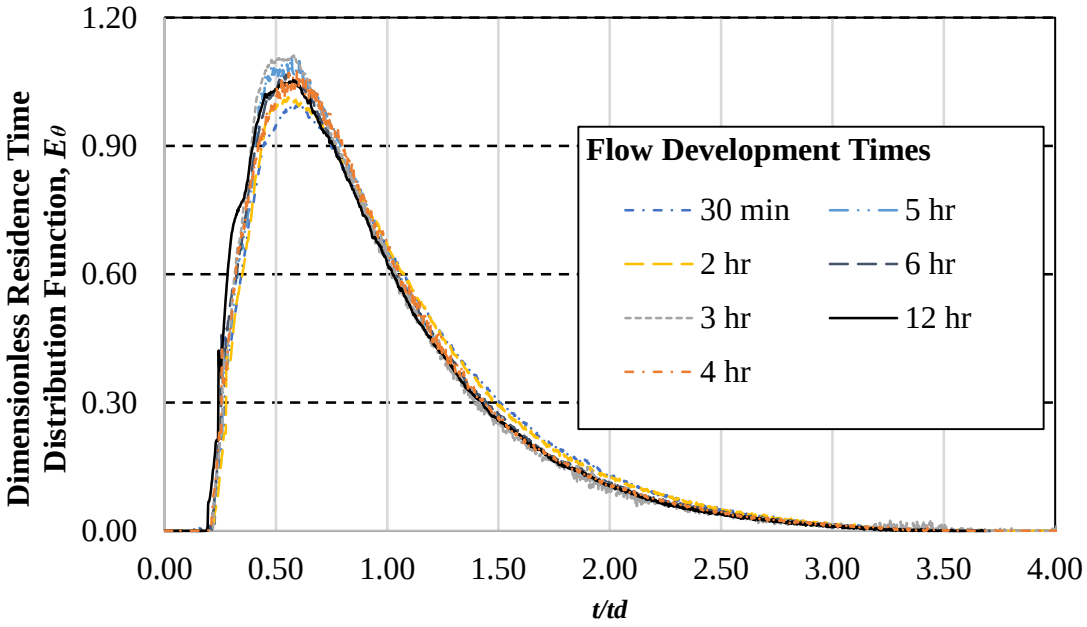

Figure 4.1: Dimensionless residence time distribution curves for different flow development times in the 100:2 pond model at 0.76 L/s (prototype flow rate = 4 m^3/s) and 65 mm flow depth without berm around the outlet

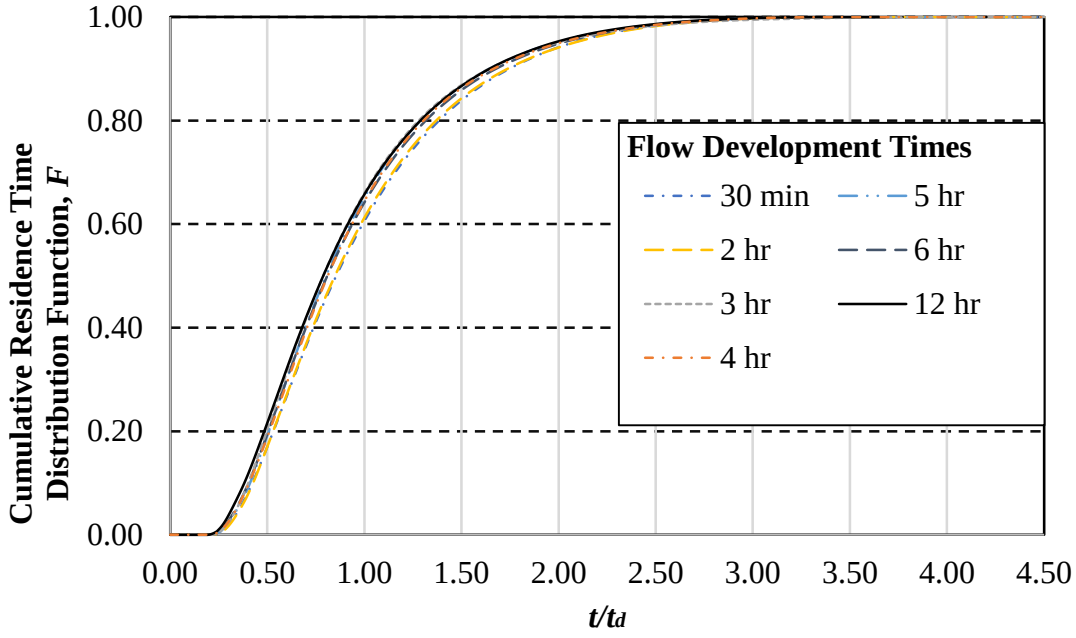

Figure 4.2: Dimensionless cumulative residence time distribution curves for different flow development times in the 100:2 pond model at 0.76 L/s (prototype flow rate = 4 m^3/s) and 65 mm flow depth without berm around the outlet

The flow development times used for the 100:2 pond model were made dimensionless using the theoretical retention time of the pond. The purpose of this dimensionless parameter is to compare the flow development times among tests carried out at different flow rates, flow depths and different aspect ratios of the model. Since the theoretical retention time is the ratio of the flow volume to the flow rate in the model and thus includes most of the parameters affected by the different test conditions, it is often used to make time dimensionless in RTD curves.

The RTD and CRTD plots for the 100:2 pond in Figures 4.1 and 4.2 show that both curves vary little with flow development time. The parameters that are typically used to describe RTD obtained from these tests are summarized in Table 4.1. The baffle factors obtained from these tests were in the range of 0.38 – 0.43 and have an average of 0.41. This implies that 10% of tracer material would exit the 100:2 prototype pond within about 24 minutes, which is 41% of the theoretical retention time of the prototype pond. The time required to reach the centroid of the dimensionless RTD curves varied between 580 – 618 s in the model and are equivalent to 54 – 57 minutes in the prototype. These are 92 – 99% of the theoretical retention times, which is calculated by taking the ratio of the flow volume to the flow rate in the model. The Morril dispersion indices in the 100:2 pond model were in the range of 4.0 – 4.3 indicating that the time required for 90% of tracer to exit the pond is about only 4 times the exit time required for the initial 10% of tracer. This provides an indicator for the dispersion characteristics of the flow. The plug flow fraction was found to be in the range of 36 – 39%, the mixed flow fraction 56 – 60% and the dead space fraction 0.8 – 8.1% in the 100:2 pond. Plug flow and mixed flow are defined in Section 2.6.1 and sample calculation for plug flow, mixed flow and dead spaces are shown in Appendix. The close similarities in the shape of the RTD curves to each other in Figure 4.1, the close similarity in the shape of the CRTD curves in Figure 4.2, narrow ranges of retention time parameters and lack of any general trend in those results for tests carried out over a wide range of flow development times from 30 min to 12 hr indicate that there is very little or no effect of flow development time on the RTD characteristics of flow in the 100:2 pond model without any berm around the outlet.

Similar tracer tests were carried out in 50:2 pond model at a flow of 1.56 L/s and a flow depth of about 148 mm. The dimensional flow development times (in min or hr) were selected for these tests to have similar dimensionless flow development times as those in 100:2 pond model. The RTD and the CRTD curves for the 50:2 pond are shown in Figures 4.3 and 4.4. The retention

time parameters derived from these curves are summarized in Table 4.2. It is seen that the RTD and CRTD curves for the 50:2 pond model for the different flow development times almost superimpose on each other. Therefore, the flow characteristics in the pond are not dependent on the flow development time.

Table 4.1: Retention time parameters obtained from tracer tests in the 100:2 pond model without berm at 0.76 L/s flow rate (prototype flow rate = 4 m^3/s) and 65 mm flow depth; injected tracer concentration = 1190 ppm and tracer volume = 30 mL

Parameters		Unit	Dimensionless Flow Development Times (t_f/t_d)						
Symbols	Definitions		2.9	11.5	17.2	23.0	28.7	34.4	68.4
t_f	Flow development time	hr	0.5	2.0	3.0	4.0	5.0	6.0	12.0
t_d	Theoretical retention time that is the ratio of system volume to discharge.	s	627	627	627	627	627	627	632
t_{10}/t_d	Baffle Factor		0.42	0.43	0.41	0.41	0.41	0.40	0.38
t_g/t_d	Index of average detention time		0.99	0.98	0.93	0.94	0.93	0.94	0.92
t_{50}/t_d	Index of mean detention time		0.86	0.85	0.81	0.81	0.80	0.81	0.79
t_{90}/t_{10}	Morril dispersion index		4.1	4.1	4.1	4.1	4.0	4.2	4.3
t_i/t_d	Short circuiting index		0.21	0.22	0.20	0.21	0.19	0.20	0.18
t_p/t_d	Index of model detention time		0.57	0.55	0.60	0.60	0.57	0.56	0.58
P	Plug flow fraction		39%	39%	37%	37%	37%	36%	35%
m	Mixed flow fraction		60%	60%	56%	57%	56%	58%	56%
d	Dead space fraction		1%	1%	8%	6%	7%	6%	8%
R	Tracer mass recovery rate		81%	81%	81%	83%	82%	85%	87%

The baffle factors obtained from the tests in the 50:2 pond model at different flow development times are seen to be in the range of 0.21 – 0.24, with an average of 0.23. Therefore, the initial 10% of the inflow mass exits the 50:2 prototype pond before 11.5 minutes, which is about 23% of the theoretical retention time. The short-circuiting index is in the range of 0.04 – 0.06 indicating that the first inflow particle reaches to the outlet within about 2.5 minutes of entering into the 50:2 prototype pond. The Morril dispersion indices are seen to be in the range of 8.3 – 9.0 indicating that 90% of the tracer mass spent up to 8.6 times longer inside the pond than the initial 10% of tracer spent. The plug flow, mixed flow and dead space fractions are in the range of 21 – 24%, 74 – 78% and 0 – 4%, respectively.

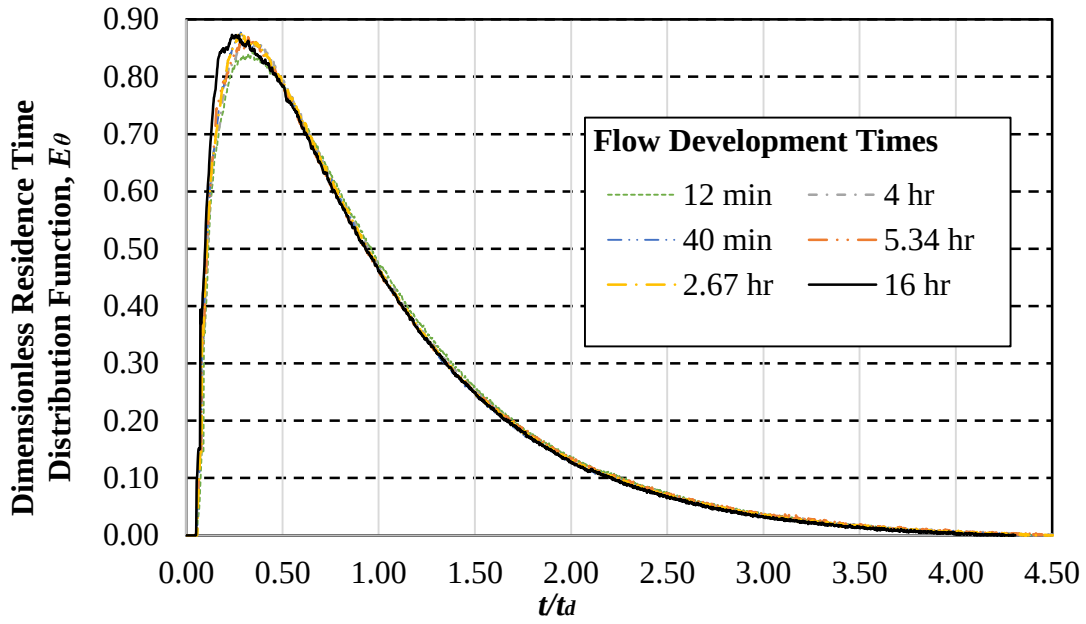

Figure 4.3: Dimensionless residence time distribution curves for different flow development times in the 50:2 pond model at 1.56 L/s (prototype flow rate = 1 m^3/s) and about 148 mm flow depth without berm around the outlet

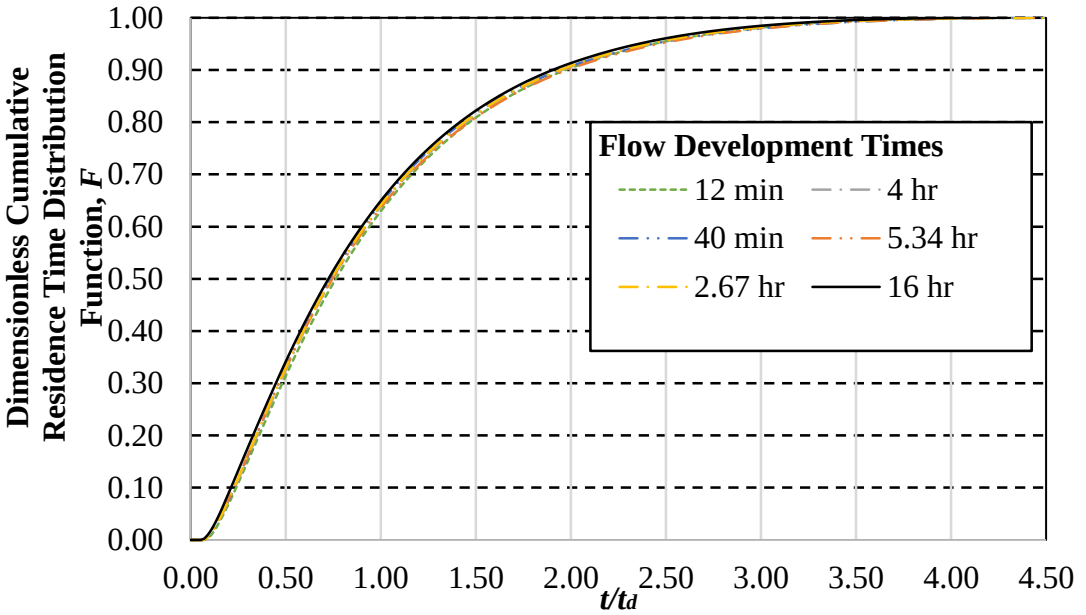

Figure 4.4: Dimensionless cumulative residence time distribution curves for different flow development times in the 50:2 pond model at 1.56 L/s (prototype flow rate = 1 m^3/s) and about 148 mm flow depth without berm around the outlet

Table 4.2: Retention time parameters obtained from tracer tests in the 50:2 pond model without berm at 1.56 L/s flow rate (prototype flow rate = 1 m^3/s) and about 148 mm flow depth; injected tracer concentration = 2380 ppm and tracer volume = 50 mL

Parameters	Definition	Units	Dimensionless Flow Development Times (t_f/t_d)					
			0.9	2.9	11.8	17.8	23.7	70.4
t_f	Flow development time	hr	0.2	0.7	2.7	4.0	5.3	16.0
t_d	Theoretical retention time that is the ratio of system volume and discharge.	s	804	823	818	811	811	818
h	Depth	mm	146	148	148	147	147	148
t_{10}/t_d	Baffle Factor		0.24	0.23	0.23	0.23	0.23	0.21
t_g/t_d	Index of average detention time		0.96	0.94	0.94	0.94	0.95	0.92
t_{50}/t_d	Index of mean detention time		0.76	0.74	0.74	0.74	0.74	0.72
t_{90}/t_{10}	Morril dispersion index		8.3	8.5	8.5	8.5	8.7	9.0
t_i/t_d	Short circuiting index		0.06	0.06	0.05	0.04	0.04	0.04
t_p/t_d	Index of modal detention time		0.34	0.30	0.28	0.31	0.32	0.24
P	Plug flow fraction		24%	21%	22%	22%	21%	22%
m	Mixed flow fraction		76%	75%	75%	76%	78%	74%
d	Dead space fraction		0%	3%	3%	2%	1%	4%
R	Tracer mass recovery rate		99%	100%	103%	104%	106%	99%

4.3.2 Comparison of the Residence Time Distribution Characteristics of Flow for the 100:2 and 50:2 Ponds

Figure 4.5 shows the RTD curves for the 100:2 and 50:2 pond models obtained from the tracer test results carried out with similar dimensionless flow development times. The effects of flow development time on the RTD characteristics were found to be negligible over the range of times tested in both ponds. The dimensionless RTD curves obtained using the longest flow development times in both models were chosen to make comparison between models. It was assumed the longest flow development times tested would be the most representative of fully

developed flow, and any unknown effects of the flow development time on the RTD characteristics would be very small.

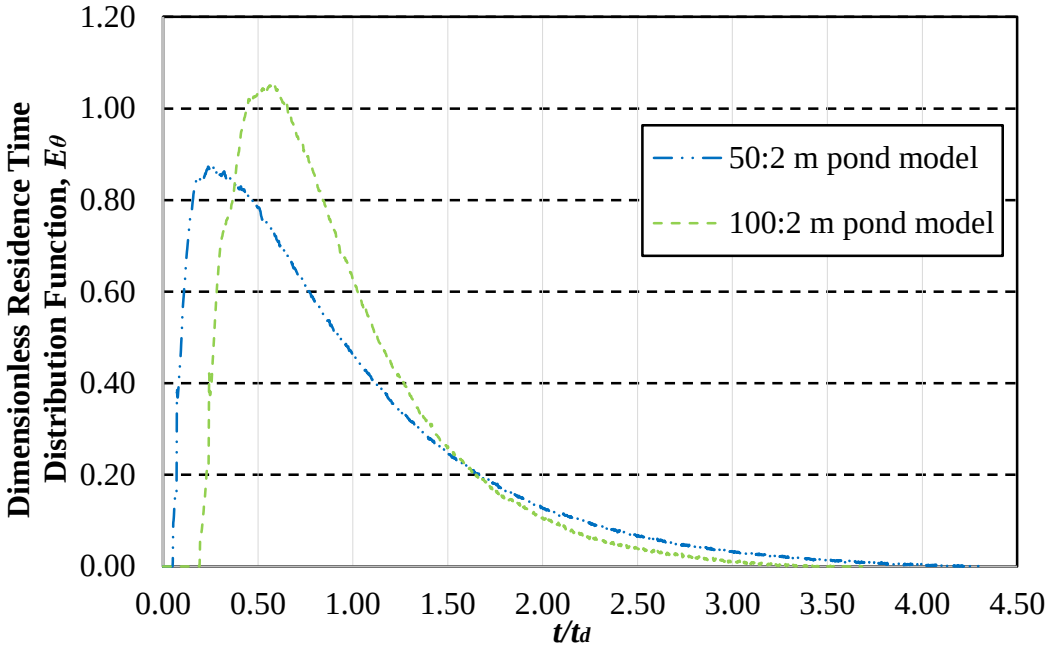

Figure 4.5: Comparison of dimensionless residence time distribution characteristics between the 100:2 and 50:2 pond models at 0.76 L/s and 1.56 L/s flow rates and for dimensionless flow development times 68.4 and 70.4 respectively; flow depths are 65 mm and 148 mm

It is seen that the first tracer particle arrived more quickly at the outlet for the 50:2 pond than the 100:2 pond. The short-circuiting indices calculated from the residence time distribution curves were 0.18 in the 100:2 pond and 0.04 in the 50:2 pond. This implies that the first inflow particle takes about 10.8 min to reach the outlet in the 100:2 prototype pond whereas it takes only 2.2 min in the 50:2 pond. The baffle factor is 0.38 in the 100:2 pond and 0.21 in the 50:2 pond. Therefore, the initial 10% of inflow mass spends up to 22.3 min in the 100:2 pond and 10.5 min in the 50:2 pond before exiting through the outlet. The RTD curve for the 50:2 pond is more spread out than the 100:2 pond indicating higher dispersion in the 50:2 pond. The Morril dispersion index is 9.0 in the 50:2 pond and 4.3 in the 100:2 pond. The plug flow fraction is higher in the 100:2 pond and the mixed flow fraction is higher in the 50:2 pond. Though the inflow jet velocity is about 2.0 m/s in both the 100:2 and 50:2 ponds, the inflow of the 100:2 pond has a much longer flow path that should result in a higher fraction of plug flow. Persson (2000) showed that the flow becomes more similar to plug flow with increased flow path length and increased length to width

ratio of the pond. The flow path length required for the inflow jet to dissipate is significant for the 50:2 pond due to its relatively shorter flow path to the outlet as compared to the 100:2 pond. Therefore, the mixing created by the same inflow jet velocity in the smaller flow volume of the 50:2 pond makes the mixed flow fraction higher than in the 100:2 pond.

Flow patterns in the 100:2 and 50:2 pond obtained from the flow visualization tests in the scale models support the flow characteristics interpreted from the RTD curves. Figure 4.6(a – f) and 4.7(a – f) show the flow patterns in the 100:2 and the 50:2 pond models, respectively. After entering into the pond, the inflow follows a circular flow path in both ponds and travels around the outer periphery of the pond. The top width of the outer peripheral strip with circular flow pattern is about 10.8 m in the 100:2 prototype pond; about 22% of the radius at the flow surface. In the case of the 50:2 prototype pond, the width of the outer peripheral strip is about 12.6 m which is about 50% of the pond radius at the flow surface. Then the flow goes through a transition region in both ponds before entering a high velocity vortex region surrounding the pond outlet. The high velocity vortex region surrounding the central outlet was identified by the degree of color around the outlet, combined with visual observation during the flow visualization tests, and was about 9.2 m radius in the 100:2 pond and 6.6 m radius in the 50:2 pond. The high velocity vortex regions are about 18% of the top flow radius in the 100:2 pond and 26% in the 50:2 pond. Therefore the width of the transition area between the outer peripheral region and the high velocity central region are about 60% of the top flow radius in the 100:2 pond and 24% of the top flow radius in the 50:2 pond. Due to a narrower transition region, the first tracer particles reached the outlet in 2.2 min in the 50:2 pond whereas it took about 10.8 min for the 100:2 pond. The baffle factor was also lower in the 50:2 pond due to this narrower transition region.

The flow patterns in the transition region of both ponds are the result of the simultaneous actions of a radial velocity component, v_r, and a tangential velocity component, v_θ, on the flow. When the flow circulates in the outer peripheral region, the tangential velocity component, v_θ dominates in the flow. However, a radial velocity component also develops in that region acting on the bottom layer of flow toward the center. As a result, the bottom layer of flow moves toward

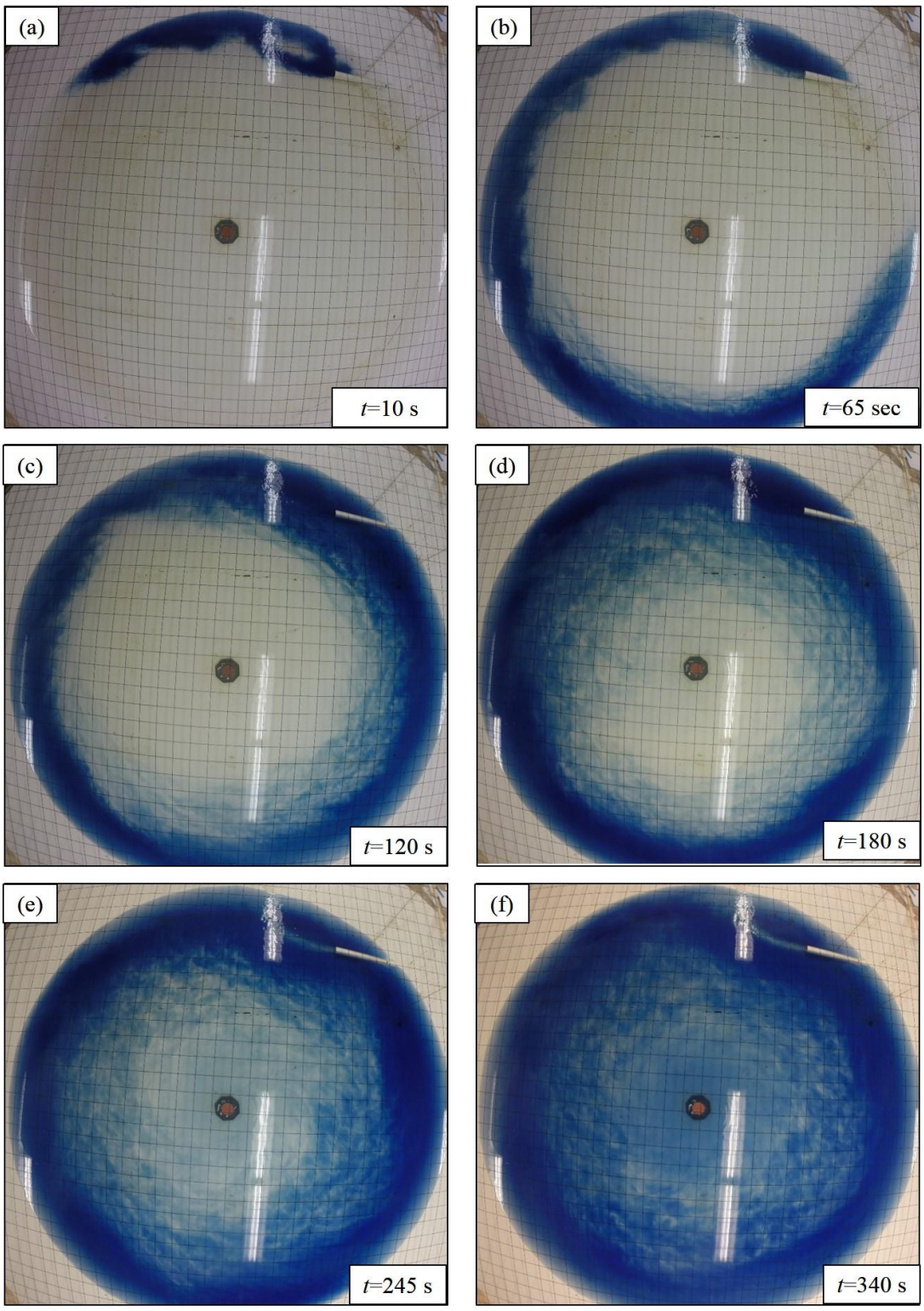

Figure 4.6: Flow pattern in the 100:2 pond model at 0.76 L/s and 65 mm flow depth with approximate time after insertion of dye at (a) t = 10 s, (b) t = 65 s, (c) t = 120 s, (d) t = 180 s, (e) t = 245 s , and (f) t = 340 s

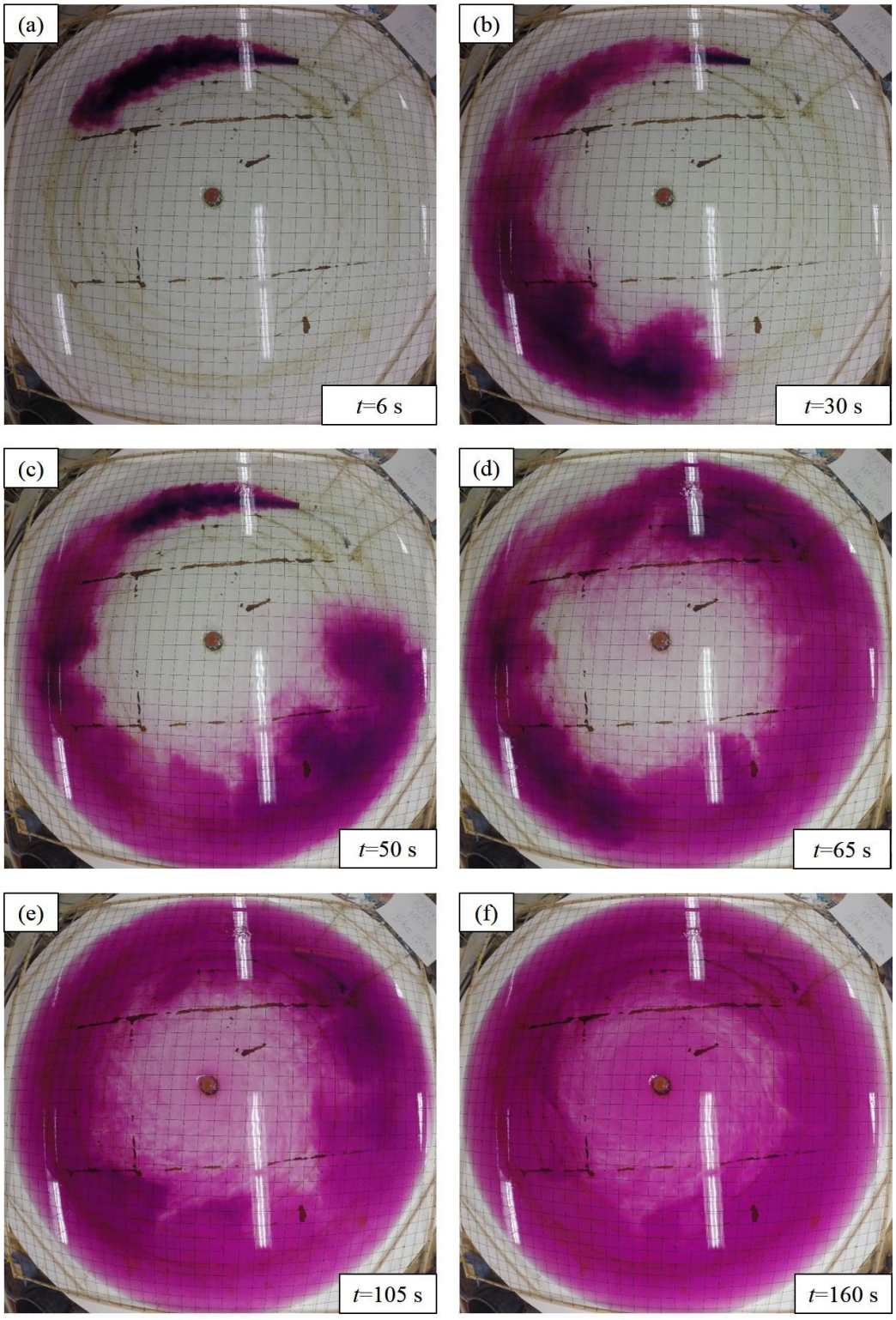

Figure 4.7: Flow pattern in the 50:2 pond model at 1.55 L/s and 148 mm flow depth with approximate time after insertion of dye at (a) t = 6 s, (b) t = 30 s, (c) t = 50 s, (d) t = 65 s, (e) t = 105 s, and (f) t = 160 s

the center whereas the top layer slowly moves away from the center. The effect of v_r becomes more significant as the flow moves toward the center creating a spiral flow pattern and eventually the flow moves to the high velocity vortex region around the center before passing through the outlet. The flow directions in the different regions of the 100:2 pond models are shown in Figure 4.8. The arrows in this sketch do not represent the velocity vectors; they represent only the flow directions.

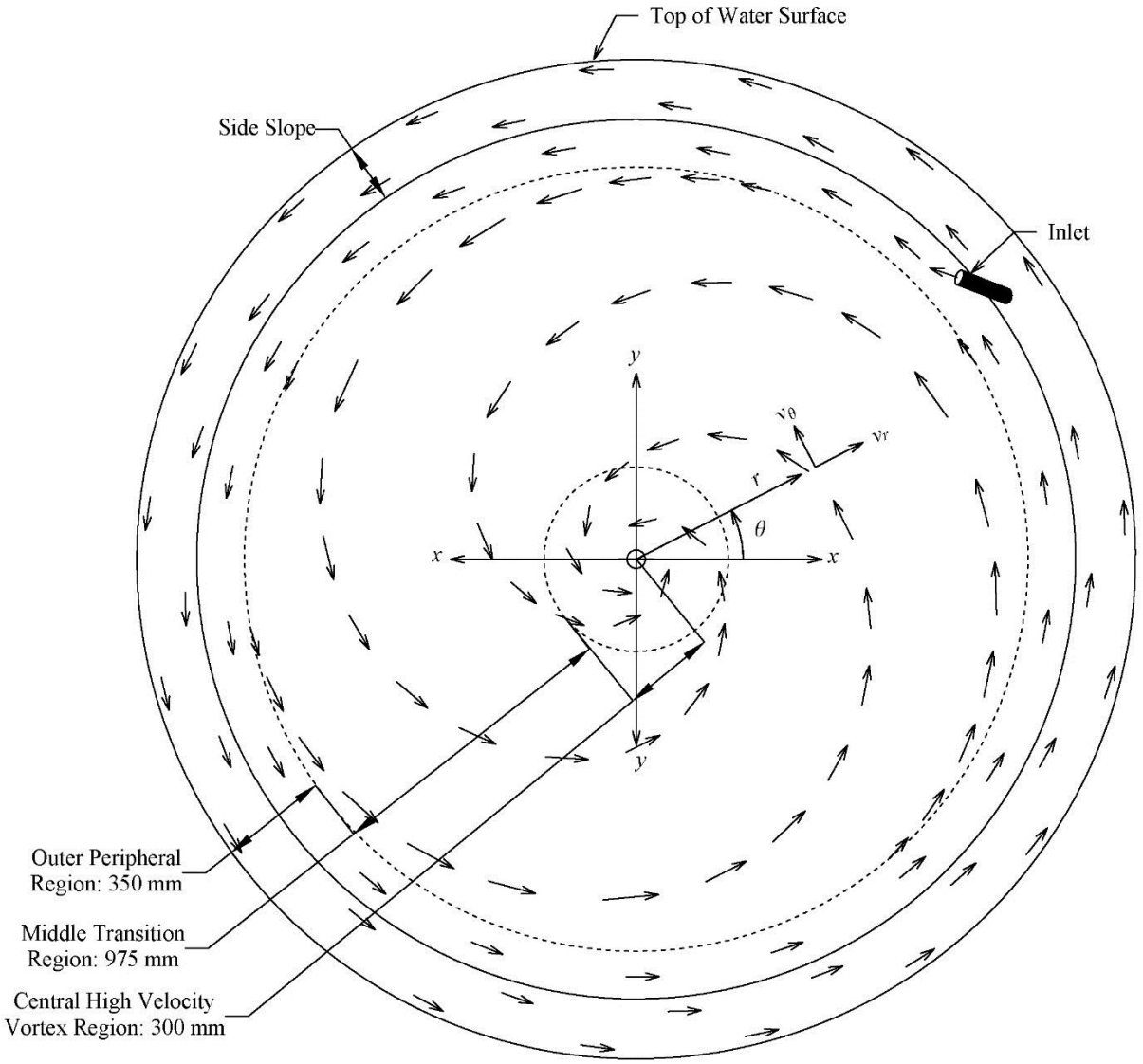

Figure 4.8: A qualitative sketch of flow pattern in different regions of the 100:2 pond model at 0.76 L/s flow rate and 65 mm depth

The radial velocity component in a circular flow is formed due to two fundamental reasons: the formation of a high velocity vortex at the center of the pond; and the deceleration of flow near

the model bed. The high velocity vortex creates a low pressure zone at the center. As a result, a radial force acting toward the center is developed due to the pressure gradient. A centrifugal force also acts upon the circular flow; but this force is very weak at the bottom layer of flow due the very low tangential velocity near the bed. Therefore, the resulting radial force acting on the top layer of the flow can be neutralized by the centrifugal force. However the radial pressure force along the bottom layer of flow is not neutralized due to the very weak centrifugal force near the model bed and as a result, a radial velocity component toward the center is developed in the bottom layer. This radial velocity component toward the center can be called a secondary flow. Mashauri (1986), Paul et al. (1991) and Athar et al. (2002) used secondary flow components generated in the circulatory flow of vortex settling basin to remove sediments from the flow.

The flow patterns in both ponds obtained from the flow visualization tests show that there are no areas in either pond where the flow remains stagnant. Therefore there should be no dead space fraction in the flow. However, the analysis of tracer data showed 0.8 – 8.1% dead space fraction in the 100:2 pond and 0.3 – 4.4% fraction in the 50:2 pond. These fractions likely indicate the low velocity areas of the flows near the side slopes of the ponds.

The flow visualization tests in both ponds were also carried out at different flow development times. However there were no differences among those flow patterns; this supports similar observations for the RTD in both ponds.

4.3.3 Influence of Flow Rates on Residence Time Distribution Characteristics

Tracer tests were carried out in both the 100:2 and 50:2 pond models to investigate the effect of flow rate on the RTD characteristics of the pond. Five flow rates between 0.10 – 1.0 L/s, equivalent to 0.53 – 5.25 m^3/s in the prototype, were tested in the 100:2 pond model. The corresponding range of inlet jet Reynolds number tested in the 100:2 pond model is 1,890 – 18,900. In the 50:2 pond model, four flow rates between 0.20 – 1.56 L/s with inlet jet Reynolds number 3,170 – 24,600 were tested. These are equivalent to flow rates of 0.13 – 1.0 m^3/s in the prototype pond. Tests were carried out in both models with the same dimensionless flow development times of $t_f/t_d \approx 69$.

The inflow jet Reynolds number in the 100:2 pond model for 0.10 L/s flow rate was 1,890 indicating that the spreading angle of the inflow jet was not independent of the inflow jet Reynolds number (Rajaratnam and Flint-Petersen 1989). The model was originally designed for a 0.76 L/s flow rate, equivalent to 4 m^3/s in the prototype. The inflow jet Reynolds number was 14,400 in the model at that flow rate. Later there was a change in testing in an attempt to investigate what would happen if the flow rate was unsteady, rising from very low to the peak flow. This change caused the inlet jet Reynolds number for the lowest flow rate, 0.10 L/s, to become lower than the threshold Reynolds number for a turbulent jet, 3000, at which the spreading rate of the jet becomes approximately constant (Rajaratnam and Flint-Petersen 1989). However, it was still thought to be useful to evaluate the RTD characteristics in the model at this flow rate. As the conventional procedure of tracer testing is not compatible with unsteady state flow rates by setting an inflow hydrograph, it was decided to test the flow rates separately in steady state conditions and compare the RTD characteristics. The inflow jet Reynolds numbers for the other flow rates in the 100:2 pond were greater than 7500.

The flow depth in the 100:2 pond model varied between 34 – 84 mm for the flow rates between 0.1 – 1.0 L/s. The outlet of the Nautilus Pond™ being perforated between 50% - 75% of height allows the flow depth in the pond to vary with a change of flow rates. Therefore, when the flow is just initiated in the prototype pond due to a rainfall, the pond aspect ratio, A_R, would be different than during peak flow rates. The different aspect ratios during varied flow rates in the 100:2 pond are shown in Table 4.3.

Figures 4.9 and 4.10 show the dimensionless RTD and the CRTD curves in the 100:2 pond model obtained from tests carried out at different flow rates. Table 4.3 shows the retention time parameters obtained from these curves. The dimensionless RTD curve for 0.10 L/s shows multiple peaks. The first peak is the highest one, which is followed by the two less prominent peaks.

A flow visualization test was also carried out in the 100:2 pond model at the 0.10 L/s flow rate in order to investigate the shape of the RTD curve which had multiple peaks. Figure 4.11(a – f) shows the flow patterns obtained from the flow visualization test at the 0.10 L/s flow rate. A 1 hr flow development time was used for this test considering the flow development time was previously found to have little effect on the shape of RTD curves. As seen in Figure 4.11, the

inflow in the pond started to follow the circular path after entering into the pond. However, the momentum for a large fraction of the inflow at 0.10 L/s was not sufficiently strong to drive the flow throughout the circular path near the periphery. Most of the dye starts to accumulate along the halfway of the circumference distance and go to the outlet from that point. The first high peak in the RTD curve for 0.10 L/s is thought to be produced by this accumulated dye. Some fractions of the dye complete the full circular flow path along the periphery and join the inflow jet for recirculation. When these fractions of the dye starts to reach the outlet, the second and third peak in the RTD curve are seen.

As the flow rate was increased, the inflow momentum increased and the prominent multiple peaks disappeared from the RTD curve. The RTD curves for 0.76 L/s and 1.0 L/s had only a single peak. The peak of the RTD curve was also reduced with the increase in flow rates. However, the dispersion in the flow increased with the increase in flow rates. The increased local velocity gradient in the pond for the higher flow rates resulted in increased dispersion in the flow. The Morril dispersion index increased from 4.1 to 6.2, a 51% increase, when the flow rate increased from 0.10 L/s to 1.0 L/s. The increased dispersion characteristics of larger flow rates are also evident from the fact that the dimensionless time required for the first tracer particle to move to the outlet, short-circuiting indices, decreased with the increase of flow rates. The baffle factor also decreased with the flow rates resulting in the higher dispersion in the flow.

The increase in flow rates also increased the inflow momentum. The higher inflow momentum kept the flow circulating in the outer peripheral area for longer times before going to the outlet. However, an increase of flow rates would also increase the radial velocity component of the flow and counteracts the increased travel time in the outer peripheral area by radially pushing the flow towards the outlet. This is the reason that the time for occurrence of peak did not shift to any particular direction with the increase of flow rates. At a certain flow rate it is likely the radial velocity component becomes more dominant than the tangential component in the pond and the flow pattern become symmetric around the outlet. This is the flow rate where the single peak starts to occur in the RTD curves. In the 100:2 model, this flow rate is in between 0.60 L/s and 0.76 L/s.

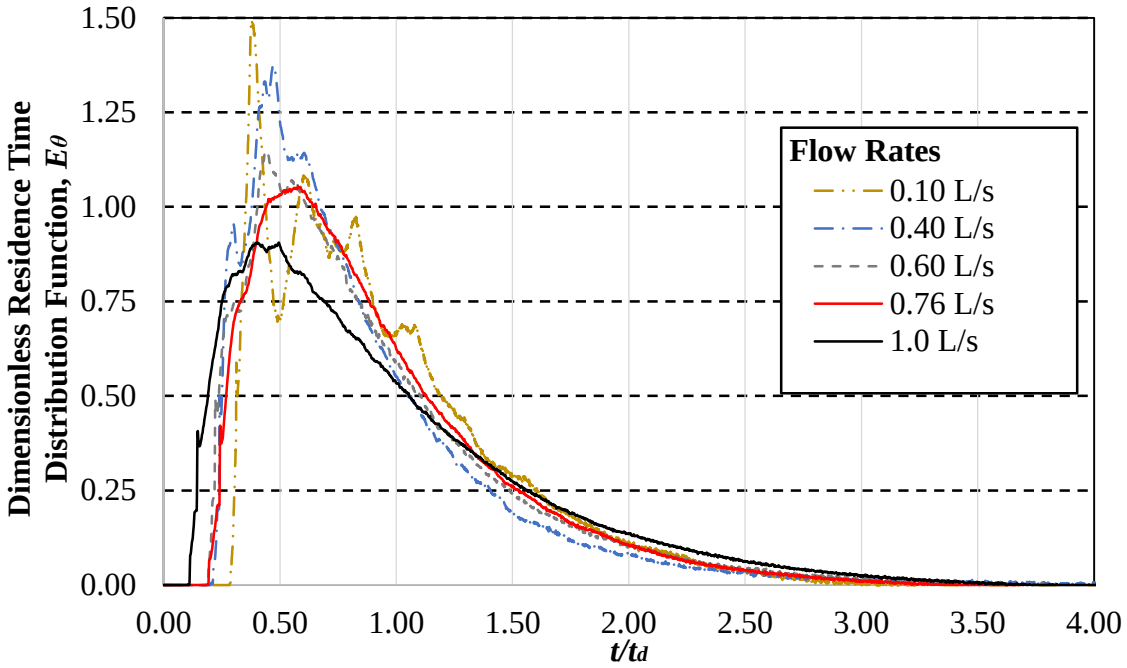

Figure 4.9: Dimensionless residence time distribution curves for the 100:2 pond model at different model flow rates with similar dimensionless flow development times and with fully developed flows

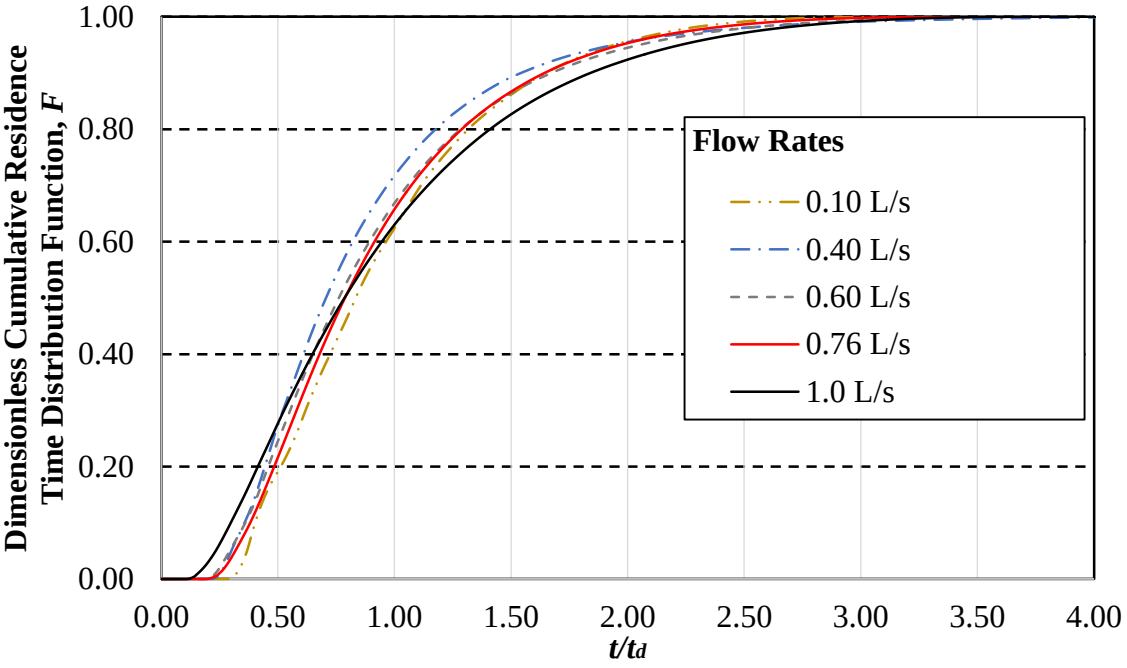

Figure 4.10: Dimensionless cumulative residence time distribution curves for the 100:2 pond model at different model flow rates with similar dimensionless flow development times and with fully developed flows

Table 4.3: Retention time parameters obtained from tracer tests at different flow rates in the 100:2 pond model without berm; injected tracer concentration=1190 ppm

Parameters	Unit	Flow Rates				
		0.10 L/s	0.40 L/s	0.60 L/s	0.76 L/s	1.0 L/s
t_f	hr	47.0	18.5	14.4	12.0	12.0
t_f/t_d		72.2	68.7	68.8	68.4	67.5
h	mm	34	54	62	65	84
A_R		100 : 1.1	100 : 1.7	100 : 1.9	100 : 2.0	100 : 2.5
V	mL	10	30	30	30	50
t_d	s	2,342	969	753	632	640
t_{10}/t_d		0.40	0.36	0.36	0.38	0.30
t_g/t_d		0.95	0.86	0.91	0.92	0.95
t_{50}/t_d		0.83	0.71	0.76	0.79	0.79
t_{90}/t_{10}		4.1	4.3	4.7	4.3	6.2
t_i/t_d		0.28	0.20	0.18	0.18	0.10
t_p/t_d		0.38	0.47	0.44	0.58	0.40
P		42%	33%	37%	39%	33%
m		53%	53%	57%	60%	66%
d		4%	14%	7%	1%	1%
R		81%	72%	69%	81%	69%

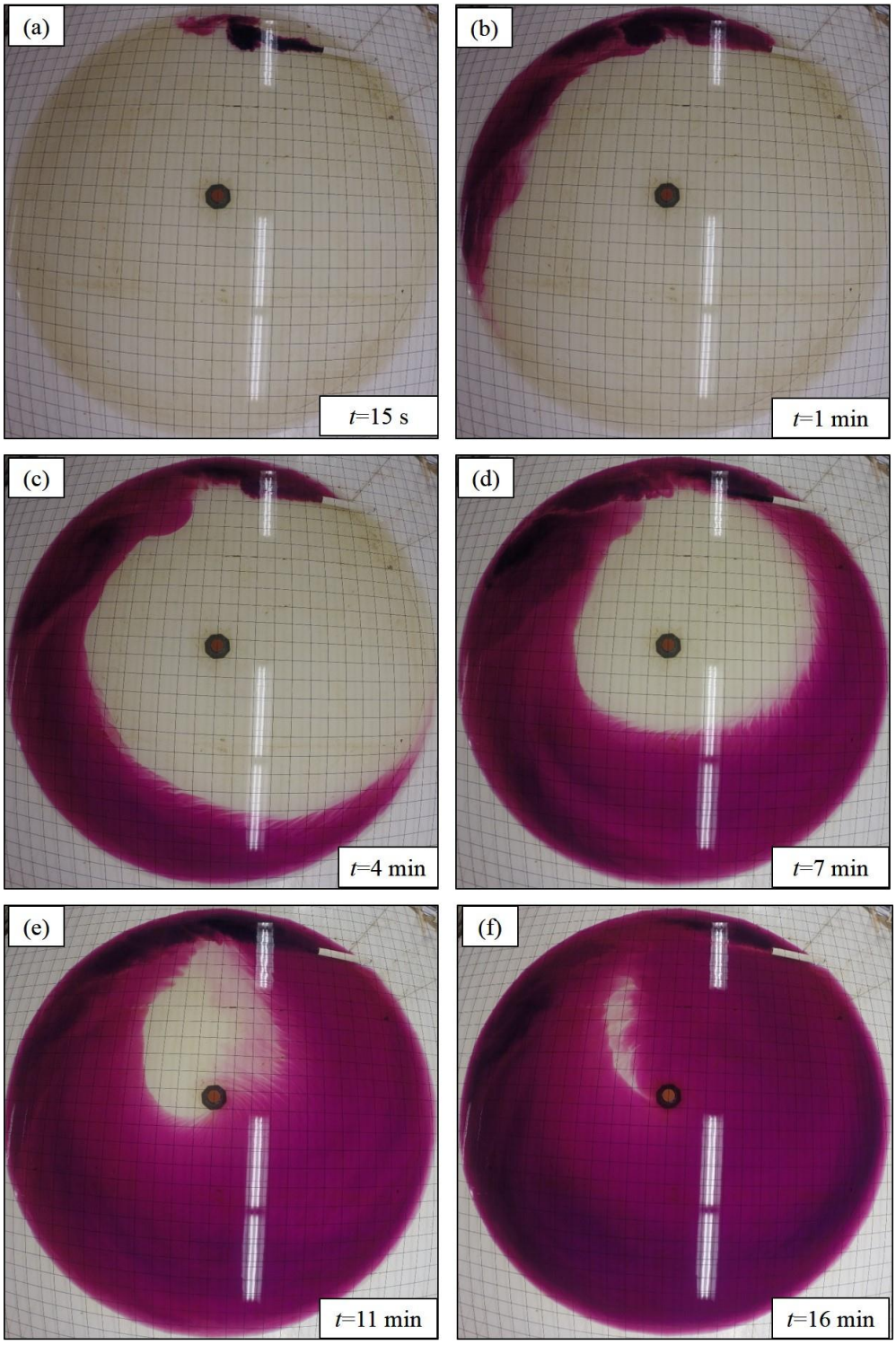

Figure 4.11: Flow pattern in the 100:2 pond model at 0.10 L/s and 34 mm flow depth with approximate time after insertion of dye at (a) t = 15 s, (b) t = 1 min, (c) t = 4 min, (d) t = 7 min, (e) t = 11 min , and (f) t = 16 min

The turbulent mixing was higher for the increased flow rates as there were more eddies to dissipate in the flow. The mixed fraction of the flow increased from 53% to 66% and consequently the plug flow fraction decreased from 42% to 33% when the flow rate was increased from 0.10 L/s to 1.0 L/s. The dead space fraction was also lower during high flow rates. The high inflow momentum during high flow rates caused more areas of the pond to become active that was left undisturbed during low flow rates.

Figures 4.12 and 4.13 show the dimensionless residence time and the cumulative residence time distribution curves in 50:2 pond model obtained from tests carried out at different flow rates. Table 4.4 shows the retention time parameters obtained from these RTD curves. It is seen that the influence of flow rates on the RTD characteristics of 50:2 pond model is similar to the 100:2 pond model in terms of the retention time parameters.

The peak of the dimensionless residence time distribution curve for the 0.20 L/s flow rate is much higher than the other flow rates and the long flat tail of the curve indicates that there are some dead spaces available in the pond at this flow rate. It was found from the application of the Rebhun and Argaman (1965) model fitting the tracer test data that there was about 32% dead space in the pond at this flow rate. This high fraction of dead space is exceptional in the Nautilus Pond™ since the dead spaces at 0.8 L/s, 1.2 L/s and 1.55 L/s were found to be about 6%, 3% and 4% respectively using the same method of calculation. This is likely due to the fact that the inflow did not have sufficient momentum at this flow rate and some flow area in the pond remained quiescent. Those areas became part of the effective volume of the pond when the flow rate was higher. The mixed flow fractions in the model for 0.8 L/s, 1.2 L/s and 1.56 L/s flow rates were found to be about 65%, 70% and 74%, respectively, whereas it was only 43% for 0.2 L/s. The plug flow fraction for 0.2 L/s was nearly the same as the higher flow rates. Therefore it is evident that a significant dead space fraction became part of mixed flow when the flow rate was increased.

A comparison between the RTD characteristics of the 100:2 pond at the 0.1 L/s flow rate and the 50:2 pond at the 0.2 L/s flow rate, shown in Figures 4.9 and 4.12, illustrates the effect of aspect ratio of the pond on the multiple peaks of the RTD curves in the 100:2 pond during low flow rates. The actual aspect ratio of the tests at these low flow rates in the 100:2 and 50:2 pond models are 100:1.1 and 50:1.1 respectively due to the change in flow depths in the ponds. The flow

path is significantly longer in the 100:1.1 than the 50:1.1 aspect ratio of the pond. The low inflow momentum cannot drive the flow through a long path up to the outlet in 100:2 pond causing multiple peaks where the flow path being shorter in the 50:2 pond there was a single peak in the RTD curve at the 0.2 L/s flow rate.

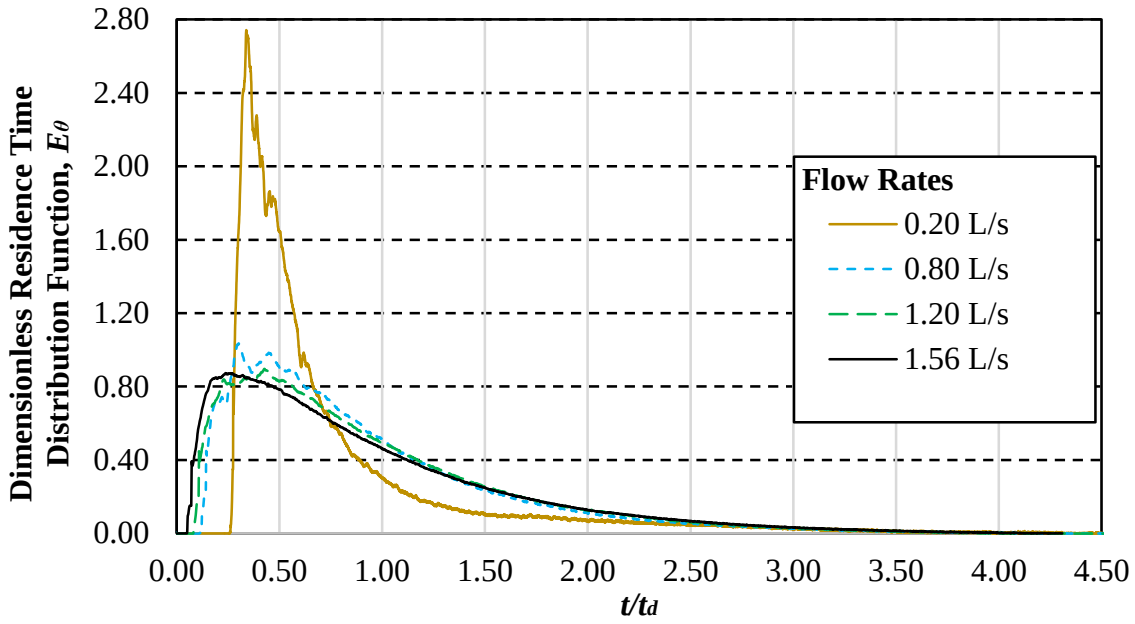

Figure 4.12: Dimensionless residence time distribution curves for the 50:2 pond model at different model flow rates with similar dimensionless flow development times and with fully developed flows

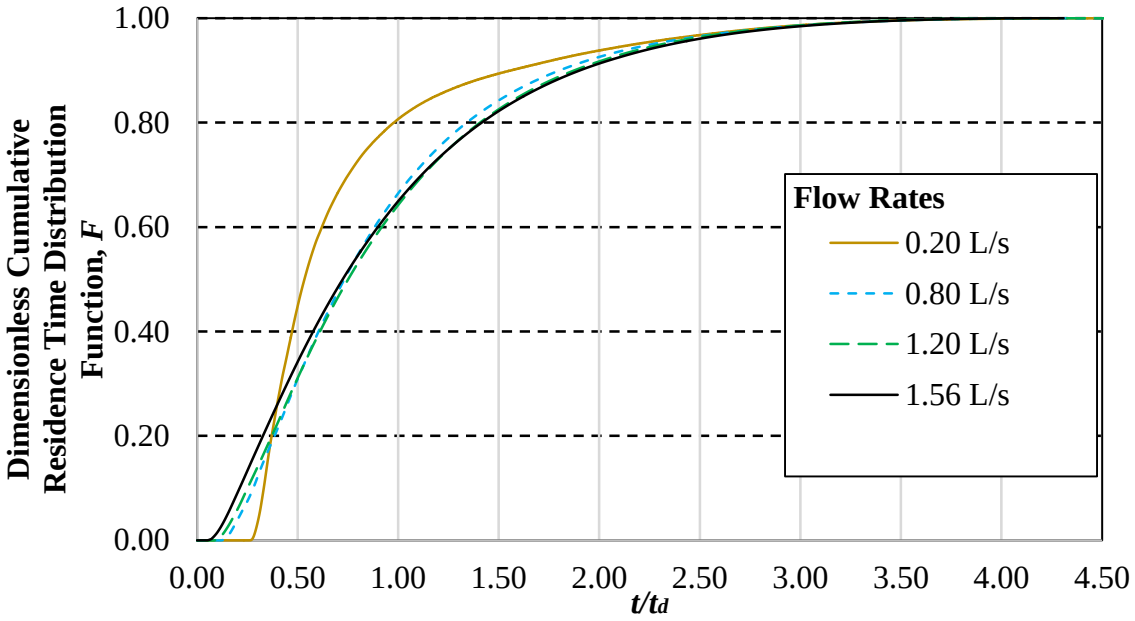

Figure 4.13: Dimensionless cumulative residence time distribution curves for the 50:2 pond model at different model flow rates with similar dimensionless flow development times and with fully developed flows

Table 4.4: Retention time parameters obtained from tracer tests at different flow rates in the 50:2 pond model without berm; injected tracer concentration = 2380 ppm

Parameters	Units	Flow Rates			
		0.20 L/s	0.80 L/s	1.20 L/s	1.56 L/s
t_f	hr	53.0	17.8	15.0	16.0
t_f/t_d		67.0	70.0	68.4	70.4
h	mm	76	94	116	148
A_R		50 : 1.1	50 : 1.4	50 : 1.6	50 : 2.0
V	mL	8	20	30	50
t_d	s	2,849	913	790	818
t_{10}/t_d		0.33	0.28	0.25	0.21
t_g/t_d		0.76	0.91	0.93	0.92
t_{50}/t_d		0.53	0.73	0.75	0.72
t_{90}/t_{10}		4.7	6.5	7.5	9.0
t_i/t_d		0.26	0.11	0.08	0.04
t_p/t_d		0.34	0.30	0.43	0.24
P		25%	29%	27%	22%
m		43%	65%	70%	74%
d		32%	6%	3%	4%
R		96%	102%	108%	99%

Tracer recovery rates for the 0.4, 0.6 and 1.0 L/s flow rates shown in Table 4.3 are lower than reported elsewhere in the thesis though the tests were carried out until all of the tracer was recovered and the fluorometer concentration readings became zero. This is because all of these three tests were carried out with the same stock solution of Rhodamine WT tracer, the concentration of which was different than the intended 1190 ppm due to a pipetting error of the 20% Rhodamine WT solution during its dilution. However, the standard used for the calibration

of the fluorometer was not prepared by diluting this stock solution of tracer. Therefore, though the RTD characteristics obtained from the fluorometer readings were valid and tests were carried out until all of the tracer was recovered, the recovery rates calculated based on the 1190 ppm inlet concentration gave lower than the true recovery rates of tracer. As soon as a correctly prepared stock solution of tracer was used for injection at the inlet, the tracer recovery rates became higher again.

4.3.4 Sediment Deposition Patterns in Both Ponds without Berm

The 100:2 and 50:2 ponds were tested for sediment deposition pattern at their design flow rates using walnut shells as sediments. The same dimensionless flow development time, $t_f/t_d \approx$ 17.5, was used for both tests. The dimensionless flow development time, 17.5, was selected arbitrarily as the flow development time was found to have no effect on flow characteristics.

Figure 4.14 shows the sediment deposition pattern in the 100:2 pond without a berm. It is seen that more sediments per unit area are deposited in the outer peripheral region of the model than the inner regions. The deposition behavior in this outer peripheral region can be explained using the flow pattern seen in this region, shown in Figure 4.6. The flow kept circulating in this region multiple times before moving to the adjacent middle transition region of flow, as described in Section 4.3.2, due to the radial velocity component acting towards the pond outlet. Therefore the flow in this outer peripheral region had a longer flow path and more sediments were deposited.

The middle transition region of the 100:2 pond model where spiral flow patterns were noticed in Figure 4.6 show almost a uniform sediment deposition per unit area of the model bed. There is a slight variation in the degree of color of deposited sediments along the radius, changing from darker to less dark towards the center. The degree of color indicates the size of the deposited sediments. The coarser walnut shells form dark brown color in water and finer walnut shell makes lighter color. The high quantity of sediment depositing just outside the central region indicates that a lot of sediments also entered the central region and escaped through the outlet. The central region is defined as the circular area of 300 mm radius around the outlet. The high velocity vortex prevents any settling of sediments in this region. Therefore based upon the model results, a 100:2 prototype pond will have about an 18.5 m diameter area around the outlet where no sediment deposition occurs. This central area near the outlet is about 4.4% of the total area of the pond bed.

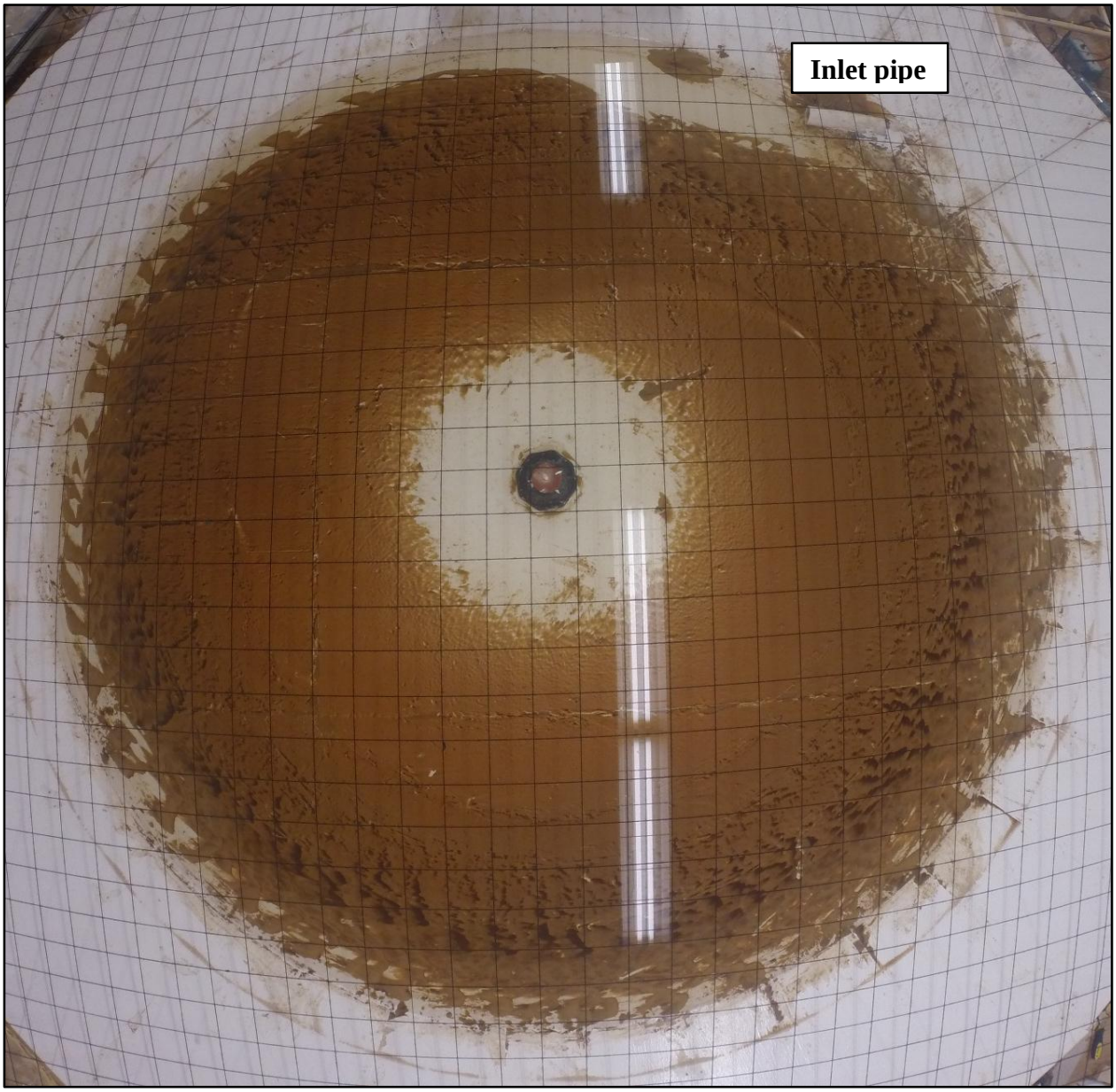

Figure 4.14: Sediment deposition pattern in the 100:2 pond model without berm at 0.76 L/s (prototype flow rate = 4 m^3/s), 65 mm flow depth and 17.2 dimensionless flow development time

Samples of the deposited sediments in the 100:2 pond model were collected from the different areas of the model bed, as described in Section 3.4.3.3. Sieve analysis was carried out to determine the particle size distributions of the deposited sediment samples. The results are given in Figure 4.15 and Table 4.5. It is seen that 84% of the weight of Sample 5 consists of particles

smaller than 53 microns. This is significantly greater than the other samples where the smaller than 53 micron fractions were in the range of 44 – 64%. The larger than 75 micron size fractions were 4% in Sample 5 whereas it was 16 – 37% in Samples 1 – 4. The location of Sample 5 is the inner 60% of model bed radius and the finer particle fraction is higher in the deposited sediment of this region. The locations of Samples 1 – 4, shown in Figure 3.15(a), were at the periphery and larger-sized particles mostly deposited in these regions.

Figure 4.16 shows the sediment deposition pattern in the 50:2 pond model. Unlike the deposition pattern in the 100:2 pond model, only a very small quantity of sediments are deposited in the outer peripheral region. The inflow jet is stronger in the 50:2 m pond model and takes a longer path to dissipate its energy. Only a small quantity of sediments are seen to be deposited as scattered ripples in the outer peripheral region. Most of the sediments were deposited in between 44 – 84% of model bed radius from the center where a spiral flow pattern dominates. Then the sediments move to the central region of high velocity vortex where no sediments can deposit. The diameter of this central region is about 1.0 m in the model which is 12.3% of the total bed area of the 50:2 pond as compared to 4.4% in the 100:2 pond.

The particle size distribution of the samples of the deposited sediments in the 50:2 pond model without berm are shown in Figure 4.17 and Table 4.6. The sediments deposited inside the 60% of bed radius distance from the center, Samples 5 and 6 in Figure 3.15(a), do not show any significantly different particle size distribution than Samples 1 – 4 taken from the pond periphery. This is in sharp contrast to the deposition pattern in the 100:2 pond model where a significantly greater fraction of finer particles deposited inside the 60% of bed radius distance from the central outlet. The deposition in the 50:2 pond mainly occurred in the middle transition region of flow. As described in Section 4.3.2, the width of the middle transition region is about 24% of the top flow radius in the 50:2 pond as compared to the 60% in the 100:2 pond; there is no significant differences found in the particle size distribution of the deposited sediments in different areas of the 50:2 pond model.

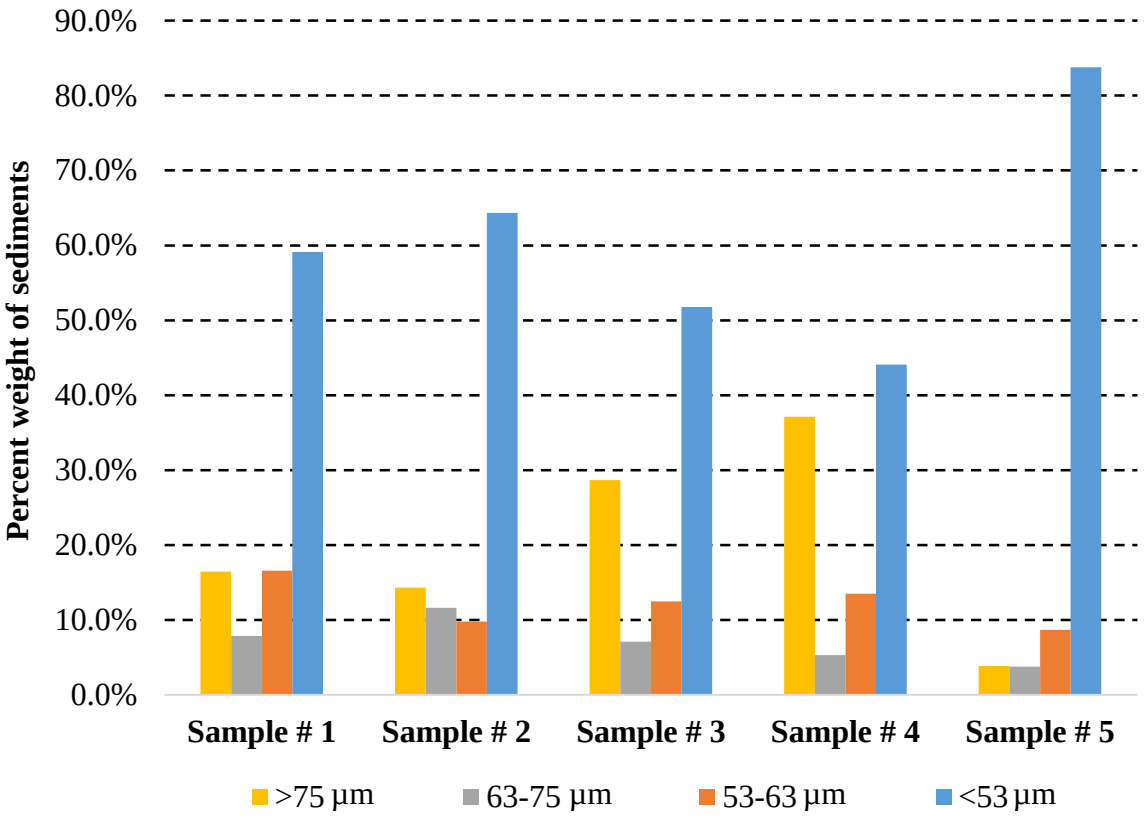

Figure 4.15: Particle size distribution of the deposited sediments in the 100:2 pond model without berm at 0.76 L/s (prototype flow rate = 4 m^3/s), 65 mm flow depth and 17.2 dimensionless flow development time

Table 4.5: Particle size distribution data of the deposited sediments in the 100:2 pond model without berm at 0.76 L/s (prototype flow rate = 4 m^3/s), 65 mm flow depth and 17.2 dimensionless flow development time

Sample #	Sample size (g)	% of total weight			
		< 53 µm	53-63 µm	63-75 µm	> 75 µm
1	40.67	59.1	16.6	7.9	16.4
2	60.94	64.3	9.8	11.6	14.3
3	49.1	51.8	12.5	7.1	28.7
4	36.1	44.1	13.5	5.3	37.1
5	9.36	83.8	8.7	3.7	3.8

Figure 4.16: Sediment deposition pattern in the 50:2 pond model without berm at 1.56 L/s (prototype flow rate = 1 m^3/s), 147 mm flow depth and 17.8 dimensionless flow development time

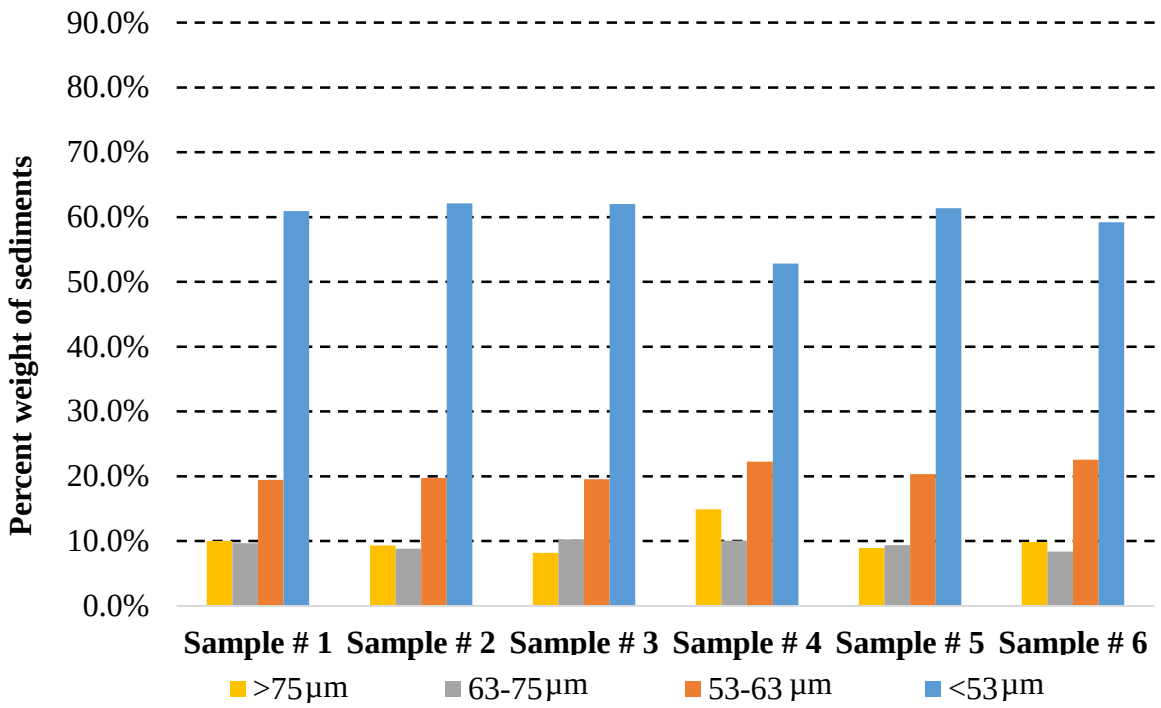

Figure 4.17: Particle size distribution of the deposited sediments in the 50:2 pond model without berm at 1.56 L/s (prototype flow rate = 1 m^3/s), 147 mm flow depth and 17.8 dimensionless flow development time

Table 4.6: Particle size distribution data of the deposited sediments in the 50:2 pond model without berm at 1.56 L/s (prototype flow rate = 1 m^3/s), 147 mm flow depth and 17.8 dimensionless flow development time

Sample #	Sample size (g)	% of total weight			
		< 53 µm	53-63 µm	63-75 µm	> 75 µm
1	42.22	60.9	19.4	9.6	10.0
2	37.65	62.1	19.8	8.8	9.3
3	31.97	62.0	19.5	10.3	8.2
4	48.45	52.8	22.2	10.1	14.9
5	19.03	61.4	20.3	9.4	8.9
6	25.65	59.2	22.6	8.4	9.9

4.3.5 Tracer Tests and Sediment Deposition Pattern Tests with a Berm

Tracer tests were carried out in the 100:2 pond model with three different berm positions between 60 – 80% of the bed radius from center (the berm in the prototype was represented by an annular ring in the model). The RTD curves obtained from these tests at different positions of the berm were compared to each other to determine its best position. The dimensionless residence time and the cumulative residence time distribution curves are shown in Figure 4.18 and Figure 4.19, respectively. Table 4.7 shows the retention time parameters obtained from these curves. The representation of the berm within the model is shown in Figures 4.20, 4.21 and 4.28. The opening in the berm is about one twelfth the length of the total circumference of the berm.

It is seen that the RTD curves for all positions of the berm are very similar to each other. The baffle factors, Morril dispersion indices and the short-circuiting indices varied between 0.42 – 0.45, 3.8- – 3.9- and 0.16 – 0.18 respectively for the three positions of the berm. These small variations of the retention time parameters do not provide any clear indication about the best position of the berm.

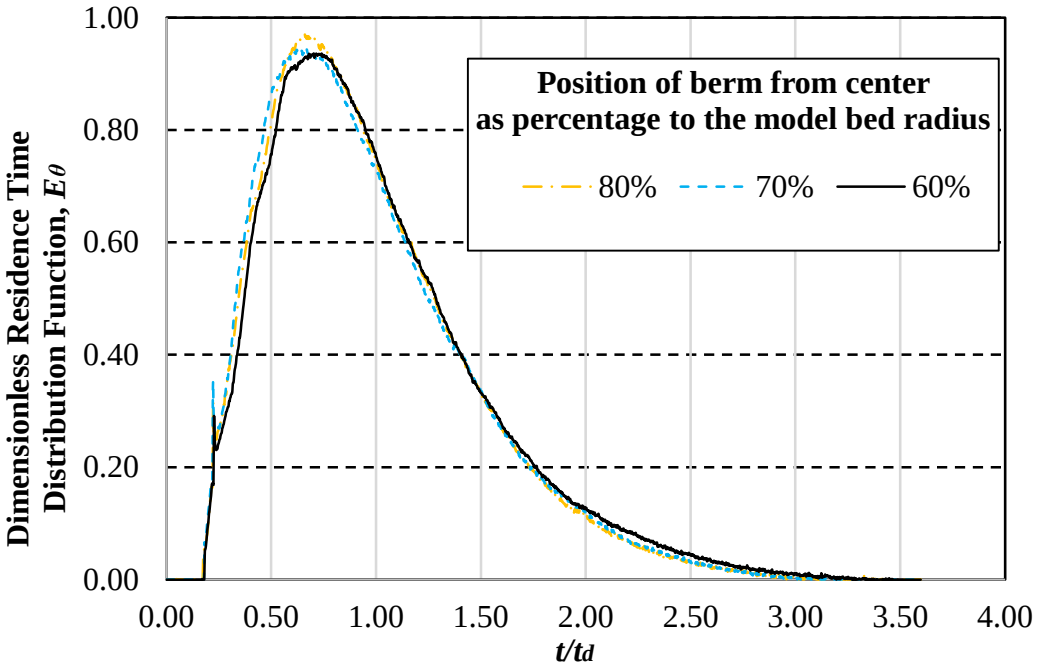

Figure 4.18: Dimensionless residence time distribution curves for the 100:2 pond model with berm at 60%, 70% and 80% of the model bed radius; tests carried out at 0.76 L/s (prototype flow rate = 4 m^3/s), 68 mm flow depth and 16.4 dimensionless flow development time

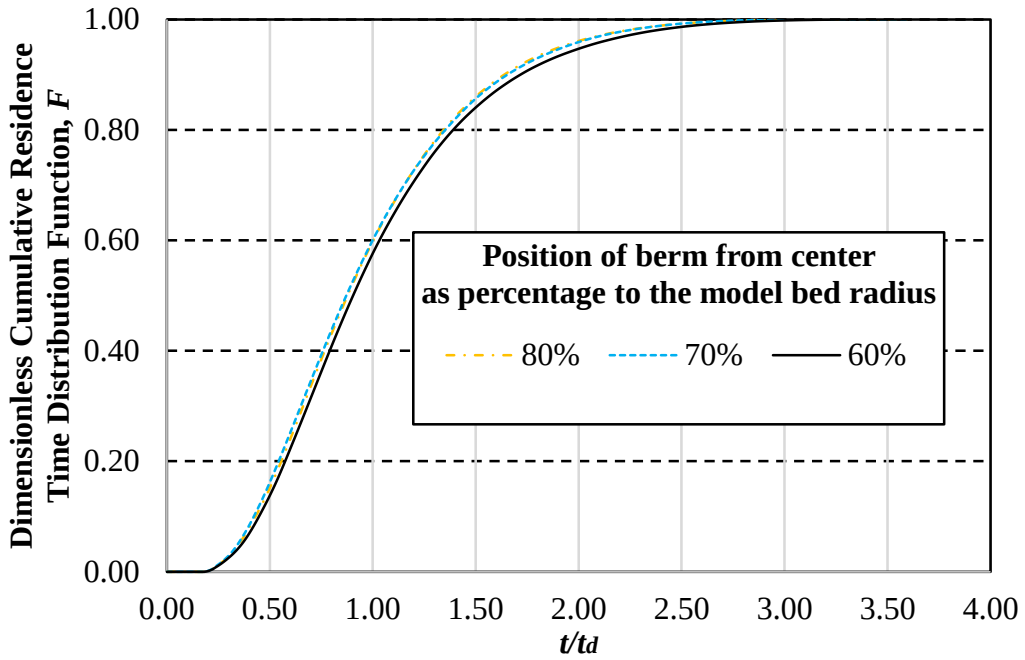

Figure 4.19: Dimensionless cumulative residence time distribution curves for the 100:2 pond model with berm at 60%, 70% and 80% of the model bed radius; tests carried out at 0.76 L/s (prototype flow rate = 4 m^3/s), 68 mm flow depth and 16.4 dimensionless flow development time

The sediment deposition pattern tests were carried out in the 100:2 pond model with berm positions at 60% and 80% of model bed radius in order to the better position and also to relate the RTD characteristics, obtained earlier with tracer tests, with the sediment deposition pattern of the pond. Test conditions were kept the same as the tracer tests with berms.

Figures 4.20 and 4.21 show the sediment deposition pattern in the 100:2 pond model with berm positions at 80% and 60% of the model bed radius respectively. The sediment deposition pattern with a berm at 70% bed radius was not recorded as the comparison of sediment deposition characteristics with a berm at 60% and 80% of the bed radius is sufficient to understand the effect of the berm on the deposition pattern. Comparison of these two deposition patterns show that more sediments have been deposited outside the berm in the case of its position at 60% of the bed radius. The flow pattern tests in the 100:2 model shown in Figure 4.6 showed that the width of the outer peripheral region having the longest flow path was about 350 mm measured at the water surface and its location was outside of 89% of the model bed radius from the center. Therefore the berm at 80% of the bed radius from center should be able to retain most of the sediments outside the berm. However, the opening in the berm is located near the inlet pipe with the intention that the flow could have the maximum flow path before entering inside the berm. With the berm at the

80% position the inflow jet creates a bottleneck with the wall of the berm near the opening and as a result a fraction of the inflow passes through the opening before even completing a full circle along the flow path. On the other hand, there is a wider space available between the inflow jet and the wall of the berm in the case of its position at 60% of the bed radius from the center. As a result, the flow can keep circulating outside the berm without interference from the inflow jet. The flow has a much longer flow path outside the berm when it is located at the 60% position. Therefore, it can deposit most of the sediments outside the berm. A significant amount of sediments were deposited inside the berm in the case of its position at 80% of the bed radius. The deposition of most of the sediments near the periphery is considered to be a major benefit of the Nautilus Pond™ as it would facilitate the operation and maintenance work throughout the lifetime of the pond. Therefore the berm position at 60% of model bed radius is considered to be the best position among those tested in this study.

Table 4.7: Retention time parameters in the 100:2 pond model with berm positions at 60%, 70% and 80% of the model bed radius; tests carried out at 0.76 L/s (prototype flow rate = 4 m^3/s), 68 mm flow depth and 16.4 dimensionless flow development time; injected tracer concentration = 1190 ppm and tracer volume = 30 mL

Parameters	Unit	Position of the berm from the center as percentage of model bed radius		
		80%	70%	60%
t_d	s	660	660	660
t_{10}/t_d		0.43	0.42	0.45
t_g/t_d		0.97	0.97	1.01
t_{50}/t_d		0.88	0.87	0.90
t_{90}/t_{10}		3.8	3.9	3.8
t_i/t_d		0.16	0.18	0.17
t_p/t_d		0.66	0.66	0.74
P		66%	51%	54%
m		34%	49%	46%
d		0%	0%	0%
R		95%	92%	95%

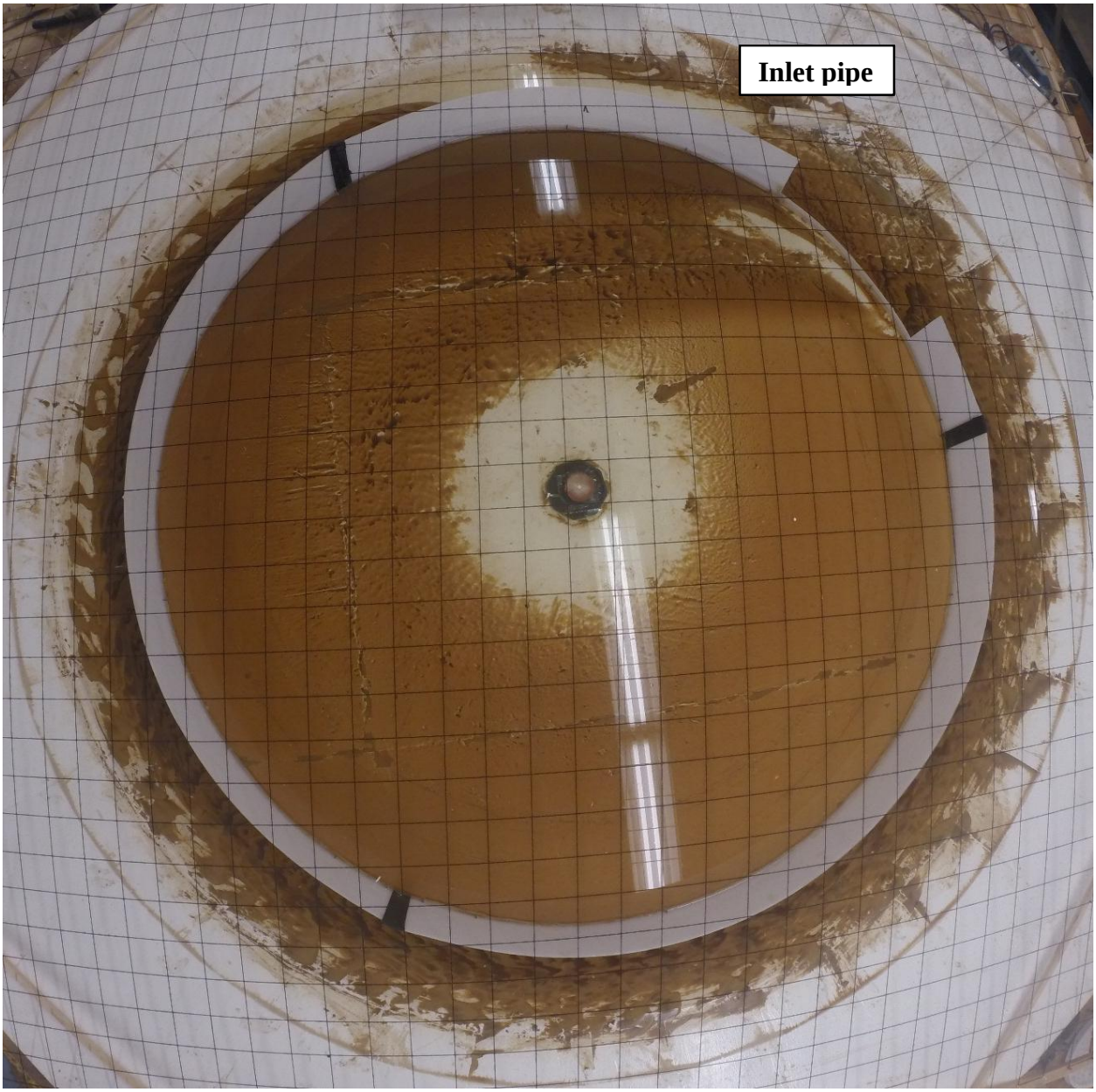

Figure 4.20: Sediment deposition pattern in the 100:2 pond model with berm position at 80% of the model bed radius; tests carried out at 0.76 L/s (prototype flow rate = 4 m^3/s), 68 mm flow depth and 16.4 dimensionless flow development time

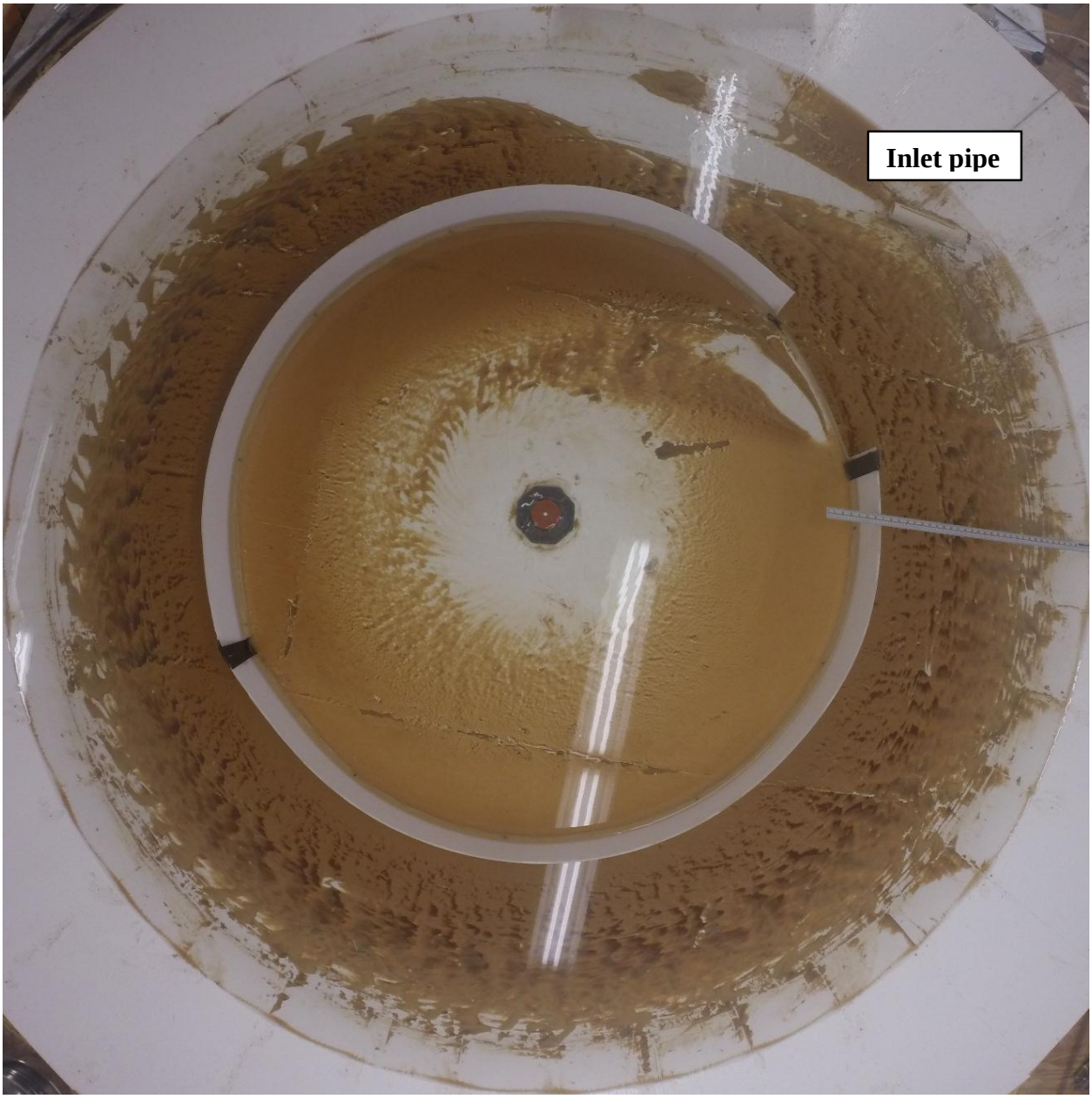

Figure 4.21: Sediment deposition pattern in the 100:2 pond model with berm position at 60% of the model bed radius; tests carried out at 0.76 L/s (prototype flow rate = 4 m^3/s), 68 mm flow depth and 16.4 dimensionless flow development time

Figure 4.22 and Table 4.8 show the particle size distribution of the deposited sediments in the 100:2 pond model with berm at 80% of the model bed radius. Similarly, Figure 4.23 and Table 4.9 show the particle size distribution when the berm was at 60% of model bed radius. The sample locations are shown in Figure 3.15(b).

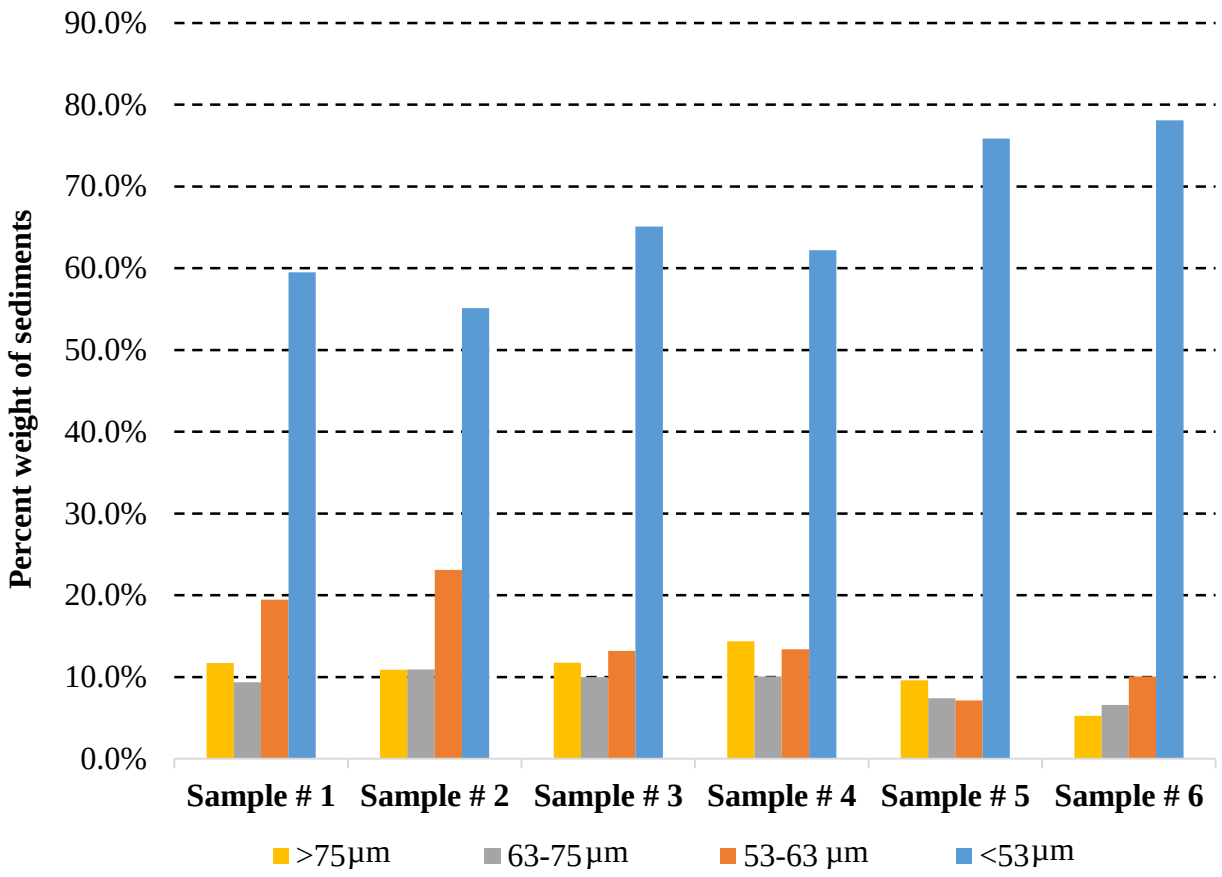

Figure 4.22: Particle size distribution of sediments deposited in the 100:2 pond model with berm position at 80% of the model bed radius; test carried out at 0.76 L/s (prototype flow rate = 4 m^3/s), 68 mm flow depth and 16.4 dimensionless flow development time

Table 4.8: Particle size distribution data of sediments deposited in the 100:2 pond model with berm position at 80% of the model bed radius; test carried out at 0.76 L/s (prototype flow rate = 4 m^3/s), 68 mm flow depth and 16.4 dimensionless flow development time

Sample #	Sample size (g)	% of total weight			
		< 53 µm	53-63 µm	63-75 µm	> 75 µm
1	30.97	59.5	19.4	9.4	11.7
2	31.79	55.1	23.1	10.9	10.9
3	34.98	65.1	13.2	10.0	11.7
4	26.47	62.2	13.4	10.0	14.4
5	24.00	75.9	7.1	7.4	9.6
6	13.71	78.1	10.1	6.6	5.3

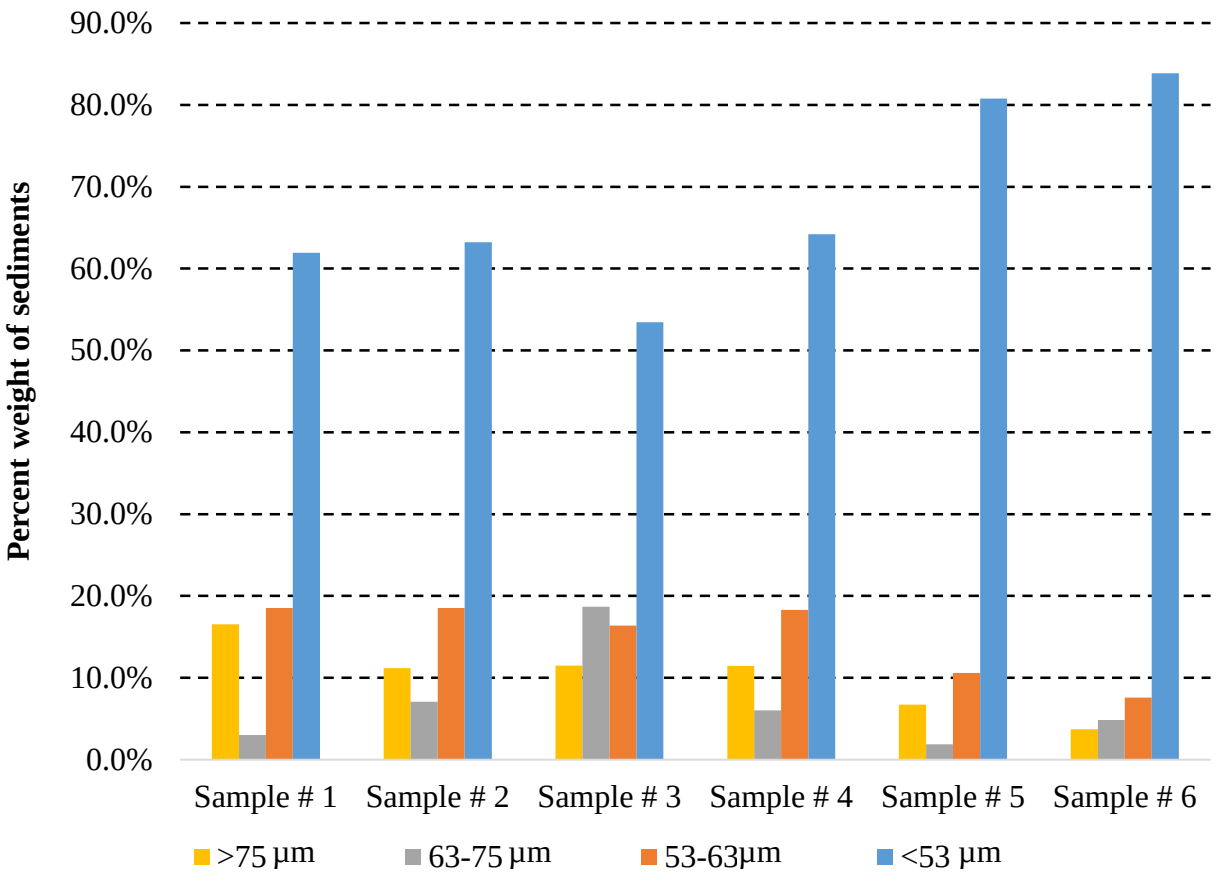

Figure 4.23: Particle size distribution of sediments deposited in the 100:2 pond model with berm position at 60% of the model bed radius; test carried out at 0.76 L/s (prototype flow rate = 4 m^3/s), 68 mm flow depth and 16.4 dimensionless flow development time

Table 4.9: Particle size distribution data of sediments deposited in the 100:2 pond model with berm position at 60% of the model bed radius; test carried out at 0.76 L/s (prototype flow rate = 4 m^3/s), 68 mm flow depth and 16.4 dimensionless flow development time

Sample #	Sample size (g)	% of total weight			
		< 53 µm	53-63 µm	63-75 µm	> 75 µm
1	53.14	61.9	18.5	3.0	16.5
2	64.65	63.2	18.5	7.1	11.2
3	63.01	53.5	16.4	18.7	11.5
4	49.69	64.2	18.3	6.0	11.5
5	29.04	80.8	10.6	1.9	6.7
6	20.82	83.9	7.6	4.9	3.7

When the berm was positioned at 80% of the model bed radius, sediments deposited outside the berm consisted of an average of 12.2% particles larger than 75 μm and 60.5% particles smaller than 53 μm. The sediments deposited inside the berm had 7.5% particles larger than 75 μm and 77% particles smaller than 53 μm in size. Therefore, the berm played an important role depositing coarser sediments mainly outside the berm. It provided a longer flow path outside the berm for some fractions of the inflow. When the berm was positioned at 60% of model bed radius, sediments deposited outside the berm had 12.7% of particles larger than 75 μm and 60.7% of particles smaller than 53 μm. These fractions are approximately same as the berm position at 80% of the model bed radius. However, in the case of the berm position at 60% of model bed radius, sediments deposited inside the berm had 5.2% particles larger than 75 μm and 82.4% particles smaller than 53 micron. The higher fraction of fine sediments deposited inside the berm at 60% of model bed radius indicates that the berm at this position functions better in keeping larger sized sediments outside the berm. This is likely due to the less constricted section between the inflow jet and the wall of the berm providing longer flow path for the most of the inflow fraction outside the berm with its position at 60% of the model bed radius. Therefore, the better position of the berm is at the 60% of the model bed radius from the center.

A comparison between Figure 4.14 and Figure 4.21 shows that more sediments traveled up to the high velocity vortex region at the center and perhaps escaped through the outlet when there was no berm present in the 100:2 pond. The berm (representing a berm in the prototype) caused most of the sediments to be deposited outside the berm making the pond more beneficial in terms of the operation and maintenance in future.

4.3.6 Comparison of the Residence Time Distribution Characteristics for the 100:2 Pond with and without the Berm

The RTD characteristics obtained for the 100:2 pond with a berm at 60% of the model bed radius was compared with the model without the berm. Figures 4.24 and 4.25 show the comparisons in terms of the dimensionless residence time distribution curve and the cumulative residence time distribution curve respectively. The test conditions and the flow development times were same in both cases.

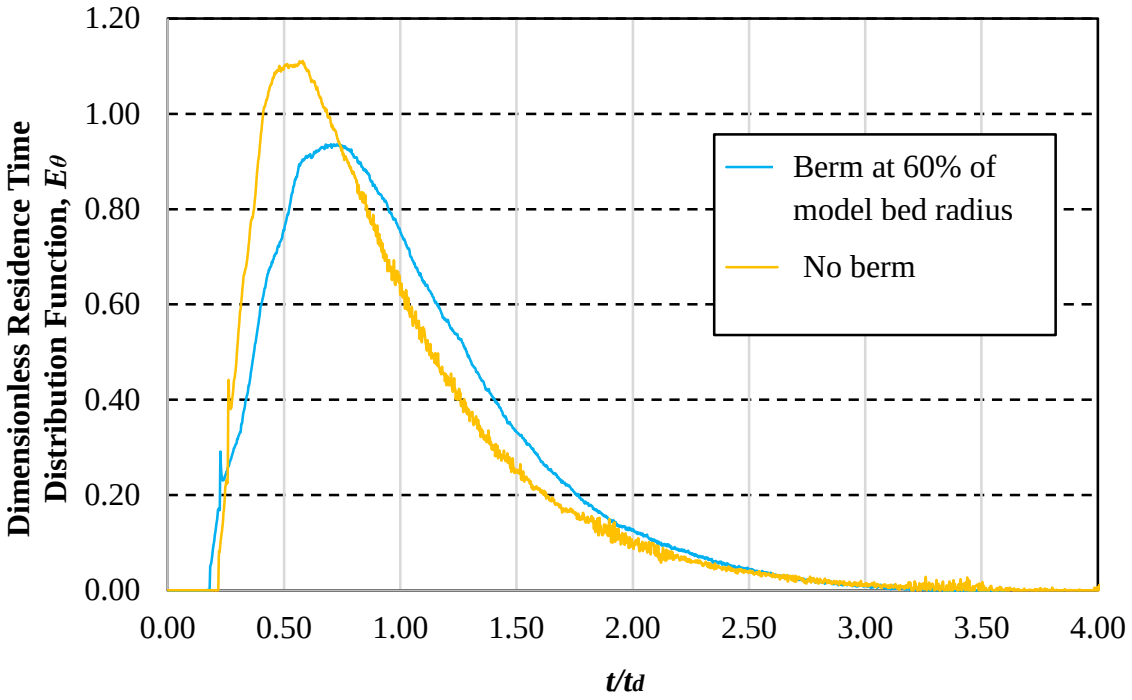

Figure 4.24: Comparison of the dimensionless residence time distribution curves for the 100:2 pond model with and without the berm at 0.76 L/s (prototype flow rate = 4 m^3/s) with 3 hr flow development time

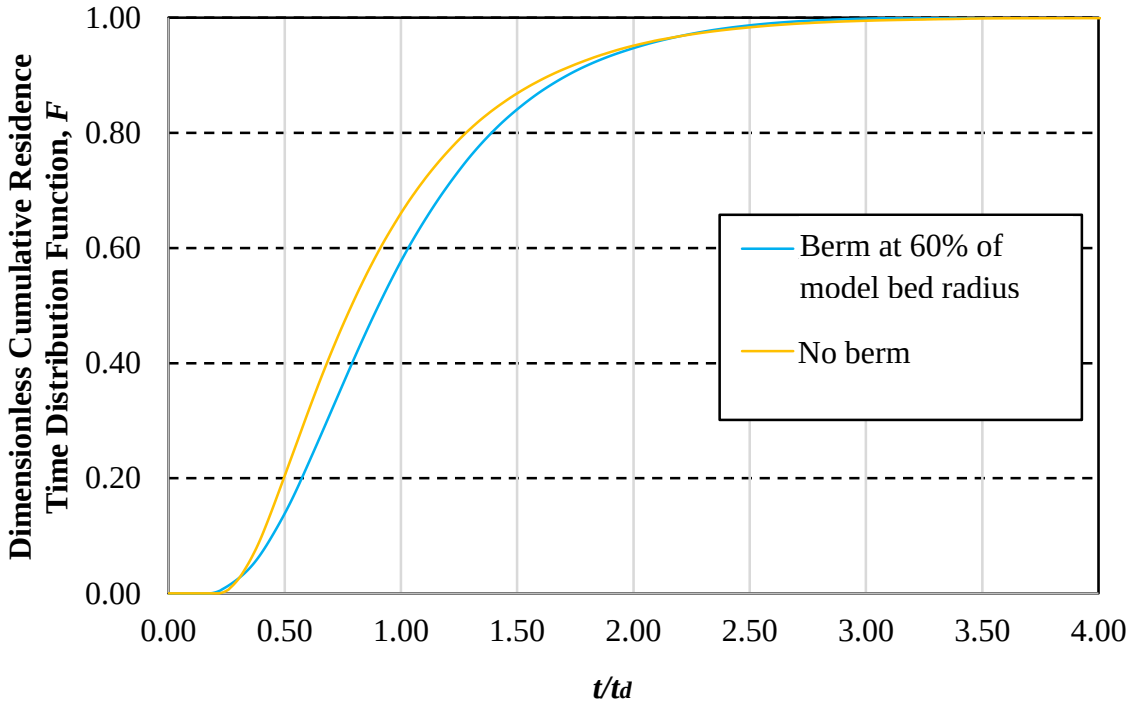

Figure 4.25: Comparison of the dimensionless cumulative residence time distribution curves for the 100:2 pond model with and without the berm at 0.76 L/s (prototype flow rate = 4 m^3/s) with 3 hr flow development time

The dimensionless RTD curves in Figure 4.24 show that the first tracer particle arrived more quickly to the outlet when there was a berm in the pond. The short-circuiting indices, shown in Table 4.1 and 4.7, were 0.20 and 0.17 for the 100:2 pond without and with the berm. This is contrary to one of the expectations of installing berm that it would actually increase the initial dye arrival time to the outlet by putting an impediment to the radial force acting toward the center and increase the travel time along the periphery. Though the berm does provide an impediment to the radial flow component, it also provides a more direct flow path toward the outlet through the berm opening and creates a spiral flow pattern inside the berm which has a much smaller path length than would have been available in that same area without the berm. After entering inside the berm, the flow moves away from the wall of the berm and has a spiral flow pattern of shorter path length. As a result the first tracer particle entering inside the berm reaches the outlet within a short time. However, the flow path length outside of the berm also increases since the flow can stay a longer time outside the berm and circulate along the periphery without a significant influence of the radial force component. Therefore the peak of the dimensionless residence time distribution curve can be found at a later time when the berm is installed in the pond. The parameter representing the time to peak of the RTD curve is 23% higher in the case of the berm in the pond. The baffle factor increased from 0.41 to 0.45 and the plug flow fraction increased from 37% to 54% in the case of the berm installed around the outlet. The dispersion and mixing decrease with the berm around the outlet. This is represented by the Morril dispersion index decreasing from 4.1 to 3.8 and the mixed flow fraction decreasing from 56% to 46% when there is berm at the 60% of the model bed radius from the center. These results indicate that the berm provides some improvement over the RTD characteristics of the 100:2 pond that would increase the water quality of the pond outflow. However, a cost-benefit analysis of installing a berm in a real pond and providing increased maintenance for removal of the additional settled solids over the pond life cycle in relation to improved outlet water quality would be required to provide a clearer picture whether the benefits outweigh the costs.

4.3.7 Tracer Tests with Berm in the 50:2 Pond Model

A tracer test was carried out in the 50:2 pond model with a berm placed at 60% of the model bed radius from the center keeping the test conditions the same as used for the design of the pond without the berm. The dimensionless flow development time was kept at 17.8; approximately

same as the test with berm in the 100:2 pond model. Figures 4.26 and 4.27 show the dimensionless residence time and the cumulative residence time distribution curves respectively. These were also compared with the RTD curves in the 50:2 pond without a berm around the outlet. Table 4.10 shows the retention time parameters obtained from the RTD curves.

A comparison between the RTD curves in 50:2 pond model with and without the berm shows that the first tracer particle arrives at the outlet at a later time in the pond when there is an berm around the outlet. As a result the short-circuiting index in the Table 4.10 is 0.11 when there is a berm in the pond whereas it is 0.04 when there is no berm in the 50:2 pond. The width of the transition region between the outer peripheral area and the high velocity central area being too short in the 50:2 pond, as described in Section 4.3.2, the first tracer particle reaches to the outlet very quickly if there is no berm in the pond. The berm works as a barrier to the short-circuiting flow and increase the flow path length significantly. The baffle factor increased by about 43%, from 0.23 to 0.33, due to the increased flow path length. The peak of the dimensionless RTD curve was higher and the time required for the occurrence of peak in the 50:2 pond was longer when the berm was installed in the pond. This indicates that most of the flow kept circulating outside the berm multiple times before entering inside the berm and reaching the outlet together. The RTD curve was more spread out for the case with no berm indicating higher dispersion in the flow. The Morril dispersion index decreased from 8.5 to 5.2 when the berm was installed in the pond. The plug flow fraction increased from 22% to 38% and the mixed flow fraction decreased from 76% to 60% due to the berm as it works as a barrier to the radial flow component and increased tangential flow component outside the berm increasing the flow path significantly. The dead space fraction increased from 2% to 3% due to the berm in the pond. This is likely caused by the additional friction between the flow and the wall of the berm.

The effectiveness of berm also depends on the aspect ratio of the pond. The berm in the 50:2 pond works more effectively in improving RTD characteristics than the berm in the 100:2 pond. The flow path length in the 100:2 pond is significantly longer than the 50:2 pond when there is no berm in the pond. The berm cannot increase the flow length as much for the 100:2 pond as it does for the 50:2 pond. As a result the improvements in the RTD characteristics, represented by the retention time parameters shown in Table 4.10, is more significant in the 50:2 than the 100:2 pond when the berm is installed in the pond.

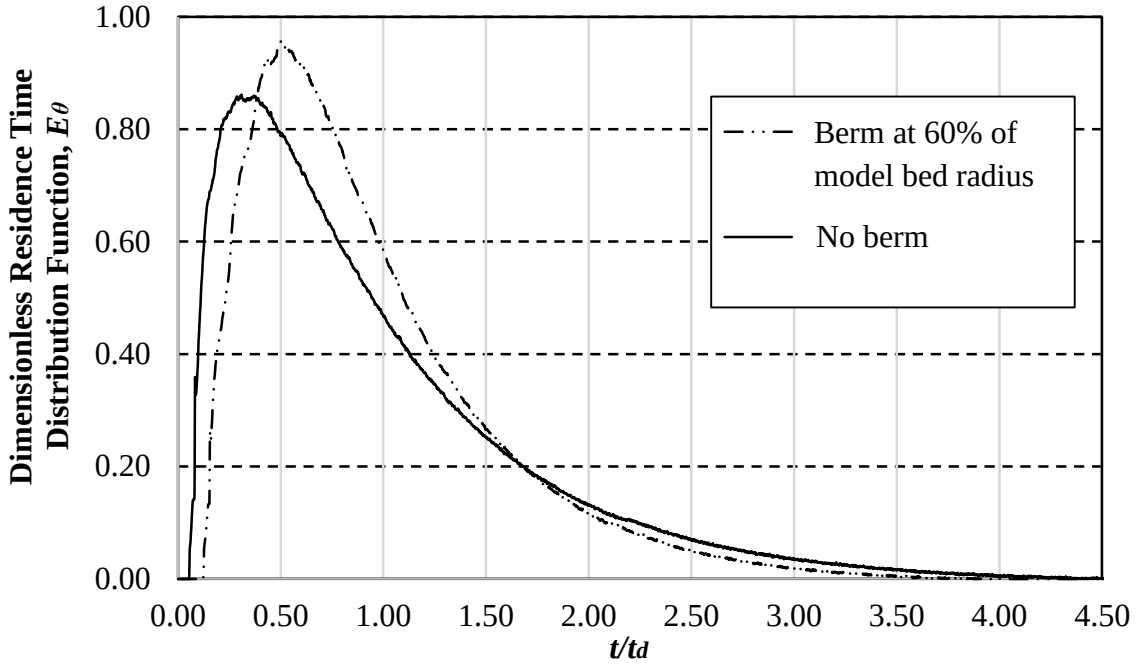

Figure 4.26: Dimensionless residence time distribution curves for the 50:2 pond with and without the berm at 1 m^3/s prototype flow rate with 4 hr flow development time

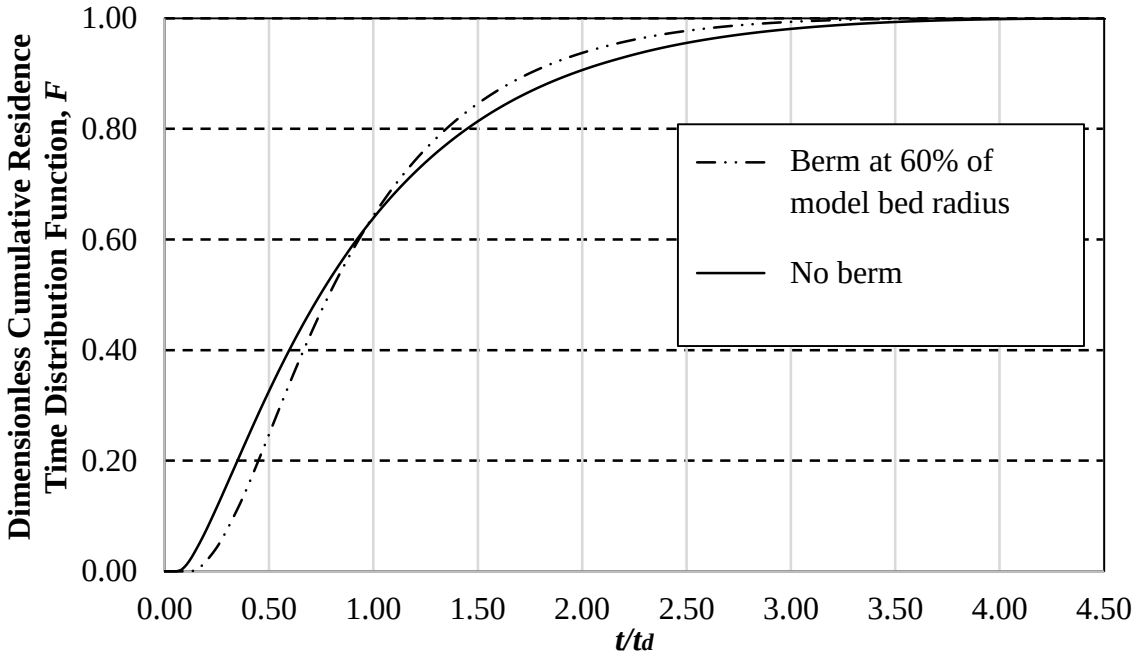

Figure 4.27: Dimensionless cumulative residence time distribution curves for the 50:2 pond with and without the berm at 1 m^3/s prototype flow rate with 4 hr flow development time

Table 4.10: Retention time parameters for the 100:2 and 50:2 pond models with and without berm around the outlet

Parameters	Unit	50:2 pond model		100:2 pond model	
		Berm at 60% of bed radius	No berm	Berm at 60% of bed radius	No berm
t_f	hr	4	4	3	3
t_f/t_d		18.9	17.8	16.4	17.2
Q	L/s	1.55	1.56	0.76	0.76
h	mm	139	147	68	65
C	ppm	2380	2380	1190	1190
V	mL	50	50	30	30
t_d	s	760	811	660	627
t_{10}/t_d		0.33	0.23	0.45	0.41
t_g/t_d		0.93	0.94	1.01	0.93
t_{50}/t_d		0.79	0.74	0.90	0.81
t_{90}/t_{10}		5.2	8.5	3.8	4.1
t_i/t_d		0.11	0.04	0.17	0.20
t_p/t_d		0.50	0.31	0.74	0.60
P		37%	22%	54%	37%
m		60%	76%	46%	56%
d		3%	2%	0%	8%
R		114%	104%	95%	81%

4.3.8 Sediment Deposition Pattern in the 50:2 Pond Model with Berm

Figure 4.30 shows the sediment deposition pattern in the 50:2 pond model with berm at the 60% of the model bed radius. The test conditions were kept the same as used for the test with no berm in the pond. This deposition pattern is almost similar to the pattern observed for the 50:2 pond without berm, as shown in Figure 4.17. However, the high velocity vortex region at the center, where no sediments deposit, is slightly smaller in size when there is berm around the outlet. Therefore, more areas of the pond become effective in depositing sediments. This might be caused by a reduction of the radial velocity component in the flow.

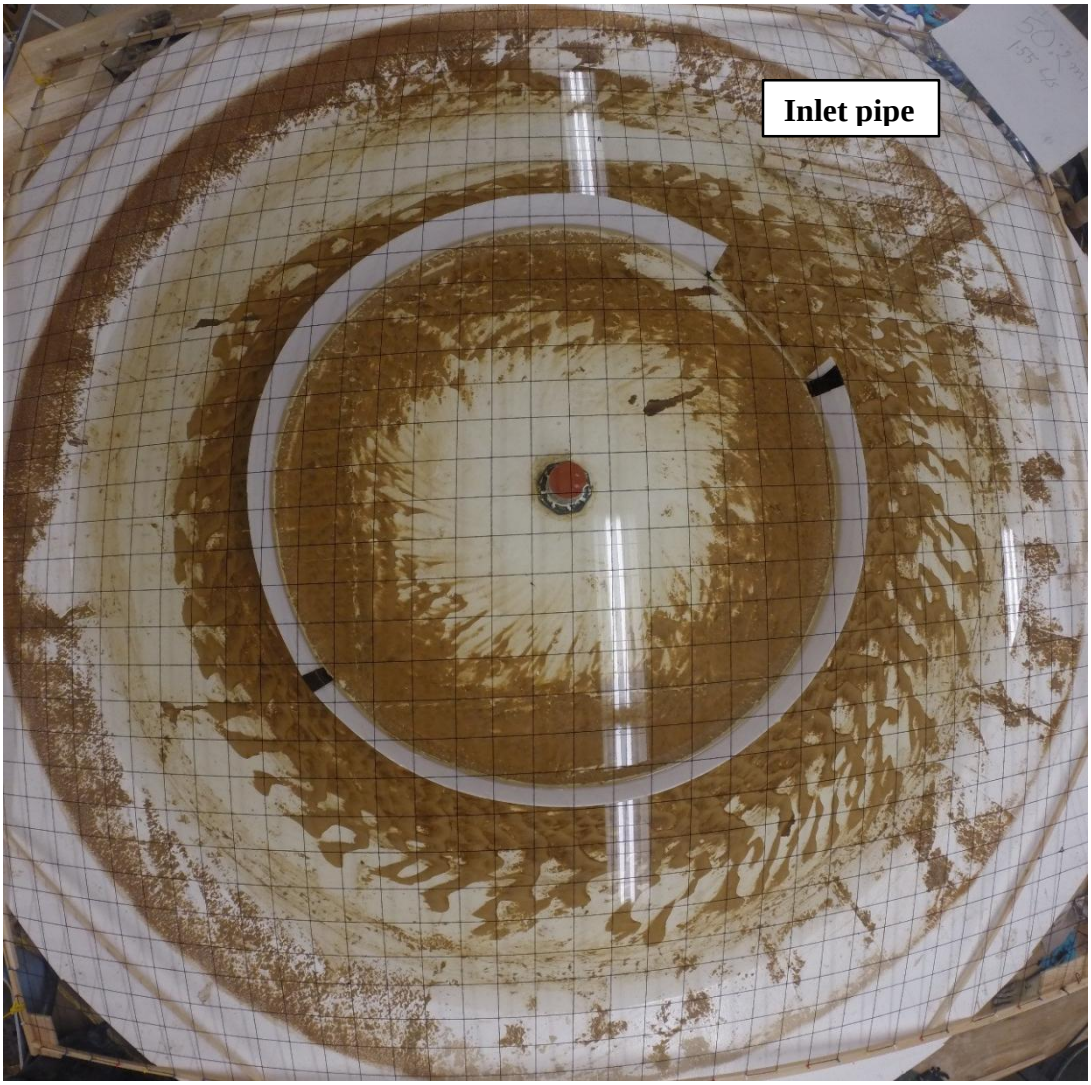

Figure 4.28: Sediment deposition pattern in the 50:2 pond model with berm position at 60% of the model bed radius; tests carried out at 1.55 L/s (prototype flow rate = 1 m^3/s), 139 mm flow depth and 18.9 dimensionless flow development time

Sieve analysis was carried out with the samples of deposited sediments in the 50:2 pond model collected from both outside and inside the berm. Figure 4.29 and Table 4.11 show the particle size distribution of the deposited sediment samples. Sediments deposited outside the berm consist of an average 12.8% of particles larger than 75 µm and 56.9% smaller than 53 µm. There were 10.5% particles larger than 75 µm and 62.9% particles smaller than 53 µm inside the berm. The differences of the particle size distribution between inside and outside the berm is not significant to conclude that the berm kept most of the coarser sediments outside the berm. This result is in sharp contrast to the sediment deposition pattern in the 100:2 pond with berm where the deposited sediments inside the berm consisted of 82.5% particles smaller than 53 µm and it was only 60.5% outside the berm.

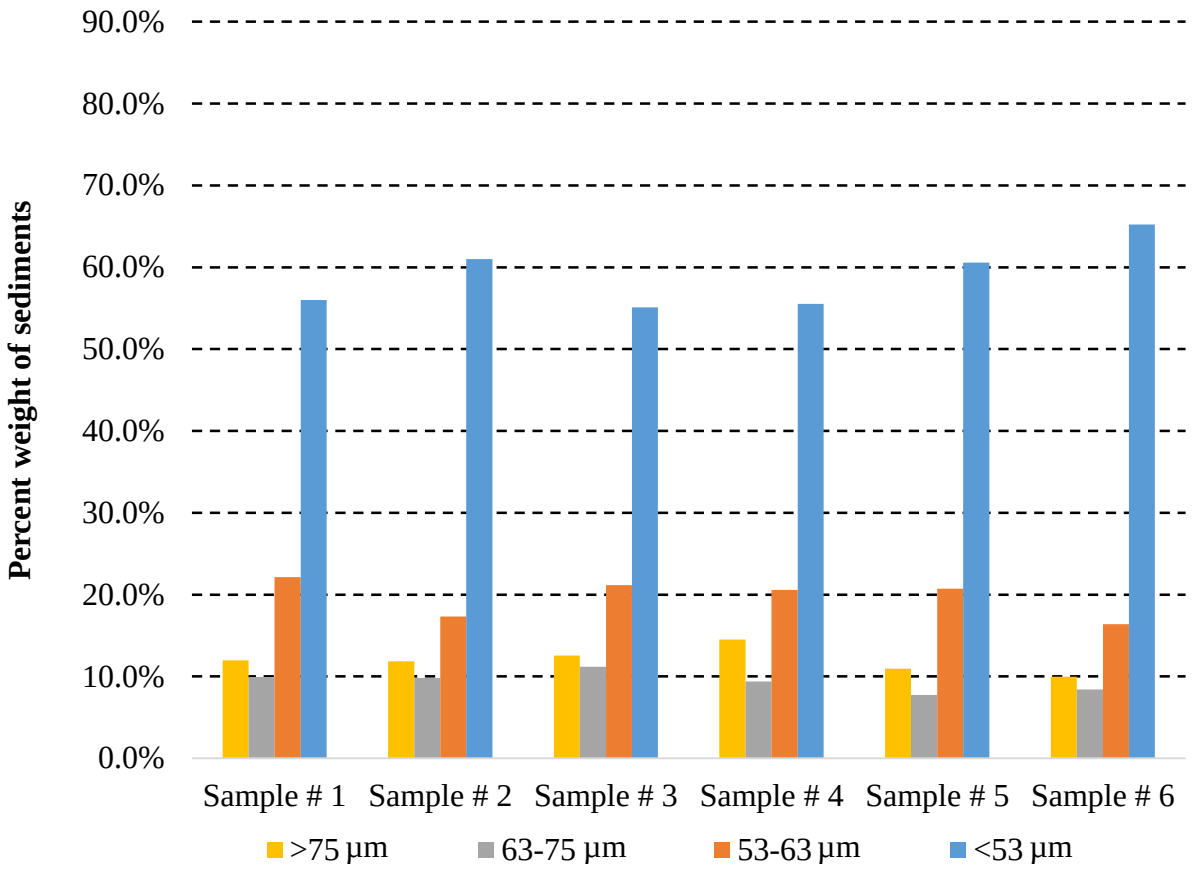

Figure 4.29: Particle size distribution of deposited sediments in the 50:2 pond model with berm at 60% of the model bed radius; flow rate = 1.55 L/s, depth = 139 mm and dimensionless flow development time = 18.9

Table 4.11: Particle size distribution data of deposited sediments in the 50:2 pond model with berm at 60% of the model bed radius; flow rate = 1.55 L/s, depth = 139 mm and dimensionless flow development time = 18.9

Sample #	Sample size (g)	% of total weight			
		< 53 µm	53-63 µm	63-75 µm	> 75 µm
1	44.30	56.0	22.1	9.9	12.0
2	43.83	61.0	17.3	9.8	11.9
3	42.97	55.1	21.2	11.2	12.6
4	62.76	55.5	20.6	9.4	14.5
5	43.86	60.6	20.7	7.8	10.9
6	45.13	65.2	16.4	8.4	10.0

4.4 Estimation of Uncertainty

The tracer tests carried out in the physical models of the Nautilus Ponds™ are experimental in nature and the results are subject to measurement errors. Therefore uncertainty estimations are required to assess the accuracies of the RTD curves and retention time parameters obtained from the tracer studies. The methods described in Topping (1957) were used for error estimation in this study. The calculated errors represent the worst case scenarios possible.

The major input parameters of a tracer study required for the calculation of RTD functions were flow rate, flow depth, model geometry, tracer concentration readings in the outflow and elapsed time. The flow rate was measured with a magnetic flow meter which has an accuracy of about ±0.01%. Considering a small variation of flow rate throughout the test duration, the accuracy in the flow rate can be considered to be ±1.0%. The flow depth was accurate within ±1 mm. If the model bed diameter is considered to be accurate within ±5 mm, the error in the 100:2 pond model volume at 0.76 L/s flow rate and 65 mm flow depth becomes ±4.3%. The theoretical retention time being the ratio of flow volume to the flow rate becomes ±5.3%.

The length of each time step was 1 s and the LabVIEW software recorded concentration readings at 1 s intervals in the computer. Therefore the time step length was considered to have no errors. However the time lag between the outlet sampling point and the fluorometer in the tracer

test was considered to have an error of about 2 s. The time lag was measured by injecting some tracer near the outlet and recording the time required to get a response in the LabVIEW. The 2 s error in measuring the time lag is the combination of instrumental error of stopwatch and the measurement error.

The total error in the measured concentration readings were considered to be about ±10%. The errors in the concentration readings are the cumulative errors originated from the instrumental error of the fluorometer, calibration error and the sampling error of the outflow. After calibration, the fluorometer was checked with a few other different concentrations and the maximum calibration error in concentration was found to be about 6%. Considering the small instrumental error in the fluorometer and the error due to the sample tracer concentration in the outflow, possibly, being slightly different than the cross-sectional average, the maximum error in the tracer concentration reading of the fluorometer was considered to be about ±10%.

The application of uncertainty theory described in Topping (1957) in the tracer tests results of 100:2 pond model at 0.76 L/s flow rate, 65 mm flow depth and 12 hr flow development time produces an error of about ±20% in RTD and CRTD function values at different time steps. The effect of these errors in the uncertainty of corresponding dimensionless time can be used to calculate the errors in the retention time parameters.

The error in the short-circuiting index was found to be ±7.0%. The errors in the concentration readings have negligible effect on the short-circuiting index as the short-circuiting index only represents the arrival of the first tracer particle to the outlet. The baffle factor, however, is more affected by the errors in concentration readings as it represents the time for the 10% of total tracer mass to leave the pond. Considering the errors associated with $F = 0.1$ and errors in the dimensionless time, the error in the baffle factor was found to be about 12%.

CHAPTER 5: CONCLUSIONS AND RECOMMENDATIONS

5.1 Conclusions

The first objective of this study was to investigate flow development times, residence time distribution characteristics and flow patterns under a steady state inflow in hydraulic models of the 100:2 and 50:2 Nautilus Pond™. The RTD characteristics and the flow patterns obtained from tracer tests and flow visualization tests carried out over a wide range of dimensionless flow development times, 0.9 – 70.4, in both models show that the flow development time has little effect on the residence time distribution characteristics and flow pattern of the Nautilus Pond™.

In the 100:2 pond model, the shape of the RTD curves obtained from eight tracer tests carried out at a 0.76 L/s flow rate with 1.0 – 68.4 dimensionless flow development times are similar to each other. The baffle factors were found in the range of 0.38 – 0.43, short-circuiting indices 0.18 – 0.22, Morril dispersion indices 4.0 – 4.3, plug flow fractions 36 – 39%, mixed flow fractions 56 – 60% and dead space fractions 1 – 8%. The close similarities of the shape of the RTD curves, narrow ranges of retention time parameter and lack of any general trend in those results over the range of flow development times tested show that there is very little or no effect of flow development time on the RTD characteristics of the 100:2 pond.

In the 50:2 pond model, RTD curves obtained from six tracer tests carried out at 1.56 L/s flow rate with 0.9 – 70.4 dimensionless flow development times show that these curves almost superimpose on each other. The baffle factors, short-circuiting indices, Morril dispersion indices, plug flow fractions, mixed flow fractions and dead space fractions was in the range of 0.21 – 0.24, 0.04 – 0.06, 8.3 – 9.0, 21 – 24%, 74 – 78% and 0 – 4% respectively. The narrow ranges of the retention time parameters for a wide range of flow development times show that the flow development time has little effect on the RTD characteristics of the 50:2 pond.

The flow patterns in both the 100:2 and 50:2 pond model obtained from flow visualization tests also showed little variation with different flow development times. Upon entering the pond the flow circulates along its outer periphery. The flow path length and the travel time are the longest in this region. The width of this outer peripheral region is about 22% of top flow radius in

the 100:2 pond and 50% of top flow radius in the 50:2 pond. Next, due to the effect of a radial velocity component, the flow moves to the middle transition region. The radial velocity component in this region becomes increasingly dominant over the tangential component of velocity as the flow moves toward the center. As a result, a spiral flow pattern is formed in this region. The width of this middle transition region is about 60% and 24% of the top flow radius in the 100:2 and 50:2 pond respectively. Lastly the flow moves to a central region around the outlet. This central region is characterized by a high velocity vortex and the flow moving into this area exits the pond very quickly. The radius of this central region is about 18% of top flow radius in the 100:2 pond and 26% of top flow radius in the 50:2 pond.

The second objective of this study was to investigate the effect of flow rate on the RTD characteristics of both the 100:2 and 50:2 ponds. In order to accomplish this objective, tracer tests were carried out in the 100:2 pond model at five flow rates between 0.1 – 1.0 L/s keeping the dimensionless flow development times approximately same; $t_f/t_d \approx 69$. The shapes of the RTD curves were significantly different for different flow rates. There were multiple peaks in the RTD curves for low flow rates; the highest peak occurred for 0.10 L/s and the lowest peak occurred for 1.0 L/s flow rate. The short-circuiting indices decreased from 0.28 to 0.10, a 64% decrease, and the baffle factor decreased from 0.40 to 0.30, a 25% decrease, when the flow rate increased from 0.10 to 1.0 L/s in the 100:2 pond model. The Morril dispersion index and the mixed flow fraction increased from 4.1 to 6.2 and from 53% to 66% respectively due to the increase of flow rate from 0.10 L/s to 1.0 L/s. The dead space fraction varied in the range of 1 – 14% in the 100:2 pond model.

In the 50:2 pond model, four tracer tests were carried out with flow rates between 0.20 – 1.56 L/s keeping the same dimensionless flow development time as the 100:2 pond model. The peak of the dimensionless RTD curve for 0.20 L/s was sharply higher than the other flow rates. The short-circuiting index decreased from 0.26 to 0.04, the baffle factor decreased from 0.33 to 0.21, the Morril dispersion index increased from 4.7 to 9.0 and the mixed flow fraction increased from 43% to 74% due to the increase of flow rate from 0.20 to 1.56 L/s in the 50:2 pond model. The dead space fraction at 0.20 L/s was found to be significantly higher, 32%, as compared to the 3 – 6% fraction in case of flow rates 0.80 – 1.56 L/s. The plug flow fractions were in the range of 22 – 29% for these flow rates.

The third objective of this study was to investigate the sediment deposition patterns in both the 100:2 and 50:2 ponds for the deposition of 50 μm particles. The deposition pattern in the 100:2 pond model obtained from a test carried out at 0.76 L/s flow rate with ground walnut shells showed that a higher quantity of sediments deposited per unit area in the outer peripheral region of the model bed. There was almost a uniform deposition of sediments in the middle transition region of flow. Sediment deposition did not occur at all in the central region around the outlet dominated by the high velocity vortex. The area of this central region is about 4.4% of the total area of the pond bed. The sediment deposition also did not occur near the inlet due to the high velocity inflow jet. The particle size distribution of the sediments deposited within the 60% of model bed radius from the center in the 100:2 pond model showed that there were 83.8% of sediments smaller than 53 μm, 8.7% between 53 – 63 μm, 3.7% between 63 – 75 μm and 3.8% larger than 75 μm in size. Sediments deposited outside the 60% of bed radius from the center consisted of 44 – 64% sediments smaller than 53 μm, 10 – 17% between 53 – 63 μm, 5 – 12% between 63 – 75 μm and 14 – 37% particles larger than 75 μm in size. Therefore, the larger sized sediment fractions deposited mainly in the outer peripheral region and the smaller sized sediments deposited more inside of the 60% of bed radius from the center.

The sediment deposition pattern in the 50:2 pond without a berm showed that only a small amount of sediments deposited near the outer peripheral region due to the high velocity inflow jet. The sediment mainly deposited between 44 – 84% of the model bed radius from the center. There was a central region around the outlet with 12.3% of total bed area where no sediment deposition occurred at all. The particle size distribution of the sediments deposited in the different areas of the 50:2 pond model did not show any significant differences. There were 53 – 62% particles smaller than 53 μm, 19 – 22% particles between 53 – 63 μm, 9 – 10% particles 63 – 75 μm and 8 – 15% particles larger than 75 μm in size deposited inside the 60% of the model bed radius from the center. The sediments deposited outside the 60% of the model bed radius composed of 59 – 61% particles smaller than 53 μm, 20 – 23% particles between 53 – 63 μm, 8 – 9% particles between 63 – 75 μm and 9 – 10% particles larger than 75 μm in size.

The fourth objective of this study was to determine the best of three positions of a berm to improve the flow and the residence time distribution characteristics of the pond. The berm position at 60% of the model bed radius, as measured from the pond center, was considered as the best of

the three positions tested. The RTD curves obtained for the 100:2 pond model with berm at 60%, 70% and 80% of the model bed radius from the center were very similar to each other. The short-circuiting indices, baffle factors and Morril dispersion indices were in the range of 0.16 – 0.18, 0.42 – 0.45 and 3.8 – 3.9 respectively. The close ranges of these retention time parameters did not provide any clear indication about the best position of the berm. However, the sediment deposition pattern in the 100:2 pond model with an berm position at 60% and 80% of the model bed radius showed that the most of the sediments deposited outside the berm in case of its position at 60% of model bed radius from the center. Considering the operation and maintenance benefits for most sediments depositing outside the berm, the 60% position was considered as the best.

The fifth objective of this study was to investigate the effect of a berm at its best position on the sediment deposition pattern. As mentioned earlier, a berm at the 60% of bed radius position in the 100:2 pond kept most of the sediments outside the berm. The particle size distribution of the deposited sediments outside the berm showed 54 – 64% particles smaller than 53 μm, 16 – 19% particles in between 53 – 63 μm, 3 – 18% particles in between 63 – 75 μm and 11 – 17% particles larger than 75 μm in size. The sediments deposited inside the berm in the 100:2 pond composed of 81 – 84% particles smaller than 53 μm, 8 – 11% particles between 53 – 63 μm, 2 – 5% particles between 63 – 75 μm and 4 – 7% particles larger than 75 μm in size.

In the 50:2 pond model with an berm at 60% of model bed radius from the center, a large proportion of sediments entered and deposited inside the berm. However, there was no significant difference in the particle size distribution of the sediments deposited inside and outside of the berm. There were 55 – 61% particles smaller than 53 μm, 17 – 22% particles in between 53 – 63 μm, 9 – 11% particles in between 63 – 75 μm and 12 – 15% particles larger than 75 μm in size deposited outside the berm. The deposited sediments inside the berm were composed of 61 – 65% particles smaller than 53 μm, 16 – 21% particles 53 – 63 μm, 8% particles 63 – 75 μm and 10 – 11% particles larger than 75 μm in size.

5.2 Future Research

Based on the results of this research, the following recommendations can be considered as guidance for future research on the Nautilus Pond™:

- The radial velocity component toward the outlet, a secondary flow, has significant effect on the flow pattern, the RTD characteristics, and the sediment deposition pattern of the pond. A strong radial velocity component creates a spiral flow pattern of short flow-path length and a dominant tangential velocity component creates circular flow pattern of long flow path-length. Therefore, future studies should be undertaken to measure the actual velocity at different radial positions in the pond model and to minimize the radial velocity component of the flow within the Nautilus Pond^{TM}.

- The inflow jet velocity is important for the efficient functioning of the pond. A high velocity inflow jet prevents sediment deposition along its flow path before dissipating most of its kinetic energy whereas a low velocity inflow jet cannot drive the flow circulating around the periphery of the pond shortens the flow-path length. Future research should be conducted to determine an optimum range of inflow jet velocity and momentum required for more efficient functioning of the Nautilus Pond^{TM} for different aspect ratios.

- The sediment deposition study in this research was qualitative in nature. Future research could be based on quantitative measurements of the sediment deposition and retention within the pond to estimate sediment removal efficiency. .

- There are several components in the Nautilus Pond^{TM} for which the effects of size, shape and position on flow characteristics and sediment deposition have not been investigated and are unknown at this stage. These components include side slope, size and location of the berm opening, presence or absence of a sill in the berm opening, inlet and outlet pipe diameters, inlet jet angle, and so on. Future research should focus on the geometry of each of these components separately and determine their effects on the pond performance.

REFERENCES

Abderrezzak, K.E.K., Moran, A.D., Mosselman, E., Bouchard, J.P., Habersack, H., and Aelbrecht, D. 2014. A physical, movable-bed model for non-uniform sediment transport, fluvial erosion and bank failure in rivers. Journal of Hydro-Environment Research, **8**(2): 95-114.

Acros Organics. 2011. Safety data sheet. Available from http://www.acros.com/DesktopModules/Acros_Search_Results/Acros_Search_Results.aspx?Type=WERCS&URL=http%3a%2f%2fwercs.acros.com%2fwercsdata%2fresults.aspx%3fX__LANGUAGE%3dEN%7cx__SKU%3dACR44697%7cx__PLANT%3dACR%7cx__SUBFORMAT%3dCLP1 [cited 23 March 2016].

Albers, C., and Amell, B. 2010. Changing the stormwater pond design game. In Proceedings of the NOVATECH Conference, Lyon, France, 27 June - 1 July 2010.

Ali, K.H.M., Hedges, T.S., and Whittington, R.B. 1978. A scale model investigation of the circulation in reservoirs. In Proceedings of the Institution of Civil Engineers, **65**(Part 2): 129-161.

Alkhaddar, R.M., Higgins, P.R., Phipps, D.A., and Andoh, R.Y.G. 2001. Residence time distribution of a model hydrodynamic vortex separator. Urban Water, **3**(1): 17-24.

American Society of Civil Engineers, ASCE. 2000. Hydraulic modeling: concepts and practice. ASCE manuals and Reports on Engineering Practice No.97. *Edited by* R. Arndt, P. Roberts, and T. Wahl. American Society of Civil Engineers, Reston, Virginia, USA.

Ansari, M.A., and Athar, M. 2013. Design parameters of vortex settling basin. Proceedings of the ICE – Water Management, **166**(5): 262–271.

ASTM C325-07(2014), Standard Guide for Wet Sieve Analysis of Ceramic Whiteware Clays, ASTM International, West Conshohocken, PA, USA, 2014, www.astm.org.

Athar, M., Kothyari, U.C., and Garde, R.J. 2002. Sediment removal efficiency of vortex chamber type sediment extractor. Journal of Hydraulic Engineering, **128**(12): 1051–1059.

Bishop, M.M., Morgan, J.M., Cornwell, B., and Jamison, D.K. 1993. Improving the disinfection detention time of a water plant clearwell. Journal of American Water Works Association, **85**(3): 68–75.

CALTRANS, Division of Environmental Analysis. 2004. BMP retrofit pilot program. California Department of Transportation, Report ID CTSW–RT–01–050, Sacramento, California, USA.

Chapokpour, J. 2011. Turbulent flow measurement in vortex settling basin. Iranica Journal of Energy & Environment, **2**(4): 382–389.

Clar, M.L., Barfield, B.J., and O'Connor, T.P. 2004. Stormwater best management practice design guide, Volume 3 Basin Best Management Practices. EPA/600/R-04/121B. United States Environmental Protection Agency, Washington, D.C., USA.

Comings, K.J., Booth, D.B., and Horner, R.R. 2000. Storm water pollutant removal by two wet ponds in Bellevue, Washington. Journal of Environmental Engineering, **126**(4): 321-330.

Crozes, G.F., Hagstrom, J.P., Clark, M.M., Ducoste, J., and Burns, C. 1999. Improving clearwell design for CT compliance. AWWA Research Foundation, American Water Works Association, Denver, Colorado, USA.

Danckwerts, P.V. 1953. Continuous flow systems: distribution of residence times. Chemical Engineering Science, **2**: 1–13.

Dodge, R.A. 1983. Model Similitude – Extended for Active Sediment Transport PAP-450. USBR Water Resources Research Laboratory. Denver, Colorado, USA.

Drake, J., and Guo, Y. 2008. Maintenance of wet stormwater ponds in Ontario. Canadian Water Resources Journal, **33**(4): 351-368.

Dunn, H.J., Pinsky, D.E., and Padmanabhan, M. 1991. A hydraulic investigation of flow patterns and disinfection requirements for a circular clearwell. *In* Proceedings of the 1991 Annual Conference, Philadelphia, Pennsylvania, USA, 23 - 27 June 1991, American Water Works Association, pp. 323-344.

Erickson, A.J., Weiss, P.T., and Gulliver, J.S. 2013. Optimizing stormwater treatment practices. Springer, New York, NY, USA.

Falconer, R.A., and Tebbutt, T.H.Y. 1986. A theoretical and hydraulic model study of a chlorine contact tank. Proceedings of the Institution of Civil Engineers, Part 2, **81**(6): 255–276.

Falconer, R.A., and Liu, S.Q. 1987. Mathematical model study of plug flow in a chlorine contact tank. Water and Environment Journal, **1**(3): 279-290.

Farrell, E.J., and Sherman, D.J. 2015. A new relationship between grain size and fall (settling) velocity in air. Progress in Physical Geography, **39**(3): 361-387.

Farjood, A., Melville, B.W., and Shamseldin, A.Y. 2015. The effect of different baffles on hydraulic performance of a sediment retention pond. Ecological Engineering, **81**: 228-232.

Ferrara, R.A., and Witkowski, P. 1983. Stormwater quality characteristics in detention basins. Journal of Environmental Engineering, **109**(2): 428-447.

Fischer, H.B., and Holley, E.R. 1971. Analysis of the use of distorted hydraulic models for dispersion studies. Water Resources Research, **7**(1): 46-51.

Fischer, H.B., List, E.J., Koh, R.C.Y., Imberger, J., and Brooks, N.H. 1979. Mixing in inland and coastal waters. Academic Press, San Diego, California, USA.

Fogler, H.S., and Brown, L.F. 1992. Distributions of residence times for chemical reactors. Elements of Chemical Reaction Engineering, 708-758.

Gain, W.S. 1996. The effects of flow-path modification on water-quality constituent retention in an urban stormwater detention pond and wetland system. Water-Resources Investigation Report 95-4297, U.S. Geological Survey, Tallahassee, Florida, USA.

Gharabaghi, B., Fata, A., Seters, T.V., Rudra, R.P., MacMillan, G., Smith, D. and Tesa, G. 2006. Evaluation of sediment control pond performance at construction sites in the Greater Toronto Area. Canadian Journal of Civil Engineering, **33**(11): 1335-1344.

Gill, T.W., and Pugh, C.A. 2009. Sediment transport similitude for scaled physical hydraulic modeling. In Proceedings of the 33rd IAHR Congress, Vancouver, Canada, 9–14 August 2009.

Gorrick, S., and Rodríguez, J.F. 2014. Scaling of sediment dynamics in a laboratory model of a sand-bed stream. Journal of Hydro-Environment Research, **8**(2): 77-87.

Grayman, W.M., Deiniger, R.A., Green, A., Boulous, P.F., Bowcock, R.W., and Godwin, C.C. 1996. Water quality and mixing models for tanks and reservoirs. Journal of American Water Works Association, **88**(7): 60–73.

Greb, S.R., and Bannerman, R.T. 1997. Influence of particle size on wet pond effectiveness. Water Environment Research, **69**(6): 1134-1138.

Gursul, I., Lusseyran, D., and Rockwell, D. 1990. On interpretation of flow visualization of unsteady shear flows. Experiments in Fluids, **9**(5): 257-266.

Hai-feng, L., Hong-xun, C., Zheng., M., and Yi, Z. 2009. Formation and influencing factors of free surface vortex in a barrel with a central orifice at bottom. Journal of Hydrodynamics, **21**(2): 238 - 244.

Hart, F.L. 1979. Improved hydraulic performance of chlorine contact chambers. Jounal of Water Pollution Control Federation, **51**(12): 2868–2875.

Heinking, G., and Wilcoxon, N. 1985. Use of a swirl concentrator management for combined sewer overflow management. Jounal of Water Pollution Control Federation, **57**(5): 398–402.

Ho, J., Coonrod, J., Gill, T., and Mefford, B. 2010. Case study: Movable bed model scaling for bed load sediment exclusion at intake structure on Rio Grande. Journal of Hydraulic Engineering, **136**(4): 247-250.

Holland, J.F., Martin, J.F., Granata, T., Bouchard, V., Quigley, M., and Brown, L. 2004. Effects of wetland depth and flow rate on residence time distribution characteristics. Ecological Engineering, **23**(3): 189–203.

Hurtig, K.I. 2003. Hydraulic modelling of water treatment storage tanks for disinfection contact time. M.Sc. thesis, Department of Civil and Environmental Engineering, University of Alberta, Edmonton, Alberta, Canada.

Hunt, W.F., Smith, J.T., Jadlocki, S. J., Hathaway, J.M., and Eubanks, P.R. 2008. Pollutant removal and peak flow mitigation by a bioretention cell in urban Charlotte, N.C. Journal of Environmental Engineering, **134**(5): 403–408.

Julien, P.Y., 2002. River mechanics. Cambridge University Press, Cambridge, United Kingdom.

Kantrowitz, I.H., and Woodham, W.M. 1995. Efficiency of a stormwater detention pond in reducing loads of chemical and physical constituents in urban streamflow, Pinellas County, Florida. Water-Resources Investigations Report 94-4217, U.S. Geological Survey, Tallahassee, Florida, USA.

Keshavarzi, A.R., and Gheisi, A.R. 2006. Trap efficiency of vortex settling chamber for exclusion of fine suspended sediment particles in irrigation canals. Irrigation and Drainage, **55**(4): 419–434.

Khan, S., Melville, B.W., and Shamseldin, A. 2013. Design of storm-water retention ponds with floating treatment wetlands. Journal of Environmental Engineering, **139**(11): 1343–1349.

Kiviniemi, O., and Makusa, G. 2009. A scale model investigation of free surface vortex with particle tracking velocimetry. Master's Thesis, Department of Civil and Environmental Engineering, Luleå University of Technology, Luleå, Sweden.

Kjellin, J., Wörman, A., Johansson, H., and Lindahl, A. 2006. Controlling factors for water residence time and flow patterns in Ekeby treatment wetland, Sweden. Advances in Water Resources, **30**(4): 838-850.

Kleinhans, M.G., van Dijk, W.M., van de Lageweg, W.I., Hoyal, D.C.J.D., Markies, H., van Maarseveen, M., Roosendaal, C., van Weesep, W., van Breemen, D., Hoendervoogt, R., and Cheshier, N. 2014. Quantifiable effectiveness of experimental scaling of river-and delta morphodynamics and stratigraphy. Earth-Science Reviews, **133**: 43-61.

Kleynhans, S.H. 2012. Physical hydraulic model investigation of critical submergence for raised pump intakes. Master's Thesis, Department of Civil Engineering, Stellenbosch University, Stellenbosch, South Africa.

Knauss, J. 1987. Swirling Flow Problems at Intakes. A.A. Balkerma, Rotterdam, The Netherlands.

Kobus, H. 1980. Hydraulic modeling. Bulletin No. 7, German Association for Water Resources and Land Improvement, Pitman Publishing Inc., Marshfield, Massachusetts, USA.

Levenspiel, O. 2012. Tracer technology: modeling the flow of fluids. Springer, New York, NY, USA.

Liebens, J. 2001. Heavy metal contamination of sediments in stormwater management systems: the effect of land use, particle size and age. Environmental Geology, **41**(3-4): 341-351.

Liem, L.E., Stanley, S.J., and Smith, D.W. 1999. Residence time distribution analysis as related to the effective contact time. Canadian Journal of Civil Engineering, **26**(2): 135–144.

Livingston, E.H., Shaver, E., Skupien, J.J., and Horner, R.R. 1997. Operation, maintenance, and management of stormwater management systems. Watershed Management Institute and Office of Water, United States Environment Protection Agency, Washington, D.C., USA.

López, P.R., Lavín, A.G., López, M.M.M., and de las Heras, J.L.B. 2008. Flow models for rectangular sedimentation tanks. Chemical Engineering and Processing, **47**(9-10): 1705–1716.

Luyckx, G., and Berlamont, J. 2004. Removal efficiency of swirl/vortex separators. Urban Water Journal, **1**(3): 251–260.

Mallin, M.A., Ensign, S.H., Wheeler, T.L., and Mayes, D.B. 2002. Pollutant removal efficacy of three wet detention ponds. Journal of Environmental Quality, **31**(2): 654-660.

Mashauri, D.A. 1986. Modelling of a vortex settling basin for primary clarification of water. Ph.D. Thesis, Tampere University of Technology, Tampere, Finland.

Mashauri, D.A. 2011. A review of the 'Tea Cup Effect' and removal of suspended solids from water. PROGRESS Multidisciplinary Research Journal, **1**(1): 72–85

McDonald, D. 2013. Pilot water quality objectives and allowable contaminant loads for the North Saskatchewan River. Alberta Environment and Sustainable Resources Development (AESRD), Version 1.0, ISBN 978-1-4601-1277-9, Alberta Government, Edmonton, Alberta, Canada.

National Research Council (NRC) 2008. Urban stormwater management in the United States. The National Academies Press, Washington, D.C.

Novak, P., and Čábelka, J. 1981. Models in hydraulic engineering: physical principles and design applications. Pitman Publishing Inc., Marshfield, Massachusetts, USA.

Novak, P., Guinot, V., Jeffrey, A., and Reeve, D.E. 2010. Hydraulic modelling–an introduction: principles, methods and applications. Spon Press, New York, NY, USA.

Odgaard, A.J. 1986. Free-surface air core vortex. Journal of Hydraulic Engineering, **112**(7): 610-620.

Ontario Ministry of Environment and Energy (OMEE) 1994. Stormwater management practices planning and design manual. Environmental Science & Standards Division, Program Development Branch, Ontario Ministry of Environment and Energy, Toronto, Ontario, Canada.

Paul, T.C., Sayal, S.K., Sakhuja, V.S., and Dhillon, G.S. 1991. Vortex settling basin design considerations. Journal of Hydraulic Engineering, **117**(2): 172–189.

Peakall, J., Ashworth, P., and Best, J.L. 1996. Physical modelling in fluvial geomorphology: principles, applications and unresolved issues. *Edited by* Bruce L. Rhoads and Colin E. Thorn. The Scientific Nature of Geomorphology: Proceedings of the 27th Binghamton Symposium in Geomorphology 27 – 29 September 1996, Chichester, West Sussex, England, pp. 221-253.

Persson, J. 2001. The hydraulic performance of ponds of various layouts. Urban Water, **2**(3): 243-250.

Phipps, D., Alkhaddar, R., Loffill, E., Faram, M., and Andoh, B. 2008. Efficiency testing of a hydrodynamic vortex seperator. *In* Proceedings of the 11th International Conference of Urban Drainage, Edinburgh, Scotland, United Kingdom, 31 August – 5 September 2008.

Quarini, G., Innes, H., Smith, M., and Wise, D. 1996. Hydrodynamic modelling of sedimentation tanks. Proceedings of the Institution of Mechanical Engineers, Part E: Journal of Process Mechanical Engineering, **210**(2): 83–91.

Rajaratnam, N. and Flint-Petersen L. 1989. Low Reynolds number circular turbulent jets. Proc. Institution of Civil Engineers, **87**: 299-305.

Rebhun, M., and Argaman, Y. 1965. Evaluation of hydraulic efficiency of sedimentation basins. Journal of the Sanitary Engineering Division, Proceedings of the American Society of Civil Engineers, **91**(SA5): 37–45.

Roy, B., Mazurek, K.A., Mccorquodale, J.A., and Machina, D. 2002. Hydraulic model study of the village of Wheatley waterworks reservoir. In Proceedings of the 2002 Joint CSCE/EWRI of ASCE Environmental Engineering Conference, 21-24 July 2002, Niagara Falls, Ontario, Canada.

Sharp, J.J. 1981. Hydraulic modeling. Butterworth & Co. (Canada) Ltd., Toronto, Ontario, Canada.

Strassler, E., Pritts, J., and Strellec, K. 1999. Preliminary data summary of urban storm water best management practices. United States Environment Protection Agency, Office of Water (4303), EPA-821-R-99-012, Washington, D.C., USA.

Sullivan, R.H., Cohn, M.M., Ure, J.E., and Parkinson, F. 1974. The swirl concentrator as a grit separator device. National Environmetal Research Center, Office of Research and Development, United States Environment Protection Agency, Chicago, Illinois, USA.

Takaijudin, H., Hashim, A.M., Rauf, N.H.A., and Jusoff, K. 2011. Assessment on pollutant removal of interconnected wet detention pond. American-Eurasian Journal of Agricultural & Environmental Sciences, **10**(3): 324-329.

Teefy, S. 1996. Tracer studies in water treatment facilities: a protocol and case studies. AWWA Research Foundation, American Water Works Association, Denver, Colorado, USA.

Thirumurthi, D. 1969. A break-through in the tracer studies of sedimentation tanks. Journal of Water Pollution Control Federation, **41**(11), Part 2: 405–418.

Topping, J. 1957. Errors of observation and their treatment. The Institute of Physics Monographs for Students. Edited by Lang, H.R. Unwin Brothers Limited, London.

U.S. Environmental Protection Agency (USEPA) 1983. Results of nationwide urban runoff program (NURP), Final Report, Water Planning Division, Washington, D.C., USA.

U.S. Environmental Protection Agency (USEPA) 2002. National Water Quality Inventory 2000 Report. EPA-841-R-02-001. Office of Water, Washington, D.C., USA.

Verstraeten, G., and Poesen, J. 2001. Variability of dry sediment bulk density between and within retention ponds and its impact on the calculation of sediment yields. Earth Surface Processes and Landforms, **26**(4): 375-394.

Waldron, R. 2008. Physical modeling of flow and sediment transport using distorted scale modeling. M.Sc. Thesis, Department of Civil and Environmental Engineering, Tulane University, New Orleans, Louisiana, USA.

Wang, G., Chen, S., Barber, M.E., and Yonge, D.R. 2004. Pond treating stormwater runoff. Journal of Environmental Engineering, **130**(11): 1315–1321.

Wilson Jr., J.F., Cobb, E.D., and Kilpatrick, F.A. 1986. Fluorometric procedures for dye tracing: US Geological Survey techniques of water resources investigations. *In* Book 3, Application of Hydraulics, Chap. A12, United States Government Printing Office, Washington, D.C., USA.

Wolf, D., and Resnick, W. 1963. Residence time distribution in real systems. Journal of Industrial and Engineering Chemical Fundamentals, **2**(4): 287–293.

Wu, J.S., Holman, R.E., and Dorney, J.R. 1996. Systematic evaluation of pollutant removal by urban wet detention ponds. Journal of Environmental Engineering, **122**(11): 983-988.

Yang, S.Q. 2009. Mechanism for initiating secondary currents in channel flows. Canadian Journal of Civil Engineering, **36**(9): 1506-1516.

Yousef, Y.A., Hvitved-Jacobsen, T., Sloat, J., and Lindeman, W. 1994. Sediment accumulation in detention or retention ponds. The Science of the Total Environment, **146/147**(1994): 451-456.

Yu, X. 2009. Modelling retention time in a clearwell. M.Sc. Thesis, Department of Civil and Geological Engineering, University of Saskatchewan, Saskatoon, Saskatchewan, Canada.

Yu, X., Putz, G., Mazurek, K. A., and Albers, C. 2008. Effect of columns on the flow behavior and residence time distribution in a water treatment plant clearwell. *In* Proceedings of the CSCE 2008 Annual Conference, Québec, Canada, 10–13 June 2008. Canadian Society for Civil Engineering.

APPENDIX

Sample Calculation for Plug Flow, Mixed Flow and Dead Spaces

A linear trend line fit to a plot of *ln(1-F)* vs t/t_d for the 100:2 pond model at 0.76 L/s flow rate (equivalent prototype flow rate = 4 m^3/s) and 12 hr flow development time (see figure A-1) produces the following equation.

$$y = -1.7725x + 0.6291 \qquad \text{[A-1]}$$

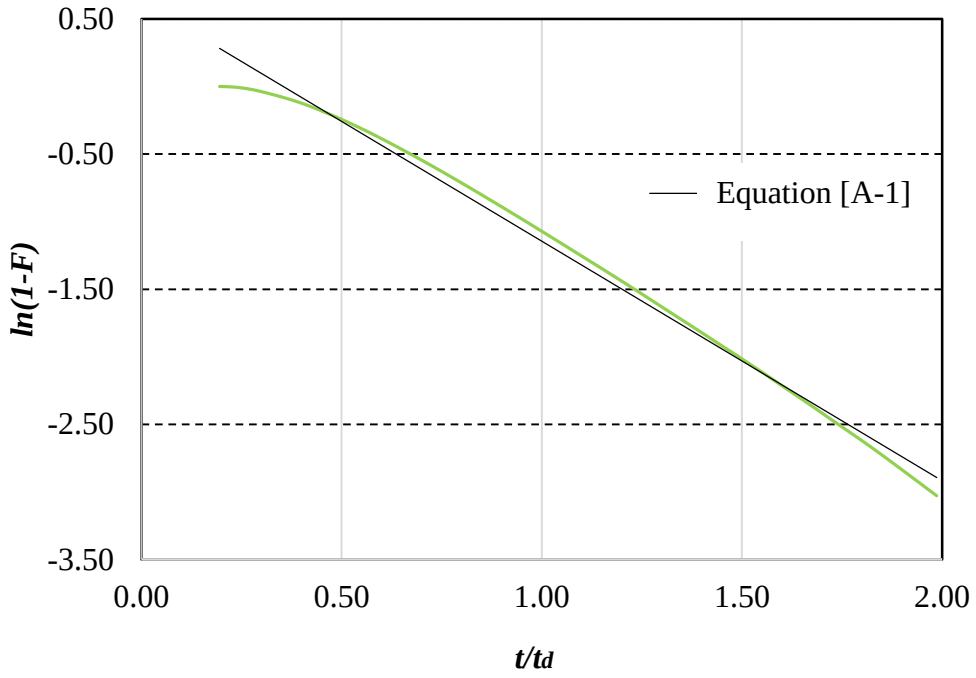

Figure A-1: Application of Rebhun and Argaman (1965) model with the tracer test data for the test carried out in the 100:2 pond model at 0.76 L/s flow rate and 12 hr flow development time

The Rebhun and Argaman (1965) model is given by

$$\ln\left(1-F\left(\frac{t}{t_d}\right)\right) = -\frac{1}{(1-P)(1-d)}.\frac{t}{t_d} + \frac{P}{1-P} \qquad \text{[A-2]}$$

Comparing Equations [A-1] and [A-2] we can get,

$$\frac{1}{(1-P)(1-d)} = 1.7725 \qquad \text{[A-3]}$$

$$\frac{P}{(1-P)} = 0.6291 \qquad \text{[A-4]}$$

Solving equations [A-3] and [A-4],

P = plug flow fraction of the effective volume = 0.39

d = dead space fraction of total volume = 0.081

m = mixed flow fraction of effective volume = $1 - P$ =1-0.39 = 0.61

Effective fraction of total volume = $1 - d$ = 1-0.081 = 92%

Therefore, the plug flow fraction of total volume = 36%

Mixed flow fraction of total volume = 56%

Dead space fraction of total volume = 8.1%